Aus dem Institut für Sportwissenschaft der Universität Rostock

# The Effect of Cycling Positions on Cardiorespiratory and Aerodynamic Parameters for Road Cyclists

Dissertation zur

Erlangung des akademischen Grades

Doctor rerum humanarum (Dr. rer. hum.)

der Medizinischen Fakultät der Universität Rostock

vorgelegt von

Wuttigrai Noipant

geb. am 06.10.1975 in Lop Buri, Thailand

Rostock, den 18. März 2016

urn:nbn:de:gbv:28-diss2016-0110-7

Gutachter:

1. Prof. Dr. phil. habil. Volker Zschorlich

   Institut für Sportwissenschaft, Philosophische Fakultät,

   Universität Rostock

2. Prof. Dr. med. habil. Dipl.-Ing. Rainer Bader

   Orthopädische Klinik und Poliklinik, Medizinische Fakultät,

   Universität Rostock

3. Prof. Dr. med. Johann-Peter Kuhtz-Buschbeck

   Physiologisches Institut, Medizinische Fakultät,

   Christian-Albrechts-Universität zu Kiel

Datum der Einreichung: 18. März 2016

Datum der Verteidigung: 27. Juli 2016

*‘‘ This masterpiece is dedicated to my parents, my family and my country. ’’*

# Acknowledgements

I would like to thank all those who have provided guidance and support while I was studying at the University of Rostock. First of all, I wish to express my sincere gratitude to Prof. Dr. Volker Zschorlich, my supervisor, for giving me the great opportunity to do my Ph.D. as well as for his inspiration, valuable guidance, constructive suggestions, and support throughout my study. I would also like to thank Prof. Dr. med. Rainer Bader and Prof. Dr. med. Johann-Peter Kuhtz-Buschbeck for their valuable reviewing to my dissertation.

I am forever grateful to Dipl.-Ing. Norbert Wolff and Dipl.-Ing. Andreas Mattke who taught me the experimental techniques and for, alongside with Dr. Ulf Reder, kindly being participants for the first tryout of the coasting down investigation.

I also would like to express my appreciation to Miss Anne Schulz, Mrs. Kerstin Daberkow, Mr. Eugen Schweitzer, Mr. Heie Ludewig, Mr. Mudar Kandkji, Dr. Sameh kassem, Dr. Tammam Tanjour, and Mr. Ulrich Creuznacher, my colleagues, for their kind support, useful discussions and friendship, which have made my time in Germany a pleasant and worthwhile experience. Also, my special thanks goes to the twenty-four participants in the experiments. Indispensably, I would like to thank Mr. Rajko Grawert very much for photographing in a part of the projected frontal area measurement as well as Miss Helen Morrison for valuable help in correction of the English text.

I deeply acknowledge the Faculty of Sports Science, Kasetsart University, Thailand, for given me the opportunity and scholarship support to accomplish my Ph.D. studies in Germany.

Certainly, this masterpiece would not have been possible without the love and encouragement of Mrs. Suwanit Nimwat and Mr. Supamongkol Noipant, my parents. I would like especially like to thank my mother for the financial support throughout my educational life. Last but certainly not least, big thanks to my wife and daughters who strengthen my willpower.

# CONTENTS

CONTENTS

CONTENTS

## List of abbreviations

| Abbreviations | Meaning | SI unit of measure |
|---|---|---|
| AP | Aero position | |
| BF | Breathing frequency | breaths·min$^{-1}$ |
| BTPS | Body temperature and pressure saturated | |
| DP | Fully dropped position | |
| HR | Heart rate | beats·min$^{-1}$ |
| NS | Not significant | |
| RER | Respiratory exchange rate | |
| rpm | Revolution per minute | |
| SD | Standard deviation | |
| SS | Sum of squares | |
| STPD | Standard temperature and pressure dry | |
| T | Temperature | °C |
| UP | Upright position | |

## List of notations

| Notations | Meaning | SI unit of measure |
|---|---|---|
| $A$ | Projected frontal area | m$^2$ |
| $a_{are}$ | Acceleration of aerodynamic drag | m·s$^{-2}$ |
| $a_{rol}$ | Acceleration of rolling friction | m·s$^{-2}$ |
| $C_1$ | First constant of integration | |
| $C_2$ | Second constant of integration | |
| $C_D$ | Drag coefficient | dimensionless |
| $C_D \cdot A$ | Drag area | m$^2$ |

# LIST OF ABBREVIATIONS, NOTATIONS, AND SYMBOLS

| Notations | Meaning | SI unit of measure |
|---|---|---|
| $°C$ | Degree Celsius | |
| $E_{kin}$ | Kinetic energy | J |
| $E_{pot}$ | Potential energy | J |
| $E_{rot}$ | Rotational energy | J |
| $F_{aer}$ | Aerodynamic drag | N |
| $F_{bea}$ | Bearing friction | N |
| $F_{gra}$ | Gravitational force | N |
| $F_{ine}$ | Inertial force | N |
| $F_{net}$ | Net force | N |
| $F_{pro}$ | Propulsive force | N |
| $F_{res}$ | Resistive force | N |
| $F_{rol}$ | Rolling friction | N |
| $g$ | Acceleration due to gravity | $m \cdot s^{-2}$ |
| $I$ | Moment of inertia | $kg \cdot m^{2}$ |
| $K$ | Aerodynamic constant | $kg \cdot m^{-1}$ |
| $K_m$ | Aerodynamic constant divided by mass | $1 \cdot m^{-1}$ |
| $m$ | Mass | kg |
| $m_{CB}$ | Mass of cyclist plus bicycle | kg |
| $m_C$ | Mass of cyclist | kg |
| $m_B$ | Mass of bicycle | kg |
| $n$ | Number of participant | |
| $P$ | Mechanical power | Watt |
| $P_{net}$ | Net mechanical power | Watt |
| $P_{aer}$ | Mechanical power of aerodynamic drag | Watt |

# LIST OF ABBREVIATIONS, NOTATIONS, AND SYMBOLS

| **Notations** | **Meaning** | **SI unit of measure** |
|---|---|---|
| $P_{rol}$ | Mechanical power of rolling resistance | Watt |
| $P$ – value | Probability value | |
| $RH$ | Relative humidity | % |
| $s$ | Displacement | m |
| $s_i$ | Initial displacement | m |
| $s_f$ | Final displacement | m |
| $s_{max}$ | Maximal displacement | m |
| $T$ | Torque | N·m |
| $t$ | Time | s |
| $t_i$ | Initial time | s |
| $t_f$ | Final time | s |
| $t_{max}$ | Maximal time | s |
| $\dot{V}O_2$ | Oxygen uptake | $ml \cdot min^{-1}$ |
| $\dot{V}CO_2$ | Carbon dioxide output | $ml \cdot min^{-1}$ |
| $\dot{V}_E$ | Minute ventilation | $L \cdot min^{-1}$ |
| $V_T$ | Tidal volume | L |
| v | Velocity | $m \cdot s^{-1}$ |
| $v_i$ | Initial velocity | $m \cdot s^{-1}$ |
| $v_f$ | Final velocity | $m \cdot s^{-1}$ |
| $v_{max}$ | Maximal velocity | $m \cdot s^{-1}$ |
| $W$ | Mechanical work | N·m |

# List of symbols

| Symbols | Meaning | SI unit of measure |
|---|---|---|
| $\alpha$ (alpha) | $\bar{a}_{rol} / K_m$ | |
| $\beta$ (beta) | $\bar{a}_{rol} \cdot K_m$ | |
| $\mu$ (mu) | Coefficient of rolling friction | dimensionless |
| $\omega$ (omega) | Angular velocity | $rad \cdot s^{-1}$ |
| $\pi$ (pi) | Ration of a circle's circumference to its diameter | |
| $\rho$ (rho) | Air density | $kg \cdot m^{-3}$ |
| $\theta$ (theta) | Slope angle | degree (°) |
| $\bar{x}$ | Mean | |
| * | $P<0.05$ | |
| ** | $P<0.01$ | |
| *** | $P<0.001$ | |

# Zusammenfassung

Die Optimierung der Sitzposition ist im Radsport ein Schlüsselfaktor für Spitzenleistung. Radfahren mit gebeugten Sitzpositionen haben einen aerodynamischen Vorteil, aber könnte Thorax-Expansion beschränken, Thorax-Volumen reduzieren und zur Steigerung der Herz-Lungen-Aktivität führen. Der Zweck dieser Studie ist es, die kardiorespiratorische Reaktionen auf einen submaximalen Spiroergometrie-Tests zu zeigen. Dabei werden die aerodynamischen Parameter, von Aufrechtlenker Sitzposition (UP), Zeitfahrlenker Sitzposition (AP) und vor allem vollem Unterlenker Sitzposition (DP) untersucht.

Für den erste Teil der Studie wurde an vierundzwanzig männlichen Freizeit-Radfahrern (randomisierte Sitzposition), an drei verschiedenen Tagen, mit jeweils mindestens zwei Tagen Erholung, in je einer Sitzposition ein Spiroergometrie-Test durchgeführt. Vor der Messung hatten die Versuchspersonen eine dreiminütige Ruhepause. Danach startete die Messung mit Radfahren auf einem modifizierten Ergometer über eine dreiminütige Aufwärmphase mit einer Leistung von 60 Watt, eine Trittfrequenz von 80 Umdrehungen pro Minute in UP zu musste eingehalten werden. Anschließend sollten die Versuchspersonen je eine drei fünfminütigen Durchgänge bei einer Leistung von jeweils 100, 140 und 180 Watt durchführen. Kardiorespiratorische Parameter einschließlich Herzfrequenz (HF), Sauerstoffaufnahme ($\dot{V}O_2$), Kohlendioxidabgabe ($\dot{V}CO_2$), Atemminmutenvolumen ($\dot{V}_E$), Atemzugvolumen ($V_T$), Atemfrequenz (AF) und Respiratory Exchange Rate (RER) wurden kontinuierlich mit einem tragbaren Telemetrie-Gasanalysesystem (Jaeger Oxycon Mobile®) aufgezeichnet. Die Ergebnisse einer einfachen ANOVA mit wiederholten Messungen zum Analysieren zeigen, dass bei den gebückten Haltungen (AP und DP) im Mittel wesentlich höhere Werte für HF, $\dot{V}O_2$, $\dot{V}CO_2$, $\dot{V}_E$ und AF im Vergleich zu UP ergeben. Ausnahme bildet hier der Mittelwert der RER. Das Mittel des $V_T$ bei UP ist signifikant höher als bei DP und AP.

Für den zweiten Teil der Studie, wurde eine alternative und nicht so kostenintensive Messmethode zum Windkanaluntersuchung für die Ausrollversuch verwendet, um den Luftwiderstandsbeiwert ($C_D$) zu bestimmen. Vier Versuchspersonen aus dem ersten Teil der Studie wurden zufällig ausgewählt, um bei zwei Geschwindigkeiten (25 und 15 $km \cdot h^{-1}$) 20 Versuche in drei Sitzpositionen Ausrollversuche zu machen. Zu Beginn des Tests beschleunigte Versuchspersonen das Messfahrrad auf die festgelegte Geschwindigkeit und rollte anschließend in einer der drei genannten Sitzposition auf einem ebenen Boden 50-Meter unter identischen Bedingungen aus. Geschwindigkeit und Zeit wurde von einem Fahrrad-Telemetrie-System erfasst und aufgezeichnet. Bei der Auswertung wurde das quadratische Mittel verwendet, um die relevanten Parameter durch ein Solver-Programm zu schätzen. Die projizierte

Stirnfläche ( $A$ ) des Radfahrers in den jeweiligen Sitzpositionen, wurde mit Hilfe von ImagJ Software bestimmt. Die Auswertung zeigt, dass das Mittel des $C_D$ für UP = 1.018 (± 0.106), AP = 0.741 (± 0.027) und DP = 0.437 (± 0.021) ergibt.

Die Ergebnisse der Widerstandskraft, der mechanischen Leistung und der Energiekosten zusammengefasst ergeben, dass Radfahren in DP und AP die aerodynamische Effizienz ergab, obwohl erhöhte die Beide die kardiorespiratorische Funktion.

*Stichworte*: Sitzpositionen, Radfahren, Aufrechtlenker, Zeitfahrlenker, Unterlenker, submaximalen Spiroergometrie, kardiorespiratorische Reaktion, Ausrollversuche, Luftwiderstandsbeiwert, Herzfrequenz, Sauerstoffaufnahme

# Abstract

The optimal cycling position is a key factor to the acquisition of high performance. Cycling in the crouched positions give an aerodynamic advantage but may restrict thorax expansion, reduce thorax volume and result to increasing of cardiorespiratory function. Therefore, the purpose of this study was to examine the cardiorespiratory responses during submaximal spiroergometry tests and investigate the aerodynamic parameters during field tests, of upright position (UP), aero position (AP) and especially, fully dropped position (DP) that has not yet been tested.

First part of the study, twenty-four recreational male cyclists were randomly assigned to perform three cycling positions on three separate days with at least two days of recovery in between. At the beginning of test trials, participants began from a 3-min rest session on a modified stationary ergometer, followed by cycling of a 3-min warm-up session with a workload of 60 Watts and were asked to maintain the cadence of 80 rpm in UP. Participants were then instructed to continuously perform a series of three 5-min cycling sessions with workload levels of 100, 140, and 180 Watts, respectively. Cardiorespiratory parameters including heart rate (HR), oxygen uptake ($\dot{V}O_2$), carbon dioxide output ($\dot{V}CO_2$), minute ventilation ($\dot{V}_E$), tidal volume ($V_T$), breathing frequency (BF), and respiratory exchange rate (RER) were continuously recorded by breath-by-breath of a portable telemetric gas analysis system (Jaeger Oxycon Mobile®). Results of a one-way repeated measures ANOVA revealed that both AP and fully DP yielded significantly the mean values of HR, $\dot{V}O_2$, $\dot{V}CO_2$, $\dot{V}_E$, and BF higher than UP, except the mean of RER. Whereas the mean value of $V_T$ in UP was significantly greater than fully DP and AP, respectively.

For second part of the study was to use a coasting down technique serves as a good alternative to measurements instead of in a wind tunnel that expensive investigation for obtaining drag coefficient ($C_D$), and model the cycling motions. Four subjects from previous study were selected to investigate with two velocities (25 and 15 km·h$^{-1}$) of 20 trials of the same three cycling positions that were measured for the cardiorespiratory study. At the beginning of coasting trials, subjects speeded up to the defined velocity and then coasted down with defined position on a flat floor 50-m long section in the University Sports Hall Rostock under identical conditions. The velocity-time function was measured by a tachogenerator mounted on a distal of front fork bicycle in combination with a bicycle-telemetry system, and the DIAdem™ software was used for data processing. The least squares method was used to estimate the relevant parameters through Solver program. Regarding projected frontal area ($A$) of cycling positions were determined via a digitizing technique through ImageJ software. The results showed that the mean values of $C_D$ for UP, AP, and fully DP yielded 1.018 (± 0.106), 0.741 (± 0.027), 0.437 (± 0.021), respectively.

From calculated aerodynamic parameters were modeled a resistive force, a mechanical power, and an energy cost. They were summarized that cycling in fully DP and AP yielded aerodynamic effectiveness, although increased the cardiorespiratory function.

*Keywords*: cycling position, submaximal spiroergometry tests, cardiorespiratory responses, coasting-down test, drag coefficient, heart rate, oxygen consumption

# CHAPTER 1: INTRODUCTION

## 1.1 Investigations of cycling positions

Lately, there has been a substantial amount of research and development on cycling science with the aim to optimise cyclist training and bicycle design. An objective of any cycling coach is to design a training program for obtaining the peak performance. Likewise, an objective of a bicycle designer is to design a new bicycle with a minimal aerodynamic drag on which the cyclist is able to maintain highest speed. In addition, the cyclists try to find the best cycling position of minimal air drag. Consequently, cycling studies should not only focus on the effectiveness of aerodynamic drag but also on the effect of physiological responses. Both branches of study have an important meaning for achieving the optimal cycling performance.

From the point of view during cycling, the cyclist's energy expenditure is synthesized from aerobic and anaerobic processes and is used to produce the mechanical power by muscular function in order to overcome aerodynamic drag, rolling resistance, friction in bearing and chain drive system, and changes in kinetic and potential energy resulting from gravitational force (Martin et al., 1998). The aerodynamic drag dominates the energy losses during cycling, when the velocity exceeds approximately 16 $km \cdot h^{-1}$. At high velocities, approximately above 48 $km \cdot h^{-1}$, 70% of mechanical power is used to overcome the air drag of the cyclist (Faria, 1992). The aerodynamic drag represents the main resistance experienced by a cyclist on level terrain at high speeds. Actually, the aerodynamic drag depends on the air density, drag coefficient, projected frontal area, and velocity (Janna, 1993). One thing that can be done by the cyclists in order to decrease the aerodynamic drag is to reduce the projected frontal area. Therefore, in order to overcome air resistance, the cyclists need to ride in a crouched position, which is a key factor to the acquisition of high speeds during competition, especially for the final period. Faria (1992) indicated that when the cyclist crouches the torso parallel to the ground, the drag force is reduced by approximately 20%. Because the crouched position gives a streamlined shape of the body, it is acquired by the cyclists just before reaching the finish line in order to decrease the air drag leading to an increased velocity (Kyle & Weaver, 2004). This can be confirmed by the aerodynamic data from wind tunnel testing, which revealed that a crouched position such as the aero position or the time trial position can decrease the drag area ($C_D \cdot A$) or drag coefficient ($C_D$), resulting in a decreased aerodynamic drag ($F_{aer}$) when compared with the upright position (García-López et al., 2008; Defraeye et al., 2010; Chowdhury et al., 2011).

However, cycling in the crouched positions, i.e. either in an aero position or a fully dropped position, for a prolonged submaximal cycling may result in a decrease of the performance level with regard to the respiratory function. Namely, the crouched position may limit chest expansion, reduce chest volume, increase respiration rates, and then, may result in reduced efficiency of both the cardio and the respiratory system. To the best of knowledge, in the last

decade, there have been investigations of the effect between upright positions and crouched position such as aero position on respiratory responses, though these investigations were mostly concerned with trained cyclists (Peveler et al., 2005; Jobson et al., 2008; Dorel et al., 2009; Hubenig et al., 2011). However, the untrained cyclists that are not familiar with the crouched position (i.e. aero position), have been less studied (Ashe et al., 2003). In particular, the fully dropped position as a crouched position that gives aerodynamic benefit has not yet been investigated with respect to respiratory function. Therefore, the effects of the upright position, the aero position, and, in particular, the fully dropped position on the energy expenditure as determined by oxygen consumption and the respiratory function should be examined and compared.

Measuring the aerodynamic drag in cycling positions can be conducted both directly and indirectly by using several different methods. To the best of knowledge, the aerodynamic parameters such as the drag area or only the drag coefficient and the aerodynamic drag can be commonly determined from the wind tunnel measurements (Martin et al., 1998; García-López et al., 2008; Gibertini et al., 2008; Chowdhury et al., 2011; Crouch et al., 2012), though these are typically very expensive. Alternative methods to measure the aerodynamic parameters and air drag can be to tow the cyclist on a bicycle with a vehicle (Capelli et al., 1993; De Groot et al., 1995), to assess the parameters from the linear regression analysis between mechanical power and energy expenditure and square velocity (Davies, 1980; Capelli et al., 1998), to determine them by using force transducers (Grappe et al., 1997; Martin et al., 2006; Edwards & Byrnes, 2007; Lim et al., 2011), or, as of recently, to simulate them using computational fluid dynamics (CFD) (Defraeye et al., 2010; Blocken et al., 2013).

Apart from these methods, the coasting down technique (also referred to as the freewheeling method or deceleration method) offers an alternative approach that is not expensive and can be used to determine the aerodynamic drag and the drag area, as well as the drag coefficient. Additionally, this technique can also calculate the rolling resistance. The coasting down method relies on Newton's second law ($\Sigma \vec{F} = m \cdot \vec{a}$) that acceleration is the negative value of deceleration. The coasting down test has been used to investigate various cycling positions in studies such as those of Candau et al. (1999) for the comparison between upright position (hands grip on upper parts of standard handlebar with straight arms) and aero position (hands grip on end portions and arms on elbow pads of aero handlebars that are mounted to the standard handlebars), Hennekam and Govers (1996) for only the racing position (hands grip on lower parts of standard handlebar with straight arms), and De Groot et al. (1995) for only hoods position (hands grip on brake-hood parts of standard handlebar with crouching torso). However, the fully dropped position (hands grip on lower parts of standard handlebar with crouching torso) has not yet been investigated with this technique. To this end, the aerodynamic drag, drag area, and drag coefficient between the upright position and the crouched positions, i.e. the aero

position and especially for the fully dropped position, will be investigated and compared in this study by using the coasting down method with a new device for obtaining data. Finally, cycling models will be created for the aerodynamic drag, the mechanical power and the energy cost for the three cycling positions.

## 1.2 Objectives

As mentioned above, effects of cycling in an upright position compare to two crouched positions such as an aero position and especially a fully dropped position that has not yet been studied should be investigated both cardiorespiratory responses and aerodynamic parameters; therefore, in this study aimed to investigated following:

### 1.2.1 Spiroergometry testing

1. To measure the response of cardiorespiratory parameters (i.e. heart rate (HR), oxygen uptake ($\dot{V}O_2$), carbon dioxide output ($\dot{V}CO_2$), respiratory exchange rate (RER), breathing frequency (BF), tidal volume ($V_T$), and minute ventilation ($\dot{V}_E$)) in the upright position (UP), the aero position (AP), and the fully dropped position (DP) at the submaximal spiroergometry level (i.e. 100, 140, and 180 Watts) by using a breath-by-breath technique through a portable telemetric gas analysis system.

### 1.2.2 Coasting down testing

1. To investigate the feasibility of the coasting down technique over a short distance by using a tachogenerator for speed measurement and a telemetry bicycle system for data transmission.

2. To determine the aerodynamic parameters (i.e. drag area ($C_D \cdot A$) and drag coefficient ($C_D$)) from the coasting down technique in the upright position (UP), the aero position (AP), and the fully dropped position (DP) by a least square method.

3. To measure the projected frontal area ($A$) in the upright position (UP), the aero position (AP), and the fully dropped position (DP) by using a digitizing method with a computer-based image analysis software.

4. To model the net force ($F_{net}$), the mechanical power ($P$), and the energy cost ($\dot{V}O_2$) in the upright position (UP), the aero position (AP), and the fully dropped position (DP).

## 1.3. Hypotheses

As mentioned earlier, although cycling in crouched positions yield the efficiency of aerodynamics, but may reduce efficiency of the cardiorespiratory system. That is, cycling in crouched position may limit chest expansion, reduce chest volume, increase respiratory rate, and then, may result in increasing both function of cardiac and lungs. Therefore, in this study is based on the following hypotheses, which it is hypothesized that if cyclists cycled in the crouched positions such as aero position (AP) and fully dropped position (DP), then:

### 1.3.1 Spiroergometry testing

1. The measured value of cardiac response such as heart rate (HR) in riding the aero position (AP) and especially the fully dropped position (DP) would be significantly *higher than* in riding the upright position (UP).

2. The measured value of gas exchanges such as oxygen uptake ($\dot{V}O_2$), carbon dioxide output ($\dot{V}CO_2$), and respiratory exchange rate (RER) in riding the aero position (AP) and especially the fully dropped position (DP) would be significantly *higher than* in riding the upright position (UP).

3. The measured value of ventilatory responses such as breathing frequency (BF), tidal volume ($V_T$), and minute ventilation ($\dot{V}_E$) in riding the aero position (AP) and especially the fully dropped position (DP) would be significantly *higher than* in riding the upright position (UP).

### 1.3.2 Coasting down testing

1. The estimated value of aerodynamic parameters such as drag area ($C_D \cdot A$) and drag coefficient ($C_D$) in riding the aero position (AP) and especially the fully dropped position (DP) would be *lower than* in riding the upright position (UP).

2. The digitized value of projected frontal area ($A$) in riding the aero position (AP) und especially the fully dropped position (DP) would be *lower than* in riding the upright position (UP).

# CHAPTER 2: THEORIES

## 2.1 Fundamentals of forces affecting road cycling motion

### 2.1.1 Conceptual outline of motion

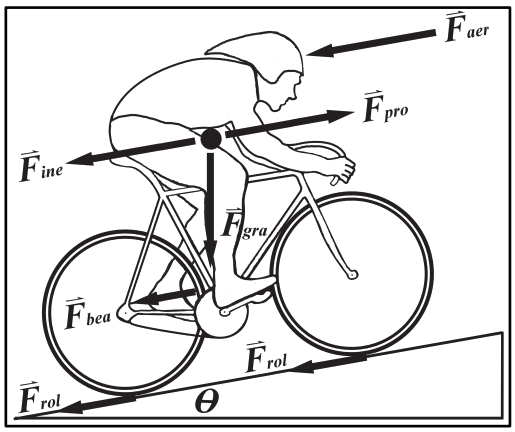


Figure 2.1 Schematic representation of a cyclist's propulsive force ( $\vec{F}_{pro}$ ), which has to overcome opposing forces during riding on an inclined road ( $\theta$ ) such as aerodynamic drag force ( $\vec{F}_{aer}$ ), rolling friction ( $\vec{F}_{rol}$ ), gravitational force ( $\vec{F}_{gra}$ ), bearing friction ( $\vec{F}_{bea}$ ), and inertial force ( $\vec{F}_{ine}$ ).

Generally, when a cyclist is moving forward, there are forces acting on both the cyclist and the bicycle. These forces are called "retarding force" or "resistive force" ( $\vec{F}_{res}$ ), which will push the cyclist and bicycle backward making it harder for the cyclist to move forward. In other words, the $\vec{F}_{res}$ is the force which hampers or hinders the forward motion of the cyclist and bicycle. Concerning the motion in cycling, the propulsive force ( $\vec{F}_{pro}$ ) that is generated by the cyclist is the forward force opposite to the direction of $\vec{F}_{res}$ that is the sum of resistive forces. This can be explained by the fact that when the cyclist is riding at a constant velocity the total forces are balanced (equilibrium). This means the forward force is equal the backward force. When the cyclist is speeding up (accelerating), the forces are unbalanced. The forces acting in the forward direction are greater than those acting in the backward direction. When the cyclist is slowing down (decelerating), the forces acting in the forward direction are smaller than those acting in the backward direction. As mentioned above, the foundation for a cycling-motion model is based on Newton's second law of motion. Applied to a cyclist on a bicycle while travelling on a road, it is defined by:

$$\sum \vec{F} = m \cdot \vec{a} = m \cdot \frac{d\vec{v}}{dt} \tag{2.1}$$

where, $m$ is the total mass of a cyclist including a bicycle, and $\vec{a}$ is the acceleration in the forward direction, resulting from the derivative of the change in velocity with time $(d\vec{v}/dt)$ with respect to the ground. Figure 2.1 shows the many forces acting on the cyclist and bicycle while travelling along a road. The acceleration is thus determined by the following sum of the forces $(\sum \vec{F})$:

$$\sum \vec{F} = \vec{F}_{pro} - \vec{F}_{aer} - \vec{F}_{rol} - \vec{F}_{gra} - \vec{F}_{bea} - \vec{F}_{ine} = m \cdot \vec{a} \quad (2.2)$$

where, $\vec{F}_{pro}$ is the propulsive force due to the force supplied to the pedal by the cyclist; $\vec{F}_{aer}$ is the aerodynamic drag that is the main force opposing motion due to air resistance; $\vec{F}_{rol}$ is the rolling friction that is necessary to overcome the mechanical resistance between the wheels and the road surface; $\vec{F}_{gra}$ is the gravitational force while cycling on an inclined road $(\theta)$; $\vec{F}_{bea}$ is the bearing friction in the cup and the cone of the wheel hubs, which is the internal resistance as a function of hub bearing types including the drivetrain system of the bicycle; and $\vec{F}_{ine}$ is the another inertial force that is associated with linear and angular motion due to the moment of inertia of the wheels (Atkinson et al., 2007; Martin et al., 2007; Dahmen et al., 2011). Note that the resistive forces are expressed with negative signs because their directions are opposite to the direction of motion. While the cyclist is riding at constant velocity (without acceleration), $d\vec{v}/dt = 0$ and Equation (2.1) becomes Newton's first law of motion, and is expressed by:

$$\sum \vec{F} = m \cdot \vec{a} = 0 \quad (2.3)$$

Hence, the propulsive force applied by the cyclist is balanced by the sum of opposing forces or resistive force:

$$\vec{F}_{pro} = \vec{F}_{aer} + \vec{F}_{rol} + \vec{F}_{gra} + \vec{F}_{bea} + \vec{F}_{ine} = \vec{F}_{res} \quad (2.4)$$

In order to maintain a constant velocity at all time, Equation (2.4) predicts the propulsive force that the cyclist must exert to overcome the resistive forces ( $\vec{F}_{aer}$, $\vec{F}_{rol}$, $\vec{F}_{gra}$, $\vec{F}_{bea}$, and $\vec{F}_{ine}$ ). These forces will slow down the speed of cyclist and bicycle; particularly, the $\vec{F}_{aer}$ is the main frictional force which is directed opposite to the movement of the cyclist and bicycle.

### 2.1.2 Aerodynamic drag force

The aerodynamic drag force ( $F_{aer}$ ) can also be called "air drag", "air friction", "air resistance" or "wind resistance", and is the dominant force which effects the cyclist and bicycle at high speeds. Kyle (1996) explained that when cycling at velocities above 13 km·h$^{-1}$, the air resistance is the dominant retarding force acting against a cyclist; on

the other hand, when the cycling velocity is below 13 km·h$^{-1}$, the rolling friction replaces it as the main force. In particular, at 50 km·h$^{-1}$, $F_{aer}$ contributes to approximately 90% of the total resistance and plays a key role to the cyclist and bicycle (Faria et al., 2005). Regarding the mechanical power, Martin et al. (1998) found that when the cyclist is travelling over a flat road at steady state, $F_{aer}$ can account for up to 96% of the cyclist's available power. Unavoidably, the power output needs to move the cyclist and bicycle through the air and increases as the cube of the riding velocity. A small increase in velocity requires an exponential growth in power output. Basically, the formula of $F_{aer}$ is obtained by integrating the total surface stress over the surface area of the cyclist-bicycle combination. If the atmosphere density is assumed to be a constant for a small region around the cyclist-bicycle, $F_{aer}$ is given by:

$$F_{aer} = 0.5 \cdot \rho \cdot C_D \cdot A \cdot \mathrm{v}^2 \tag{2.5}$$

where, $\rho$ is the air density as a function of temperature, relative humidity, and barometric pressure; $C_D$ is the drag coefficient; $A$ is the projected frontal area, also called the cross-sectional area of the cyclist and bicycle; and $\mathrm{v}$ is the relative velocity of air with respect to the cyclist-bicycle combination. Often, the $C_D \cdot A$ term is defined as the drag area or effective frontal area associated with the coefficient of drag over the characteristic surface area of the cyclist and bicycle, which is dependent on size and shape (Martin et al., 2007). Considering Equation (2.5), firstly, the value of $F_{aer}$ increases with $\rho$; this can be explained by the fact that more density means more mass or inertia which in turn leads to an increase of resistance. Secondly, the value of $F_{aer}$ also increases with $A$, which means that a greater cross-sectional area causes a greater collision with the airstream. Thirdly, $F_{aer}$ increases with $C_D$, which is used to quantify the resistance of an object in the air flow environment. The lower $C_D$, the less drag the object will experience, and it is always associated with the particular surface area. Lastly, $F_{aer}$ increases with $\mathrm{v}^2$, so that when cycling on flat terrain at high velocity, the energy is mainly dissipated through air resistance.

#### 2.1.2.1 Types of aerodynamic drag

Basically, in the nature of airflow, there are two types of drag forces which exist in cycling events, namely pressure drag or form drag and skin friction or surface drag (Gross et al., 1983) (see Appendix A: Figure 1). Both act directly opposite to the cyclist-bicycle's direction of motion. Both forces are present themselves as a part of the total drag but are not necessarily of equal magnitude. Both depend on size, shape, position, velocity, and density.

2.1.2.1.1 Pressure drag

"Pressure drag" or "form drag" is caused by differences in air pressure between the leading and trailing surface of the body segment in the airstream, and always acts perpendicular to the surface (Kyle & Weaver, 2004). Kreighbaum and Barthels (1996) described that at a velocity fast enough to produce a pattern of flow, the air particles flowing past the body will create the air pressure on the leading surface (high-pressure zone) that becomes greater than the pressure on the trailing surface (low-pressure zone) (see Appendix A: Figure 2). During the body's forward motion will occur the velocity of airstream across the body flows rapidly inducing the airstream to follow the contour of trailing side is separated. When the airflow separates from the body surface, a back flow occurs at the surface of the body, which causes the flow to separate from the surface contour. The separation of the boundary layer will cause large-scale turbulence in the low-pressure zone which is created behind the body (Gross et al., 1983). As the region of low pressure is continually being formed as the object moves though the air; this flow pattern is called the turbulent flow. The cause of turbulence behind the moving body is the force that is applied by the object to the air as it pushes its way trough. According to Newton's law of action and reaction, the air applies the equal and opposite reaction force against the object. This counterforce is the resistive drag against the object. Kyle and Weaver (2004) suggested a streamlining or a lowering frontal area could drastically reduce the pressure drag and the turbulent flow. The streamlined shapes easily and smoothly pass into the airstream, thereby reducing the high-pressure region on the leading surface, thus wasting little energy in air turbulence. For example in cycling, at low velocity, as a smooth human limb moves into the air, the airstreams on the leading surface are laminar and will separate from the limb near the widest point leaving a large low-pressure cavity. At high velocity, however, airstreams on the leading edge of the limb become turbulent, and these turbulent air packets have increased momentum and will follow the limb circumference past the limb's widest point, leaving a much smaller low-pressure cavity in the wake (Brownlie, 2009).

2.1.2.1.2 Skin friction

"Skin friction" or "surface drag" is caused by viscous shear forces in the boundary layer that act parallel to the surface (Kyle & Weaver, 2004). In other words, it is a frictional force that is caused by the air tending to rub along the body or object surface. The thin layers of air in contact with the solid surface of the object do not slide, but rather stick to it and are carried along with the moving body. This layer, in turn, tends to tow along the adjacent outer layer of air, which then drags along the next layer, and so on. From the inner to the outer layer of the surface, the difference in velocities and the subsequent rubbing or shear force become progressively less until the outer layers are reached that

have no sliding tendency at all (see Appendix A: Figure 3). Therefore, the shear forces of the inner layers near the body surface cause the skin friction among the air particles, which will consequently vary from layer to layer of air (Kreighbaum & Barthels, 1996). Smooth surfaces can easily help the air flow around the body in a laminar fashion, resulting in less drag because smooth surfaces generally create a lower shear force than rough surfaces since they trap air. The skin friction will increase with an increase in the velocity of airflow, with an increase in the amount of surface area that is parallel to the flow, i.e. with the amount of surface which is exposed to friction, and with an increase in the roughness of the surface. In cycling, Brownlie (2009) explained that the skin friction can be reduced by using aerodynamic apparel with a smooth texture, e.g. cycling skinsuits. The smooth texture will have lower skin friction, as the smooth surface causes a laminar boundary layer. In comparison, a rough texture would cause the air molecules near the body surface of the cyclist to adhere to the skin and impede the flow along the surface producing the shear force and the turbulent layer; and it would therefore provide additional viscous stress.

#### 2.1.2.2 Nature of airflow surrounding body

As mentioned above, a cyclist on a bicycle will experience two types of aerodynamic drag forces while moving into an airflow, namely pressure drag and skin friction. In general, these two types are associated with an alteration of the boundary layer around the body. Whitt and Wilson (1982) described the boundary layer is the layer of air particles adjacent to the body surface. It is a region which consists of relative motions between its layers, which can exist in one of three forms. (A) “Laminar flow” means the boundary layers of air slide smoothly over one another with minimal surface friction. The laminar-flow boundary layers are extremely sensitive because they have a tendency to separate from the surface producing very high drag. (B) “Separated flow” means that the boundary layers separate from the surface and then usually become to eddy flows. And (C) “Turbulent flow” describes the boundary layers that are largely composed of small eddy flows which greatly increase the surface friction. The turbulent-flow boundary layers will cause higher surface friction drag than the laminar-flow boundary layers; thus, they result in a higher value of drag (see Appendix A: Figure 4).

Kyle and Weaver (2004) defined the turbulent boundary layers is the intense microvortices, which transfer the momentum from the outer freestreams to the viscous interface at the body surface. The turbulent boundary layers will then result in the greater velocity gradient at the surface and the greater associated local shear force, when compared with the laminar boundary layers that without intermixing. As mentioned above, the $C_D$ of any object consists of the effects of pressure drag and skin friction. When a cyclist chooses a position of a non-streamlined body such as an

upright position, the airflow separation can cause the creation of a low-pressure cavity on the trailing surfaces of the body, thus producing vortices that spin into the cavity. At high velocity, Martin et al. (2007) indicated that the skin friction is often negligible when compared with the pressure drag because the airstreams around the cyclist-bicycle induces to the pressure drag that can be regarded as the total drag. Mostly, the airstreams flowing around the cyclist and bicycle will cause the turbulences in the regions of separated flows and the cavities leading to the increased pressured drag. Even with a fully attached flow in a streamlined body position such as an aero position, a significant pressure drag will still be created due to it induced turbulence behind the cyclist, but less so than in the case of the upright position (Kyle & Weaver, 2004).

#### 2.1.2.3 Relative influence of factors causing aerodynamic drag

##### 2.1.2.3.1 Air density

By definition, a density of an object is equal to its mass ($m$) divided by its volume ($V$). In the Earth's atmosphere, "air density" ($\rho$) is defined by the mass of air divided by a specific volume of air, e.g. cubic metre ($m^3$) or litre (L) (Kreighbaum & Barthels, 1996). This describes a measure of how compactly the atoms and molecules of air are arranged to form the air. The $\rho$ relates to the property of air viscosity, which involves the internal resistance of air to flow. An increase of air viscosity causes an increase in the forces, which are exerted on objects exposed to the air (Hall, 1999). In other words, the air viscosity is a property which causes shear stresses between adjacent layers of moving air, leading to an irreversible loss of energy as heat and to a resistance experienced by moving through the air (Bartlett, 1997). The $\rho$ varies with the height above sea level (altitude) because the air is compressed by the weight of the atmosphere (atmospheric pressure) above it. The $\rho$ will decrease in direct proportion to increasing altitude resulting in a reduced $F_{aer}$ (Kyle & Weaver, 2004). This has been established as a help to cyclist's performance, as riders can then move into the air more easily. In fact, most cycling world records have been set at high altitudes (Gross et al., 1983). Nevertheless, there are two opposing effects at high altitude for aerobic endurance events. The $\rho$ is lower, which will help increase velocity, but the oxygen absorption of the cyclist is also less due to the thinner air (Burke, 1995). Moreover, the $\rho$ decreases with increasing temperature, i.e. cool air has a higher density than warm air. The density also varies slightly with humidity (Bartlett, 1997). Atkinson et al. (2003) explained that an increase of temperature of 5°C and a decrease in barometric pressure of 15 mmHg will reduce the air density and air drag by approximately 4%.

2.1.2.3.2 Drag coefficient

Equation (2.6) shows that the "drag coefficient" ( $C_D$ ) is the ratio between the aerodynamic drag ( $F_{aer}$ ) and the product of the dynamic pressure ( $0.5 \cdot \rho \cdot \mathrm{v}^2$ ) and the projected frontal area (*A*). It depends on the relative velocity between the airflow and the object and on the roughness of the body surface, which is a dimensionless number (Debraux et al., 2011).

$$C_D = \frac{F_{aer}}{0.5 \cdot \rho \cdot \mathrm{v}^2 \cdot A} \tag{2.6}$$

Efficient streamlined shapes have low $F_{aer}$ and low $C_D$ , often less than 0.1 in magnitude, whereas the shape of the human body as a non-streamlined object for example, exceeds $C_D$ = 1.0 (Kyle, 1979). For a cyclist and a bicycle combination, the $C_D$ can be used as an indication as to how well streamlines of the airflow can follow the orientation of the body (Edwards & Byrnes, 2007). For example, the $C_D$ of the shape of the cycling positions will tell how streamlined it is. Whether a shape is considered a streamlined body or not depends not only on the shape itself but also on how the shape is presented to the passing flow. The $C_D$ will change as the velocity changes because it is based on the changing dynamics of the fluid flow, which is represented by a quantity called the Reynolds number (Kreighbaum & Barthels, 1996). The Reynolds number describes the ratio of inertial forces to viscous forces and is given in dimensionless units. One aim of an aerodynamic experiment on the object or the body is to measure its $C_D$ that is also defined as dimensionless quantity. Normally, the $C_D$ for cycling positions must be obtained by direct measurements in a wind tunnel because it varies with every change in the orientation of the body or riding positions (Whitt & Wilson, 1982).

2.1.2.3.3 Projected frontal area

The area of the object that faces the airstream is called the "frontal cross-section area" or "projected frontal area" (*A*), which is typically defined as the projected area of objects onto the plane perpendicular to the direction of motion. Thus, the *A* of a cyclist is the portion of the body surface in square units, which can be seen by an observer placed exactly in front of the cyclist's body surface, i.e. the projected surface normal to the airflow displacement (Debraux et

al., 2011). The area $A$ is increased in a non-streamlined position, which results in an increased $F_{aer}$, which in turn is also associated with an increased $C_D$. The increase in $A$ is proportional to an increase in $F_{aer}$; for example, when $A$ is doubled, $F_{aer}$ is also doubled. Obviously, the value of $A$ is affected by the rider's size, riding position, type of bicycle, and cycling accessories (Burke, 1995). The cycling position plays an important role in decreasing $A$, leading to a reduced $F_{aer}$. Riding in a crouched position, for example, is better than an upright position, which means the cyclists can go faster (Jeukendrup & Martin, 2001). By lowering $F_{aer}$, the crouched position can help to reduce the airstreams that collide with the body surface and thus can reduce the pressure drag; besides, the torso approaches the horizontal position, which means the body becomes more streamlined (Gross et al., 1983). Nowadays, aerodynamic handlebars are invented for cyclists in order to assume a low crouch with resting elbows on the bars to avoid fatigue. Thereby, the aero position can be assumed for a longer time and is more streamlining compared with the standard racing positions or dropped position (Kyle & Weaver, 2004).

#### 2.1.2.3.4 Relative velocity

The "relative velocity" (v) is the velocity of the airflow with respect to a moving cyclist-bicycle combination (Hall, 1999). That means, that the velocity of the vehicle is only the same as the relative velocity, which used to calculate the $F_{aer}$, if the air is still. When there is a headwind or a tailwind, the relative velocity is different from the velocity of vehicle. Assuming the air density, the drag coefficient and the projected frontal area of cyclist-bicycle remain constant, the retarding force due to $F_{aer}$ will increase as $\mathrm{v}^2$, and the mechanical power to overcome $F_{aer}$ is proportional to $\mathrm{v}^3$ (Grappe et al. 1999; Kyle & Weaver, 2004). Therefore, the relationship between $F_{aer}$ and v relative to the fluid is nonlinear. For example, Debraux et al. (2011) mentioned about the influence of velocity with aerodynamic drag and mechanical power that, when the rider doubles his/her speed, they will collide with twice as many air molecules that strike them twice as fast. As a consequence, this results in four times the $F_{aer}$. According to the mechanical power, represented as $P = F_{aer} \cdot \mathrm{v} = 0.5 \cdot \rho \cdot C_D \cdot A \cdot \mathrm{v}^2 \cdot \mathrm{v}$, which is required to overcome the $F_{aer}$ is greater still. Indeed, when a cyclist doubles his/her speed, for example, the energy they require will be eight times as great.

2.1.2.3.5 Drag area

The variable $C_D$ times $A$ in Equation (2.5) is called the "drag area" (Jeukendrup & Martin, 2001) or "effective frontal area" ( $C_D \cdot A$ ) (Hoffman et al., 2003). The drag area is defined as the product of drag coefficient and projected frontal area of an object or body in units of square meter ( $m^2$ ) and expresses the effects of both size and streamlining through the airflow (Edwards & Byrnes, 2007). It is given by the ratio between the aerodynamic drag and the dynamic pressure. The $C_D \cdot A$ effectively integrates all the effects associated with stresses acting on the body surface. When the cyclist and bicycle moves into air, the $C_D \cdot A$ is dominated by the turbulence in consequence of the cycling position, shape, size, and surface roughness (Martin et al., 2007).

$$C_D \cdot A = \frac{F_{aer}}{0.5 \cdot \rho \cdot v^2} \tag{2.7}$$

Usually, the $C_D \cdot A$ , as given in Equation (2.7), can be measured in the wind tunnel as well as in field tests such as on the road using a powermeter (Martin et al., 2006), in towing experiments (Capelli et al., 1993) and during coasting down tests (Candau et al. 1999). Whitt and Wilson (1982) mentioned that the streamlining of objects causes less air turbulence and thus leads to less wasted energy when moving through the airflow. Therefore, the streamlined shape can have extreme benefits in cycling.

2.1.3 Rolling friction

"Rolling friction", also referred to as "rolling resistance" ( $F_{rol}$ ) is related to the weight of cyclist and bicycle, wheel size, tire pressure, tread pattern, casing construction, road gradient and texture of riding surface (Grappe et al., 1999b). The $F_{rol}$ can influence the mechanical power more than $F_{aer}$ at low speeds in the still air. That is, at slow velocities below approximately 15 $km \cdot h^{-1}$, the $F_{rol}$ significantly contributes to the total energy expenditure of cycling (Kyle, 1996), whereas at higher velocities the $F_{rol}$ is a constant or independent of velocity and approximately accounts for 10% to 20% of the total power (Martin et al., 2007). Theoretically, the $F_{rol}$ is modelled as the normal force that is always the force perpendicular to the road surface, on which the wheel is rolling, multiplied by a coefficient of $F_{rol}$ that includes the effects of tire and surface characteristics. This simplification leads to a model formula expressed by:

$$F_{rol} = \mu \cdot m \cdot g \cdot cos\theta \quad (2.8)$$

where, $\mu$ is the coefficient of rolling friction (dimensionless); $m$ is the mass of a cyclist including a bicycle; $g$ is the acceleration due to gravity; and $\theta$ is the slope or the angle of the inclined road (Martin et al., 1998). The rolling friction coefficient can be described as the ratio between rolling resistances itself and overall weight $\mu = F_{rol} / (m \cdot g \cdot cos\theta)$. That is, the $\mu$ represents the ratio between the force acting against the forward motion of the tires and the force pressing the tires against the surface it rolls on. The term $m \cdot g \cdot cos\theta$ is the part of the vertical force that is perpendicular to the surface of slope. Faria et al (2005) mentioned that the magnitude of the $F_{rol}$ of a tire on hard surfaces is mostly the result of the bending of the tire wall or tread causes internal friction, which is wasted energy. Unavoidably, in order to support its load, the tires must sink leading them to flatten. Basically, four things cause the increased tire friction. Firstly, a most important is the added weight. Secondly, a tire inflation pressure is low. Thirdly, a surface roughness will cause the local deformation in the tire shape and add to the friction loss. Fourthly, a wheel diameter will change the area of contact patch causing increased deformation. That is, a smaller wheel, the tire must sink further than a larger wheel on the same contact area; as a result, the smaller wheel will have a higher rolling friction. Di Prampero (2000) suggested a method to easily optimise the value of $F_{rol}$, which achieves a reduction in tire width by high inflation pressures, which also results in a reduction of $\mu$; this means, the higher pressure induces lower rolling friction.

### 2.1.4 Gravitational force

Unavoidably, the "gravitational force" ($F_{gra}$) is a natural resistance which causes the effort needed to increase extremely during uphill cycling, but rapidly reduces efforts during downhill cycling. In order to move in a continuous forward and fast motion uphill, the amount of energy expenditure with each pedal cycle due to gravitational and inertial forces is maximal. Gravitational force $F_{gra}$ is also called weight in physics, which is always direct downward, but in this case the $F_{gra}$ of cycling uphill is expressed by:

$$F_{gra} = m \cdot g \cdot sin\theta \quad (2.9)$$

where, $m$ corresponds the mass of rider and bicycle; $g = 9.81$ m·s$^{-2}$ represents the gravitational acceleration; and $\theta$ is the angle of inclined road (Di Prampero, 2000). Note that the term $m \cdot g \cdot sin\theta$ is defined as the force along the

horizontal axis (parallel to the ground) and opposite to the propulsive force when cycling uphill. Mognoni and Di Prampero (2003) indicated that although the energy expenditure for a cyclist on a straight road will essentially increase due to both the force and the power production of air resistance, this is less important while riding uphill. In this case, it is fact that the greatest fraction of the mechanical power is spent to overcome the gravity. An investigation by Martin et al. (1998) indicated that during uphill cycling, a change in gravitational potential energy: $E_{pot} = m \cdot g \cdot h$ , where *h* is the height of cyclist and bicycle from the ground, account for losses equivalent to 10% to 20% of total mechanical power. Gregor and Conconi (2000) suggested a reducing of the lighter bicycle would help to diminish the effect of gravity on the required cycling power.

### 2.1.5 Bearing friction

The frictional losses in wheel bearing is called "bearing friction" ( $F_{bea}$ ). It is the internal friction acting on the cup and cone ball bearings and cartridge bearings of wheels, which is related to the load and the rotational velocity (Kyle, 1996). The torque in each bearing pair is represented as $T = 0.015 + 0.00005 \cdot \mathrm{v}_{rot}$ , where *T* is the torque in unit of newton metre (N·m), and $\mathrm{v}_{rot}$ is the rotational velocity in unit of revolution per minute (rpm) (Martin et al. (1998). The study of Wolf (2010) showed the relationship of the force due to friction in one wheel bearing. When $\mathrm{v}_{rot} = (60 / C_{whe}) \cdot \mathrm{v}$ , where v is the linear velocity of a rider and bicycle system and $C_{whe}$ is the wheel circumference calculated by: $C_{whe} = 2 \cdot \pi \cdot r_{whe}$ , where $r_{whe}$ is the wheel radius, the value of bearing friction is given by: $F_{bea} = (T / r_{whe}) = (1 / r_{whe}) \cdot (0.015 + 0.00005 \cdot \mathrm{v}_{rot}) = (1 / r_{whe}) \cdot (0.015 + 0.00005 \cdot (60 / C_{whe}) \cdot \mathrm{v})$ . In other words, the friction in the bearings of two wheels is given by:

$$F_{bea} = \beta_0 + \beta_1 \cdot \mathrm{v} \tag{2.10}$$

where, $\beta_0 = (0.03 / r_{whe})$ , and $\beta_1 = (0.006 / r_{whe} \cdot C_{whe})$ (Wolf, 2010; Dahmen et al., 2011; Dahmen & Saupe, 2011). Conveniently, Martin et al. (1998) estimate the wheel bearing friction for a general racing bicycle with the cartridge bearings by $F_{bea} = (91 + 8.7 \cdot \mathrm{v}) \cdot 10^{-3}$ , namely, the total mechanical power lost to bearing friction torque as a function of bicycle velocity. In the wheel hub, the bearing friction was found to be extremely small at approximately 1 % of the total power or 1 to 2 Watts. In addition, the losses due to the drive chain efficiency were fixed at approximately 2% of the total mechanical power or 2 to 7 Watts. Whitt and Wilson (1982) suggested that a good clean chain might reduce the frictional losses by only 1.5% of total resistance. When the bearings are not sufficiently lubricated, the rider needs more

force to overcome the bearing friction and maintain the velocity. The frictional losses in the wheel bearings and drive chain of a good-quality bicycle are extremely small, and are a function of the ball bearing types, the load, and the angular velocity of wheels (De Groot et al., 1994; Di Prampero, 2000). Additionally, Kyle and Weaver (2004) mentioned about the bearing friction can usually be included with the rolling resistance.

### 2.1.6 Inertial force

"Inertia" is the tendency of any physical object to resist any change of its motion state, including a change in direction. In other words, for linear motion in cycling, the inertia is the tendency of a rider and bicycle to keep moving in a straight line at constant linear velocity. The direction of the inertial force ( $F_{ine}$ ) is opposite to the direction of the accelerating forces, with being the joint mass of the cyclist and bicycle, and the accelerating force. While speeding up, the cyclist-bicycle system can accelerate, when the propulsive force generated from the rider exceeds the total initial force. In view of Equation (2.1), the $\vec{a}$ is directly proportional to the resulting $\vec{F}$ produced at the rear wheel contact patch, but inversely proportional to the total *m*. For this reason, the benefit of a lighter bicycle is the ability to accelerate and decelerate faster. Whitt and Wilson (1982) described that, apart from the $F_{ine}$ in linear motion, another form of inertia is the rotational inertia. It is associated with the polar mass moment of inertia (*I*) of rotating components, the total mass (*m*) and the rolling radius of the wheel ( $r_{whe}$ ) (Hertz & Ukrainetz, 1967). The moment of inertia is defined as $I = m \cdot r_{whe}^2$, with its value depending on the wheel size and on the amount and distribution of its mass. Normally, the moment of inertia of racing bicycle wheel is approximately 0.14 kg·m$^2$ (Martin et al., 1998). Theoretically, rotational inertia refers to the fact that a rotating rigid body maintains its state of uniform rotational motion. Its angular momentum is unchanged, unless an external torque is applied; this is also called conservation of angular momentum (Bartlett, 1997).

$$F_{ine} = \left( m_{CB} + \frac{I}{r_{whe}^2} \right) \cdot a \tag{2.11}$$

Because the inertia is one of the primary displays of the mass, which is a quantitative property of physical systems, Equation (2.11) expresses the mass as the static mass of cyclist and bicycle ( $m_{CB}$ ) plus the inertial mass effect of the rotating components ( $I / r_{whe}^2$ ) (Dahmen et al., 2011; Dahmen & Saupe, 2011). It can be defined as an effective mass term (Hertz & Ukrainetz, 1967) or called an extra mass term (De Groot et al., 1995): $m = m_{CB} + (I / r_{whe}^2)$ .

Consequently, Equation (2.11) becomes as $F_{ine} = m \cdot a$ . This can be explained that, during acceleration, both wheels are angularly accelerated, and their rotational inertias will resist this acceleration, which contributes to approximately 1% of the total power or 1 to 2 Watts (Martin et al., 1998).

### 2.1.7 Propulsive force

The cycling motion consists of an angular motion for the rotation of the wheel which in turn induces a linear motion so that the bicycle moves forward. The "propulsive force" or "driving force" ( $F_{pro}$ ) is generated by a cyclist through the pedal force ( $F_{ped}$ ), with the drive being handled by the rear wheel. In initial starting phase, the rider must exert a large amount of force in order to rotate the rear wheel because the rider must overcome both the static friction between wheels with surface and the inertia of the cyclist and bicycle. Technically, the rider applies $F_{ped}$ to the rear wheel primarily by the musculature of his/her leg and alternately through the feet, with repeated work in a pattern of force application to the pedal-crank system of the bicycle. During pedalling, the forces are transferred via the pedal crank through front chain rings, roller chain, and rear sprocket to the rear wheel. The $F_{ped}$ will drive the rear wheel to rotate, push the ground backwards, and lead to a forward motion of the cyclist-bicycle. As mentioned above, during a forward movement with a constant velocity, the cyclist must overcome $F_{aer}$, $F_{rol}$, $F_{gra}$, $F_{bea}$, and $F_{ine}$, these are $F_{res}$. Atkinson et al. (2007), Martin et al. (2007), and Dahmen et al. (2011) developed the mathematical model for road cycling in the form of a nonlinear differential equation, which is based on the equilibrium of the resistive torque ( $T_{res}$ ) with the pedal torque ( $T_{ped}$ ) or the propulsive torque ( $T_{pro}$ ). The torque is defined as a force that pushes or pulls to rotate an object around its axis. By assuming $T_{res} = F_{res} \cdot r_{whe}$, hence the $T_{res}$ consists of the torques gained from $F_{aer}$, $F_{rol}$, $F_{gra}$, $F_{bea}$, and $F_{ine}$ (see Appendix A: Figure 5). It can be defined by:

$$T_{res} = T_{aer} + T_{rol} + T_{gra} + T_{bea} + T_{ine} + = T_{ped} \cdot \frac{\eta}{\gamma} \tag{2.12}$$

It can also be expressed in form of the product of the applied action force and the length of the lever-arm connecting the axis to the point of force application:

$$F_{res} \cdot r_{whe} = (F_{aer} + F_{rol} + F_{gra} + F_{bea} + F_{ine}) \cdot r_{whe} = F_{ped} \cdot l_{cra} \cdot \frac{\eta}{\gamma} \tag{2.13}$$

Equation (2.13) shows that the rider generates $T_{ped}$ that is the produced from $F_{ped}$ and the length of crank $l_{cra}$. It is equal to $T_{res}$ that is the produced from $F_{res}$ and the rolling radius of the wheel $r_{whe}$. The term which contains $T_{ped}$ in Equation (2.12) is multiplied by $\eta$, that is defined to be the efficiency factor which accounts for the frictional loss in the drive chain ($\eta < 1$). This loss occurs in the drive chain between the crank and the rear wheel, and is related to the power transmitted (Martin et al. 1998). In addition, $T_{ped}$ is divided by the transmission ratio ($\gamma$) of the number of teeth on the front sprocket to the number of teeth on the rear sprocket $\gamma = n_{front} / n_{rear}$ because of a considerable factor that involves the usage of the lever principle (Dahmen & Saupe, 2011). Finally, Equation (2.13) is divided by $r_{whe}$ and the variables are substituted into each component. The result then becomes an equilibrium of forces:

$$F_{res} = \underbrace{\left(0.5 \cdot \rho \cdot C_D \cdot A \cdot \mathrm{v}^2\right)}_{F_{aer}} + \underbrace{\left(\mu \cdot m \cdot g \cdot cos\theta\right)}_{F_{rol}} + \underbrace{\left(m \cdot g \cdot sin\theta\right)}_{F_{gra}} + \underbrace{\left(\beta_0 + \beta_1 \cdot \mathrm{v}\right)}_{F_{bea}} + \underbrace{\left(m_{CB} + \frac{I}{r_{whe}^2}\right)}_{F_{ine}} \cdot a = F_{ped} \cdot \frac{l_{cra}}{r_{whe}} \cdot \frac{\eta}{\gamma} \qquad (2.14)$$

Equation (2.14) shows that during cycling with the constant velocity the cyclist will generate the propulsive force $F_{pro}$, which is the product of the pedal torque $T_{ped} = F_{ped} \cdot (l_{cra} / r_{whe}) \cdot (\eta / \gamma)$ in order to overcome the resistive force $F_{res}$. Considering Equation (2.14) again, the weight of the cyclist plus bicycle is an important factor for the required pedalling force, which affects the power demand of the cyclist. This is because weight slows the cyclist in three forces by retarding acceleration $F_{ine}$, by adding mass to be carried uphill $F_{gra}$, and by adding to the rolling resistance $F_{rol}$. However, the majority of the resistance is the net force component acting in the direction of travelling: the air resistance, which is proportional to $\mathrm{v}^2$.

## 2.2 Coasting down testing for road cycling

### 2.2.1 Experimental principle

Generally, the “coasting down” method (De Groot et al., 1995) can be called “coasting deceleration” method (Candau et al. 1999) or “freewheeling” method (Hennekam & Govers, 1996) and is compared to measurements of the aerodynamic parameters with wind-tunnel tests. It is an inexpensive experimental method of measuring the aerodynamic drag forces ($F_{aer}$) and the rolling frictions ($F_{rol}$) that are encountered under actual road-travelling

conditions. Moreover, one aim of the coasting down experiment with various cycling positions is to measure the drag coefficient ( $C_D$ ) including its dimensionless rolling friction coefficient ( $\mu$ ), which is defined as a nondimensional quantity. Taking a cyclist-bicycle as a closed system, theoretically, if no propulsive force $F_{pro} = 0$ is generated by the rider while coasting down, the sum of change in the kinetic energy of the cyclist is equal to the mechanical work due to the external forces, i.e. $F_{aer}$ and $F_{rol}$ . The kinetic energy while coasting down consists of the translational kinetic energy ( $E_{kin}$ ) and the rotational kinetic energy ( $E_{rot}$ ), whereas the change of the latter is less than 1% and is therefore negligible (De Groot et al., 1994).

The coasting down experiment should be performed in an indoor hall in the absence of wind, i.e. head, tail and side wind. That is, the wind velocity with respect to the cyclist-bicycle is equal to the velocity of the cyclist-bicycle to the ground (relative velocity) (Hennekam, 1990; Hennekam & Bontsema, 1991; Hennekam & Govers, 1996). Di Prampero (2000) suggested that the coast down technique is appropriate for assessing the constant of $F_{aer}$ and $F_{rol}$ , which in principle consists of measuring the deceleration of the coasting velocity as a function of the velocity (v) with respect to time (*t*) during free running over a flat terrain. Its great practical advantage is, that it can easily be measured over a rather short distance with the defined v. The method of measuring $F_{aer}$ is based on Newton's second law: $\sum \vec{F} = m \cdot \vec{a}$ (De Groot et al., 1995; Candau et al., 1999; Hoffman et al., 2003). The test measures the deceleration of the cyclist-bicycle on the terrain after reaching a defined v. At a specified position, before the rider stops pedalling, he/she must reach the defined v. The riding position is unchanged and reproduces the actual conditions with the turbulence, which is created by movement of the lower limbs. With this method, Debraux et al. (2011) further explained that the rider could pedal without a transmission of force (driving force) to the rear wheel during coasting trials. In this way, the cyclist slowed down due to $F_{aer}$ and $F_{rol}$ over several timing switches.

To begin with the simple principle of coasting down cycling, the cyclist will accelerate from the starting point until the defined speed is obtained, which is assigned the maximal speed. After this point, the cyclist and bicycle will freewheel run without any impulsion, and the cyclist must constantly hold the cycling position until the speed approaches zero. The data is recorded as a plot of velocity versus time and will begin to record from the defined velocity point or maximal velocity to the ending point. Precautions are: it is necessary to ensure that the wheel rotations are not retarded by the brakes, the test must take place on a smooth horizontal surface without any gradient, and the tyre pressure is always constant. Additionally, repeated testing should be performed under the same calm ambient conditions (see Appendix A: Figure 6).

2.2.2 Mathematical models for coasting down motion

Following section will explain the mathematical models for cycling motion in the coasting down experiment step-by-step. Considering the factors in Equation (2.2) for coasting down motion, the external force, being the propulsive force, is set to zero due to freewheeling $F_{pro} = 0$ . In addition, the influence of gravitational force is defined as: $F_{gra} = m \cdot g \cdot sin\theta = 0$ because $\theta = 0$ . The various internal frictions, such as the bearing friction of the bicycle $F_{bea}$ , are negligible due to the very small values, and can be combined with the rolling resistance (Kyle & Weaver 2004; Martin et al., 2007). Thus, the main resistive forces that need to be calculated consist of $F_{aer}$ and $F_{rol}$ .

Following the principle mentioned above, the model for cycling motion arises from the physics concepts of "work-energy theorem" including "Newton's second law of motion". De Groot et al., (1994, 1995) described that the kinetic energy change is equal to the mechanical work ( $W = F \cdot s$ ) that is done by the total external forces $F_{rol}$ and $F_{aer}$ during coasting down cycling across a flat floor over a certain displacement (*s*). The total kinetic energy is the sum of the translational kinetic energy: $E_{kin} = (1/2) \cdot m_{CB} \cdot \mathrm{v}^2$ and the rotational kinetic energy: $E_{rot} = (1/2) \cdot I \cdot \omega^2$ (Bartlett, 1997). If the cyclist applies no propulsive force, the $F_{rol}$ and the $F_{aer}$ act as a joint decelerating force on the cyclist-bicycle movement. It can be defined by:

$$\underbrace{\left(-F_{rol} - F_{aer}\right) \cdot s}_{Work} = \underbrace{\left(\frac{1}{2} \cdot m_{CB} \cdot \mathrm{v}^2\right)}_{E_{kin}} + \underbrace{\left(\frac{1}{2} \cdot I \cdot \omega^2\right)}_{E_{rot}} \cdot 2 \qquad (2.15)$$

The left term in Equation (2.15) shows the mechanical work that the external forces exert as negative forces because the $F_{rol}$ and the $F_{aer}$ are directed opposite to the direction of motion. The term $E_{rot}$ can be expressed by the moment of inertia ( $I = m \cdot r_{whe}^2$ ) and the angular velocity ( $\omega$ ) of the two wheels ( $\cdot 2$ ), using the relationship between the linear and the angular velocity of rotation around the axis, $\mathrm{v} = \omega \cdot r_{whe}$ , where $r_{whe}$ is the wheel radius. Consequently, from Equation (2.15) substitutes $\omega = \mathrm{v} / r_{whe}$ . Moreover, a term of the rotational energy can be regarded as: $m = m_{CB} + (2 \cdot I / r_{whe}^2)$ , where *m* can be defined the term of the extra mass, which is equal to the static mass of cyclist and bicycle combination ( $m_{CB}$ ) plus the inertia mass effect of the rotating components ( $2 \cdot I / r_{whe}^2$ ) (De Groot et al., 1995). Hence, Equation (2.15) becomes as:

$$\underbrace{\left(-F_{rol}-F_{aer}\right)\cdot s}_{Work}=\underbrace{\left(\frac{1}{2}\cdot m_{CB}\cdot \mathrm{v}^2\right)}_{E_{kin}}+\underbrace{\left(\frac{1}{2}\cdot I\cdot\left(\frac{\mathrm{v}}{r_{whe}}\right)^2\right)}_{E_{rot}}\cdot 2=\frac{1}{2}\cdot\underbrace{\left(m_{CB}+\frac{2\cdot I}{r_{whe}^2}\right)}_{Extra-Mass}\cdot \mathrm{v}^2=\frac{1}{2}\cdot m\cdot \mathrm{v}^2 \tag{2.16}$$

Taking the derivative of both terms of mechanical work that are done by resistive forces and kinetic energy, then dividing by $\mathrm{v}$ :

$$\frac{d}{dt}\left(-F_{rol}-F_{aer}\right)\cdot s=\frac{d}{dt}\left(\frac{1}{2}\cdot m\cdot \mathrm{v}^2\right) \tag{2.17}$$

The result of Equation (2.17) then becomes Equation (2.18) in the form of negative forces and effective mass times acceleration, when assuming $m$ is constant, $(ds/dt)=\mathrm{v}$ and $(d\mathrm{v}/dt)=a$ . After taking the derivative, the left term in Equation (2.17) becomes the power term $\left(-F_{rol}-F_{aer}\right)\cdot \mathrm{v}$ . Dividing both sides by $\mathrm{v}$ , hence results in:

$$-F_{rol}-F_{aer}=m\cdot a \tag{2.18}$$

Equation (2.18) can also be expressed in the decelerating form of the system when assuming $-a_{rol}=(-F_{rol}/m)$ and $-a_{aer}=(-F_{aer}/m)$ :

$$a=-a_{rol}-a_{aer} \tag{2.19}$$

Note from Equations (2.18) into (2.19), that when the cyclist applies no propulsive force (freewheeling) the cyclist-bicycle will slow down with the deceleration of rolling friction ( $-a_{rol}$ ) and deceleration of aerodynamic drag ( $-a_{aer}$ ) until stand still $\mathrm{v}=0$ due to the influence of $F_{rol}$ and $F_{aer}$ . In order to appear in the derivative form of $\mathrm{v}$ with respect to *t*, the differential Equation (2.18) must be solved for $\mathrm{v}$ :

$$\frac{d\mathrm{v}}{dt}=-a_{rol}-K_m\cdot \mathrm{v}^2 \tag{2.20}$$

Equation (2.20) is obtained from Equation (2.18) in the form of a nonlinear differential equation in order to get qualitative information. Consequently, it becomes an inverted parabola with $a_{rol}$ as a negative constant. With Newton's second law ( $\sum \bar{F}=m\cdot \bar{a}$ ), to consider Equation (2.20) with $a_{rol}=\frac{F_{rol}}{m}=\frac{\mu\cdot m\cdot g}{m}=\mu\cdot g$ , and $a_{aer}=\frac{F_{aer}}{m}=\frac{0.5\cdot\rho\cdot C_D\cdot A\cdot \mathrm{v}^2}{m}=\frac{K\cdot \mathrm{v}^2}{m}=K_m\cdot \mathrm{v}^2$ . Note that the $F_{aer}$ is directly proportional to $\mathrm{v}^2$ , but the $F_{rol}$ is independent of v. In addition, the rolling friction coefficient $\mu$ and the drag area $C_D\cdot A$ are not affected by v. Then, Equation (2.20) can be solved by integration in order to obtain a function v respect to *t* as follows:

$$\int_{v_i}^{v_f} \frac{dv}{-(a_{rol} + K_m \cdot v^2)} = \int_{t_i}^{t_f} dt \tag{2.21}$$

resulting in a tan-function form (Wohlhart, 1998):

$$-\frac{1}{\sqrt{a_{rol} \cdot K_m}} \cdot tan^{-1}\left(\frac{v}{\sqrt{\frac{a_{rol}}{K_m}}}\right) + C_1 = t \tag{2.22}$$

Or

$$-\frac{1}{\sqrt{\beta}} \cdot tan^{-1}\left(\frac{v}{\sqrt{\alpha}}\right) + C_1 = t \tag{2.23}$$

where, $\alpha = a_{rol} / K_m$ , and $\beta = a_{rol} \cdot K_m$ . Equation (2.23) can be obtained by integration after separating the variables from Equation (2.21). The solution is found in forms of trigonometric and exponential functions plus a first constant of integration ( $C_1$ ). Equation (2.23) defines the velocity v, assuming the time $t$ is the initial time $t_i$ of motion and therefore is zero: $t = t_i = 0$ , and assuming the velocity v at that time is the maximal velocity $v_{max}$ of motion and thus is the initial velocity: $v = v_{max} = v_i$ . Thus, $C_1$ is described as a function of initial velocity at initial time:

$$C_1 = \frac{1}{\sqrt{\beta}} \cdot tan^{-1}\left(\frac{v_i}{\sqrt{\alpha}}\right) \tag{2.24}$$

Substituting this solution for $C_1$ into Equation (2.23) then yields:

$$-\frac{1}{\sqrt{\beta}} \cdot tan^{-1}\left(\frac{v}{\sqrt{\alpha}}\right) + \frac{1}{\sqrt{\beta}} \cdot tan^{-1}\left(\frac{v_i}{\sqrt{\alpha}}\right) = t \tag{2.25}$$

Equation (2.25) can then be expressed as a function for v of $t$ :

$$v(t) = \sqrt{\alpha} \cdot tan\left(tan^{-1}\left(\frac{v_i}{\sqrt{\alpha}}\right) - \sqrt{\beta} \cdot t\right) \tag{2.26}$$

Equation (2.26) is the solution of Equation (2.21) for the mathematical model of $v(t)$ and is given in a tan-function form (Wohlhart, 1998), which is dependent on the parameters $v_i$ , $K_m$ and $a_{rol}$ . In other words, for the case of the cyclist-bicycle starting with $v_i = v_{max}$ on flat terrain the factors of $F_{aer}$ and $F_{rol}$ will slow the cyclist-bicycle down until stand still at the final velocity of zero $v_f = 0$ . From Equation (2.26) the final time ( $t_f$ ) at the stopping point can

be calculated, which is also called the maximal time ( $t_{max}$ ) by assuming $t = t_f = t_{max}$ , and at $\mathrm{v}_f = 0$ assuming the function $\mathrm{v}(t) = \mathrm{v}(t_f) = \mathrm{v}(t_{max}) = 0$ . The result is given by Equation (2.27):

$$t_{max} = \frac{1}{\sqrt{\beta}} \cdot tan^{-1}\left(\frac{\mathrm{v}_i}{\sqrt{\alpha}}\right) \tag{2.27}$$

In addition, a second integral of the Equation (2.26) can be obtained in order to predict the function displacement (*s*) at time $t_i$ until $t_f$ :

$$\int_{t_i}^{t_f} \mathrm{v} \cdot dt = \int_{t_i}^{t_f} \sqrt{\alpha} \cdot tan\left(tan^{-1}\left(\frac{\mathrm{v}_i}{\sqrt{\alpha}}\right) - \sqrt{\beta} \cdot t\right) \cdot dt \tag{2.28}$$

The result is:

$$s = \frac{\sqrt{\alpha}}{\sqrt{\beta}} \cdot ln\left(cos\left(tan^{-1}\left(\frac{\mathrm{v}_i}{\sqrt{\alpha}}\right) - \sqrt{\beta} \cdot t\right)\right) + C_2 \tag{2.29}$$

Equation (2.29) demonstrates the result of the second integration of Equation (2.28) with a second constant of integration ( $C_2$ ). If $C_2$ is defined as a function of $\mathrm{v}_i$ at an initial displacement ( $s_i$ ) by assuming $s = s_i = 0$ , and $t = t_i = 0$ , it is given by:

$$C_2 = -\frac{\sqrt{\alpha}}{\sqrt{\beta}} \cdot ln\left(cos\left(tan^{-1}\left(\frac{\mathrm{v}_i}{\sqrt{\alpha}}\right)\right)\right) \tag{2.30}$$

Substituting this solution for $C_2$ into Equation (2.29), the solution for Equation (2.28) is defined by:

$$s(t) = \frac{\sqrt{\alpha}}{\sqrt{\beta}} \cdot ln\left(cos\left(tan^{-1}\left(\frac{\mathrm{v}_i}{\sqrt{\alpha}}\right) - \sqrt{\beta} \cdot t\right)\right) - \frac{\sqrt{\alpha}}{\sqrt{\beta}} \cdot ln\left(cos\left(tan^{-1}\left(\frac{\mathrm{v}_i}{\sqrt{\alpha}}\right)\right)\right) \tag{2.31}$$

Equation (2.31) is the mathematical model of the function of the displacement with respect to time $s(t)$ . Then, substituting $t = 0$ in Equation (2.31), this can obtain a new formula that describing the velocity-displacement relationship $\mathrm{v}(s)$ . Thereby, Equation (2.31) becomes as:

$$\mathrm{v}(s) = \sqrt{\alpha} \cdot tan\left(cos^{-1}\left(exp\left(\frac{\sqrt{\beta}}{\sqrt{\alpha}} \cdot \left(s + \frac{\sqrt{\alpha}}{\sqrt{\beta}} \cdot ln\left(cos\left(tan^{-1}\left(\frac{\mathrm{v}_i}{\sqrt{\alpha}}\right)\right)\right)\right)\right)\right)\right) \tag{2.32}$$

Equation (2.32) describes the function $\mathrm{v}(s)$ and can be verified by the fact that at $t_i = 0$ and $s_i = 0$ , the velocity yields $\mathrm{v}(s) = \mathrm{v}_i = \mathrm{v}_{max}$ of coasting down cycling, and remembering that $\alpha = a_{rol} / K_m$ , and $\beta = a_{rol} \cdot K_m$ .

To summarize, the three formal mathematical models resulting from coasting down motion, i.e. velocity versus time $v(t)$ as in Equation (2.26), displacement versus time $s(t)$ as in Equation (2.31) and velocity versus displacement $v(s)$ as in Equation (2.32) are given. Note that these mathematical models are nonlinear models and they will be taken to create the best-fit curves for the least-squares method in the cycling-motion study (see Chapter 5: Results 5.2).

### 2.2.3 Telemetry-bicycle system

For coasting down testing, a telemetry system needs to be applied to the bicycle in order to send the measured data such as the value of velocity over time to a receiver device in the form of a wireless signal. A telemetry bicycle system mainly consists of a speed-measurement device, a signal-exchange device, and a signal-transmitter device (see Appendix A: Figure 7). In order to measure the velocity, the telemetry bicycle has a device for speed measurement called a tachogenerator. Mechanically, the tachogenerator is a speed transducer, which develops the direct current (DC) voltage proportional to the speed of the motor connected to it. With regard to technical data, this tachogenerator is a speed sensor: tachogenerator series T, type T505 (Mattke AG, Germany), output voltage 4.3 volts per 1000 revolution per minute (rpm), maximum rpm = 5000, and peak-to-peak current ripple amplitude = 7%. As the sensor, the tachogenerator is mounted on the distal of the front fork of the bicycle and it has a rotating axle or a shaft that is connected to the front hub. When the wheel rotates, the shaft of tachogenerator rotates with it, and then it converts the revolution per minute into DC voltage. This DC voltage is sent to an encoder that translates electric-currents into digital signals through a modulator, and then a wireless transmitter will send this digital signal through a transmitter antenna to the receiver device.

The data transmitter is a radio telemetry system (Biotel 99, Glonner Eletronics GmbH, Germany) at a carrier frequency of 433.92 MHz with 8 analogue and digital channels and a resolution of 12 bits. This system consists of two units: (1) a transmitter or TX unit at a transmitting power of 4.4 mW with a modulation in the form F1D (F=Frequency modulation, 1= One channel digital signal, and D=Data) and a battery 6 V, and (2) a receiver unit for input-to-output signal data at 12 V DC. The signal direction of a telemetry-bicycle system through various devices, which mainly consist of a speed sensor unit, a telemetry transmitter unit as mentioned above, and a telemetry receiver unit. Beginning from (A) the telemetry bicycle, the signal is sent through (B) a receiver antenna (Type Nr. K711721 BN 510192, KATHREIN, Germany) to (C) a radio-telemetry receiver and through (D) a connector block, after which (E) an A-D connector (analogue-digital) will again adapt the signal. Lastly, as a recording device, (F) a computer with special software will process and store the measured data (see Appendix A: Figure 8).

## 2.3 Nonlinear parameter estimation

### 2.3.1 Least-squares method

In 1795, 'Johann Carl Friedrich Gauss', a German mathematician, invented the principle of the least squares method. The least-squares technique refers to the method which finds the overall solution which minimizes the sum of squares of errors made in the results of every single equation. The least-squares method, in other words, is a standard to the approximate solution of an over-determined system (Draper & Smith, 1998). The main object of the least-squares method is to help fit the nonlinear models (curve fitting) by minimizing the error or the sum of squares function, which requires heavy iterative calculations and the use of a special program. Analysing data with nonlinear regression is quite complex, but this method can help estimate the best-fit parameter values and define a nonlinear model after a curve has been fitted.

Conceptually, the nonlinear least-squares method follows the steps of Billo (2007) and Liengme (2009). 1) Start with an initial estimated value for each parameter in the equation. 2) Generate the curve defined by the initial values. 3) Calculate the sum-of-squares, which is the residual sum of the squares of the vertical distance of the points from the curve. 4) Adjust the value of the parameters to make the curve come closer to the data points. This needs to use the algorithms for adjusting the parameters or variables. 5) Adjust the value of the parameters again so that the curve comes even closer to the points. Repeat, so as to obtain an iterative method. 6) Stop the calculations when the adjustments make virtually no difference in the sum-of-squares. 7) Report the best-fit results. Obtaining the precise values depends, in part, on the initial values that are chosen in step 1 and on the stopping criteria of the sixth step (see Appendix C: Least-squares method).

### 2.3.2 Parameter estimation by using a Solver

As mentioned above, nonlinear regression programs can be used to fit a curve to data from measurements, and obtain the best-fit values of the parameters in order to generate a model. In this case, the model is a mathematical description of a physical process. This needs to use a special program for the least-squares method to minimize the residual sum of squares (or vertical distances of the data points from the curve) and to find the best-matching parameter values. Since the measurement data from the coasting down test is not a smooth-nonlinear curve (see Appendix A: Figure 8F), it is better to fit a curve with "Solver", as this leads to more accurate results.

Solver is a program that is a part of Microsoft Excel® and normally offered with the Microsoft Office® package when installed with full options. Solver is well suited to fit data with a nonlinear regression analysis function via the use of an iterative algorithm. The aim of curve fitting of experimental data is to describe measured data in the universally accepted formula $y = f(x)$ (Harris, 1998). Generally, $f$ is a function used to describe the relationship between $x$ and $y$, which takes the form of an equation, composed of one or more parameters. The $y$ is determined as the dependent variable that is measured in the experiment, as its value on the $y$-axis is fixed, and the $x$ is controlled during the experiment and determined as the independent variable, as its value on the $x$-axis is fixed. Solver will minimize the difference between the sum of squares of the raw data to be fitted and the function to be found by the using the iterative generalized reduced gradient method (Billo, 2007; Liengme, 2009). This method relates manually entered raw data to graphed data, followed by curve fitting and displaying the resulting curve fit on top of the data. The goodness of the fit is calculated so that the accuracy of the fit a can be assessed. This interpretation of the data with Solver is conducted via the process of iterative nonlinear regression. From Equation (2.33), this process will minimize the value of the squared sum of the difference between the raw data and the fit values (Brown, 2001, 2006):

$$\mathrm{SS} = \sum_{i=1}^{n} (\mathrm{v}_{mea} - \mathrm{v}_{fit})^2 \tag{2.33}$$

where, $\mathrm{v}_{mea}$ is the measured velocity value from the coasting down experiment; $\mathrm{v}_{fit}$ is the fitted velocity value with best-fit parameters in the coasting down equation which are generated by Solver; n is the total number of points; and SS is the sum of squares of the difference between the measured velocity and the fit velocity which is minimized by the least squares method of Solver.

The first step of Solver is to calculate an initial sum of squares value, which is determined by the user providing initial estimates for the values of various parameters. The second step involves changing the parameters that were initially set by a small amount and recalculating the sum of squares. By principle, this process is repeated many times to ensure that changes in the parameter values result in the smallest possible value of the sum of squares (deviation). Solver uses the generalized reduced gradient method of iteration. The following shows an experimental sample illustrating how to apply the spreadsheet with Solver to fit the curve on the data with a user-input nonlinear equation that is known as the coasting down equation. As a reminder, Equation (2.26) is given by:

$$\mathrm{v}(t) = \sqrt{\alpha} \cdot tan\left( tan^{-1}\left( \frac{\mathrm{v}_i}{\sqrt{\alpha}} \right) - \sqrt{\beta} \cdot t \right) \tag{2.26}$$

where, $\alpha = \dfrac{\bar{a}_{rol}}{K_m}$, and $\beta = \bar{a}_{rol} \cdot K_m$. Substituting these parameters into Equation (2.26) gives:

$$\mathrm{v}(t) = \sqrt{\frac{a_{rol}}{K_m}} \cdot tan\left( tan^{-1}\left( \frac{\mathrm{v}_i}{\sqrt{\frac{a_{rol}}{K_m}}} \right) - \sqrt{a_{rol} \cdot K_m} \cdot t \right) \tag{2.34}$$

Function v($t$) illustrates the nonlinear relation between the velocity v (as the dependent variable) and the time $t$ (as the independent variable) that has passed during the deceleration of the cyclist-bicycle system since the point of initial velocity ( $\mathrm{v}_i$ ) influenced by the constant of aerodynamic drag divided by the mass of the cyclist plus bicycle ( $K_m$ ) and the acceleration of rolling resistance ( $a_{rol}$ ). In other words, the cyclist-bicycle system will be decelerated by the aerodynamic drag ( $F_{aer}$ ) and rolling friction ( $F_{rol}$ ). Equation (2.34) can be considered together with Equation (2.20) for acquisition of parameter of the $a_{rol}$ , the $K_m$ , and the $\mathrm{v}_i$ . Note that in this investigation, Equation (2.34) is used to estimate the parameter $K_m$ and $\mathrm{v}_i$ by Solver. For the parameter $a_{rol}$ can be calculated from the rolling-resistance coefficient ( $\mu$ ) times the gravity ($g$).

## 2.4 Spiroergometry

### 2.4.1 Definitions

The assessment of various cardiorespiratory functions while cycling is conducted the spiroergometry method, which mainly consists of two parts. “Spirometry” refers to a measurement of the pulmonary functions such as inhalation and exhalation through a spirometer. The spirometer is an instrument for measuring lung functions, which can test both the air volume and the airflow speed of the lungs (Foss & Keteyian, 1998). “Ergometry” refers to a form for the energetic measurement of physical work performed by the muscles, which requires a suitable measurement device that is reliable and valid such as an ergometer. A popular ergometer, for example, is a bicycle ergometer or stationary bicycle of which the front or back wheel is driven by the pedalling of a subject. The resistance or workload, defined by the exercise intensity prescription, is electronically supplied by increasing the magnetic resistance (electromagnetic braking) against the flywheel (Gregor & Conconi, 2000). Consequently, “spiroergometry” (spiro = breath, ergo = work, metry = measure), also sometimes called “ergospirometry”, is defined as the measurement of respiratory gas exchange and ventilation of a subject during physical exercise on an ergometer in order to consider the reaction of cardiorespiratory functions (Kroidl et al. 2007). The system of spiroergometry testing essentially consists of the

following instruments: (1) a device producing a defined level of physical stress, such as an ergometer, (2) a transducer for the measurement of ventilation, (3) gas analyzers for oxygen and carbon dioxide, (4) a computer for online processing of the measured data, and (5) a multichannel electrocardiograph (ECG) (Schlegelmilch & Kramme, 2011).

In sports medicine, nowadays, the spiroergometry testing procedure is carried out using either a ramp or steady-state protocols under laboratory conditions. These protocols are a powerful diagnostic testing method through the principle of stepwise increasing load to access muscle performance, metabolism and the cardiovascular system. With the stationary bicycle ergometer, during the ramp protocol, intensity is increased by 15 to 25 Watts every minute; whereas the stead-state protocol consists of several exercise stages, which usually add 25 to 50 Watts every 2 to 4 minutes (see Appendix A: Figure 9).

### 2.4.2 Lung function

The body needs to apply a respiratory system in order to create aerobic energy. The function of the "lung" or "pulmonary" is defined as the movement of respiratory gases into and out of the lungs, called pulmonary "ventilation". This function is provided by the gaseous exchange at the alveoli, also sometimes called air sacs, in form of "diffusion", which is the random movement of the molecules of the respiratory gases (Eston, 2003). Within the air sacs, the exchange of oxygen ($O_2$) and carbon dioxide ($CO_2$) occurs at the alveoli-pulmonary capillary interface, which is regulated by the partial pressure of $O_2$ and $CO_2$ between alveolar air and pulmonary capillary blood. That is, each gas moves from a higher partial pressure area to a lower partial pressure area until equilibrium is achieved, called the principle of pressure gradient (Foss & Keteyian, 1998).

Ventilatory mechanics are divided into resting and exercising conditions. At rest, during "inhalation" or "inspiration", the size of the thoracic cage is extended from the neck to the abdomen by the downward contraction of the diaphragm and extended from left to right and from front to back by the contraction of the external intercostal muscles (Kroidl et al. 2007). This extension will cause the intrapulmonary and intrapleural pressures to decrease, and the air is immediately sucked into the lungs. During maximal exercise, the scalene muscles, the sternocleidomastoid muscles, the trapezius muscles, and the extensor muscles will facilitate the extension of the thoracic cavity for inhalation. On the other hand, "exhalation" or "expiration" is passive and caused by the upward return of the diaphragm and the external intercostal muscles during resting because of the special properties of elastic tissues (Kroidl et al. 2007). During exercise, the contraction of the abdominal muscles and the internal intercostal muscles helps increase the pressure inside by decreasing the size of the cavity. That is, the pressures are reversed, leading to the inside pressure

being greater than the outside pressure, and then the air is forced out of the lungs into the environment. Normally, the volumes of inhalation and exhalation are not equal because the inspired $O_2$ volumes are greater than the expired $CO_2$ volumes (Eston, 2003).

In order to gain an understanding of the lung function, lung volumes and lung capacities need to be studied with a particular device that is called a spirometer by measuring and reading spirographs. Basically, the lung volumes are distinguished by the tidal volume ($V_T$), inspiratory reserve volume (IRV), expiratory reserve volume (ERV) and residual volume (RV). Furthermore lung capacities result from adding the special lung volumes, such as the inspiratory capacity (IC=IRV+ $V_T$), the vital capacity (VC=IRV+ $V_T$ +ERV), the functional residual capacity (FRC=ERV+RV), and the total lung capacity (TLC=IC+FRC) (Foss & Keteyian, 1998). These factors will vary with body size, age, sex and exercise intensity (see Appendix A: Figure 10).

By definition, $V_T$ is the movement of air volumes during breathing, which concerns the air that reaches the air sacs for gaseous exchange, and the air that remains in the respiratory passage or dead space volume where there is no gaseous exchange. IRV refers to the amount of air that can be maximally inspired at the end of a normal inhalation, or the reserve ability for inspiration beyond the tidal volume. In contrast, ERV is the amount of air that can be maximally expired after the normal exhalation. After maximal exhalation, the amount of air that cannot be expired is termed the RV. Regarding lung capacities, IC is defined as the amount of air that can be moved into the lungs during a full inhalation, starting from the resting inspiratory position. VC refers to the total amount of air that can be breathed out voluntarily from the lungs after a full inhalation and a full exhalation. After a normal exhalation, the amount of air that remains inside the lungs is defined as FRC, which is the balancing point where the elastic recoil force of the lung and the chest wall are equal but opposite. All of this combined results in TLC, which gives the total amount of air in the lungs at the end of a maximal inspiration until the ending point of the residual volume or a full inflation of the lungs. The changes of pulmonary parameters between rest and exercise including their definitions (see Appendix B: Table 1). During exercise, for example, $V_T$ is increased by an expansion of the airway, causing the dead space to double in order to obtain adequate alveolar ventilation. This increasing affects the IRV and ERV, which are reduced during workout since it is a natural consequence of an increase in $V_T$. Athletic training will help to increase the VC. In particular, training the shoulder girdle muscles leads to a strengthening of accessory muscles for inspiration. Pulmonary ventilation is assessed by the air volume measurement that either inspires or expires per minute. This is called minute ventilation ($V_E$), which depends on the breathing frequency (BF) and tidal volume ($V_T$) of the ventilation per breath. While resting, $V_E$, BF, and $V_T$ vary between 4 and 12 $L \cdot min^{-1}$, 10 and 20 $breaths \cdot min^{-1}$, and 0.4 and 0.6 litres, respectively (Eston, 2003).

2.4.3 Breath-by-breath principle

The breath-by-breath method is a continuous gas measurement while inhaling and exhaling at a mouthpiece, which is connected to the face or a breathing mask (Schlegelmilch & Kramme, 2011). Ideally, gas volumes are measured by using a turbine spirometer, which measures the rotations of a turbine, that is, the higher the flow, the faster the turbine rotates. Infrared detectors will detect the rate at which the light from an infrared source is interrupted by the passing of the turbine (Kroidl et al. 2007). With this information, the flow can be used to calculate the gas volumes. The samples of the respiratory gas are continuously sucked through a thin moisture-absorbing tube attached to the mouthpiece, into a device which is called the fast-response gas analyzer. A special sensor in this gas analyzer detects the respiratory gases of the inhaling and exhaling, and measures the fractional concentration together with the volume of the flow at the mouthpiece per minute. Technically, the gas flows together with the gas concentrations, need to be synchronized and precisely brought into phase. Furthermore, the response of each analyzer also requires software calculation (Kroidl et al. 2007).

Besides the various values of the respiratory variables, the body temperature and pressure saturated (BTPS) must be converted to the standard temperature and pressure dry (STPD), which must be applied by the software of the device (Schlegelmilch & Kramme, 2011). Furthermore, the values of oxygen consumption ($\dot{V}O_2$) and carbon dioxide production ($\dot{V}CO_2$) were determined by the following common technique for the breath-by-breath method with a Haldane transformation principle included in the algorithm (Rosdahl et al., 2009). The concept of the Haldane transformation is based on the fact that the amount of respiratory gaseous nitrogen ($N_2$) that the body inspires is equal to that which the body expires because $N_2$ is neither consumed while inhaling nor produced while exhaling by the body (Foss & Keteyian, 1998). This concept can therefore be applied with an open-circuit spirometry method to calculate the respiratory gases (Wilmore & Costill, 2004). The following equations, known as the Haldane transformation, describe the mathematical expression of the relationship between the inspired and expired air volumes based on the assumed constancy of $N_2$:

$$\dot{V}_{in} \cdot F_{in}N_2 = \dot{V}_{ex} \cdot F_{ex}N_2 \tag{2.35}$$

Thus, the inspired air volume is:

$$\dot{V}_{in} = \dot{V}_{ex} \cdot \left( \frac{F_{ex}N_2}{F_{in}N_2} \right) \tag{2.36}$$

And the expired air volume is:

$$\dot{V}_{ex} = \dot{V}_{in} \cdot \left( \frac{F_{in}N_2}{F_{ex}N_2} \right) \tag{2.37}$$

where, $\dot{V}_{in}$ and $\dot{V}_{ex}$ are the volumes of inspired and expired air per minute, expressed in L·min$^{-1}$; and $F_{in}N_2$ and $F_{ex}N_2$ are the fractional concentrations of nitrogen in the inspired and expired air. Wilmore and Costill (2004) commented on Equation (2.35), stating that it is not necessary to calculate both the inspired and the expired air volumes because the amount of inert gas nitrogen is always constant; that is, during the steady state, the inspired nitrogen amount ($\dot{V}_{in} \cdot F_{in}N_2$) each minute is exactly equal to the expired nitrogen amount ($\dot{V}_{ex} \cdot F_{ex}N_2$). However, during measurements using the breath-by-breath method, although the fractional concentration of oxygen ($F_{in}O_2$), carbon dioxide ($F_{in}CO_2$) and nitrogen ($F_{in}N_2$) are constant in the inspired air, the values that are recorded for the fractional concentration of oxygen ($F_{ex}O_2$), carbon dioxide ($F_{ex}CO_2$) and nitrogen ($F_{ex}N_2$) in the expired air will vary.

Under this assumption, Cooke (2003) reasoned that the values of concentration or the fraction of oxygen in the expired air will be lower than in inspired air $F_{ex}O_2 < F_{in}O_2$ because some of the oxygen ($O_2$) is extracted from the lungs into the blood capillaries. On the other hand, the values of the concentration or the fraction of carbon dioxide in the expired air will be higher than in the inspired air $F_{ex}CO_2 > F_{in}CO_2$, since the body excretes the carbon dioxide ($CO_2$) from the blood into the lungs during the gas exchange process. In fresh air, generally, the proportion of gases that are inspired by the body typically consist of: $F_{in}O_2$ = 0.2093 (20.93%), $F_{in}CO_2$ = 0.0004 (0.04%), and $F_{in}N_2$ = 0.7903 (79.03%) (Foss & Keteyian, 1998) (see Appendix A: Figure 11). Hence, the sum of the fractional concentrations of these gases is equal to 1.0 (100%) for both the inspired and expired gas volumes, which can be calculated by either $F_{in}N_2$ or $F_{ex}N_2$ (Cooke, 2003). The gas relationship for inhalation is given by (Foss & Keteyian, 1998; Cooke, 2003; Wilmore & Costill, 2004):

$$F_{in}O_2 + F_{in}CO_2 + F_{in}N_2 = 1 \tag{2.38}$$

Thus:

$$F_{in}N_2 = 1 - F_{in}O_2 - F_{in}CO_2 \tag{2.39}$$

And the gas relationship for exhalation is:

$$F_{ex}O_2 + F_{ex}CO_2 + F_{ex}N_2 = 1 \tag{2.40}$$

Thus:

$$F_{ex}N_2 = 1 - F_{ex}O_2 - F_{ex}CO_2 \quad (2.41)$$

Note: the Equation (2.36), (2.38) and (2.41) are used to determine the oxygen consumption and carbon dioxide production (see Appendix D: Calculation of respiratory gases).

### 2.4.4 Oxycon mobile® metabolic system

Since recently, the measurement of respiratory gases through spirometry can use a portable telemetric gas analyzer system in order to assess the cardiorespiratory functions. This system applies the principle of telemetry (wireless) in form of physiological radio transmission. The data of the respiratory gases are collected by a special detector at the mouthpiece and sent to a host computer system via wireless transmission. This device, the "Oxycon Mobile®" (Erich Jaeger, Viasys Healthcare GmbH, Germany), is popularly a portable device that can measure and analyze both the respiratory gas volumes and the compositions. The components of the Oxycon Mobile® portable system mainly consist of: (1) a "facemask" with a digital TripleV® volume sensor and a Nafion tube for gas samples connected to; (2) a "sensor box" (SBx) or a measuring unit for the gas and flow signals; (3) a "data exchange storage" box (DEx) or a transmitter unit; (4) a "telemetry" or receiver unit including a calibration module (PCa) that is connected to a pressure reducer with an optional gas cylinder; and (5) a "personal computer" (PC) with Oxycon Mobile®'s software for data and graphical analysis (see Appendix A: Figure 12). The respiratory gas volumes and flows are measured by the digital "TripleV®" volume sensor (Diaz et al., 2008). A critical element consists of a turbine flowmeter, which is a type of flow sensor which is small, lightweight, and has low resistance and dead space. The turbine or propeller is built into the flowtube, which is called that a "digital volume transducer" (DVT) (Eriksson et al., 2010). The DVT is connected to a facemask and protected by a windshield for outdoor tests. In addition, the facemask must be fitted carefully so as to ensure no air leakage. Technically, the turbine is stimulated or exited by the passing gas flows which lead to its rotation, upon which the rotating elements interrupt or reflect the light from a light-emitting diode (LED). The photodiodes will record the rotations, returning an electrical impulse frequency proportional to the flow, while the total count is proportional to the volume (Schlegelmilch & Kramme, 2011).

Another critical element close to the DVT is the "Nafion" tube, which is a gas sampling tube. While inhaling and exhaling through the TripleV® turbine, Oxygen ($O_2$) and carbon dioxide ($CO_2$) as respiratory gas samples are led through the Nafion tube into the sensor box (SBx). Then, in SBx, the fractional concentrations of $O_2$ are derived from an electrochemical principle in a microfuel cell with ambient air humidity that is also provided by the Nafion tube, and

the fractional concentrations of $CO_2$ are derived from a thermal conductivity principle (Diaz et al., 2008; Rosdahl et al., 2009). As mentioned above, the oxygen consumption ($\dot{V}O_2$) and the carbon dioxide production ($\dot{V}CO_2$) are then calculated by the breath-by-breath technique with the Haldane transformation (Rosdahl et al., 2009; Eriksson et al., 2010). According to the instruction manual, Oxycon Mobile® must be switched on at least 30 min before the begin of each test. Calibration must be done immediately before each test by using the built-in automated procedures (PCa). In addition, the calibration must be done under the same environmental settings as for the tests. While calibrating, high-precision gases for the calibration of the gas analyzer are sampled from the same tank, which contain 15% $O_2$ and 6% $CO_2$. After calibration, no dysfunctional signs should be detected, such as an inconstancy in the flowing $O_2$ and $CO_2$. The gas exchange and ventilation parameters are measured by using the breath-by–breath method, and averaged over 15 sec for data analysis. Regarding a reuse of the Nafion tube for the next test, it must be rested for at least 90 min after the previous test because the water vapour condensation in the sampling tube influences the respiratory gas analysis (Rosdahl et al., 2009; Eriksson et al., 2010). The accuracy of $\dot{V}O_2$ and $\dot{V}CO_2$ are specified to 3% or 0.05 L·min$^{-1}$ in the range of 0-7 L·min$^{-1}$; the accuracy of the minute ventilation ($\dot{V}_E$) is specified to 2% or 0.05 L·min$^{-1}$ (range 0-300 L·min$^{-1}$); and the accuracy of the respiratory exchange rate (*RER*) is specified to 4% in range 0.6-2.

To date, cycling performance needs to optimize between biomechanical advantage and physiological efficiency. That being said, the optimal cycling position is usually a compromise between effectiveness of aerodynamics and respiratory function, as improving cycling positions from an aerodynamic point of view does not necessarily result in an optimised respiratory function. There are three cycling positions, namely the upright position (UP), aero position (AP), and dropped position (DP), which are widely used in racing (Grappe et al., 1999a). The use of the three different positions depends on the competitive situation and racing type. The differences among the riding positions affect not only inclination of the torso that is related to altering the muscle force-length relationship for power production at the hip joint, but also the cardiorespiratory responses (Gnehm et al., 1997).

In the past two decades, several studies of effectiveness among various positions that affect energy expenditure have been conducted in field tests at constant velocity; and the results showed that the crouched position yielded the energy saving more than the upright position (Richardson & Johnson, 1994; Sheel et al., 1996; Jobson et al., 2008). In order to control the various variables under the same conditions, for example especially without wind effects, the tests were mostly performed in a laboratory. In previous laboratory works, the effect of three cycling positions on physiological responses were compared among UP, AP, and DP at submaximal exercise testing with elite cyclists (Gnehm et al., 1997; Grappe et al., 1998) and triathletes (Dorel et al., 2009). In addition, comparisons between two positions have also been conducted, such as a comparison between UP and AP with trained cyclists (Berry et al., 1994; Ashe et al., 2003; Peveler et al., 2005; Jobson et al., 2008; Hubenig et al., 2011); a comparison between UP and DP (Ryschon & Stray-Gundersen, 1991); and a comparison between AP and DP (Evangelisti et al., 1995).

Results from these investigations revealed that for UP versus AP, only the mean oxygen consumption ($\dot{V}O_2$) was significantly higher in AP than in UP for the investigations of Gnehm et al. (1997), Ashe et al. (2003), and Peveler et al. (2005), though Grappe et al. (1998) also showed a significant difference in the parameter of the respiratory exchange rate (RER). In contrast, Origenes et al. (1993), Berry et al. (1994), Grappe et al. (1998), and Dorel et al. (2009) found no significant differences in the ventilatory and gas-exchange variables. Comparing UP with DP, Grappe et al. (1998) revealed that the mean minute ventilation ($\dot{V}_E$) and RER yielded significantly higher values in DP than in UP. This appears to be in contrast to other researchers, which reported that the cardiorespiratory factors were not significantly different (Ryschon & Stray-Gundersen, 1991; Gnehm et al., 1997; Dorel et al., 2009). Finally, Gnehm et al. (1997), who compared AP to DP, found that the mean heart rate (HR), $\dot{V}O_2$, and RER yielded significantly higher values in DP than in AP. But no significant differences were found in the studies of Evangelisti et al. (1995), Sheel et al. (1996), Grappe et al. (1998), and Dorel et al. (2009). These results demonstrate that there are still many conflicts when it comes to comparing the cardiorespiratory parameters among these cycling positions in trained cyclists. This could

possibly be attributed to the fact that researchers conducted their tests with trained cyclists/triathletes who were familiar with the training programme of the crouched position. For untrained cyclists, only few studies have focused on cardiorespiratory effects in UP compared with crouched positions.

To the best of knowledge, only the study of Ashe et al. (2003) has previously investigated UP compared to AP in recreational cyclists who had never trained with aerobars (AP) before. Consequently, this present study is designed to compare the differences of cycling positions between UP and crouched positions, such as AP and fully DP, and their effects on cardiorespiratory responses during a submaximal bicycle ergometer exercise. In this present study, a fully DP was selected, during which the upper body and lower arms have to be parallel to the ground. This riding position is different from the general DP in previous studies, where participants were required to maintain elbow extension. The fully DP was chosen because, as mentioned previously, it is useful in reducing the aerodynamic drag at high speeds and it is thus the most commonly used position of cyclists with a standard handlebar. From a mechanical point of view, the crouched position is considered the most effective from an aerodynamic point of view, but may provide a disadvantage to the cardiorespiratory functions for cyclists who are inexperienced with AP and fully DP. Therefore, it is hypothesized that, cycling in crouched positions (AP and fully DP) may limit chest expansion, reduce the chest volume, increase respiration rates, and result in a reduced efficiency. In other words, the increase in the cardiorespiratory efforts may be affected by the decreased torso angle while cycling in crouched positions when compared with the upright position.

The aerodynamic drag, drag area, and drag coefficient for various cycling positions can directly or indirectly be determined by using different methods: 1) wind tunnel (Martin et al., 1998; García-López et al., 2008; Gibertini et al., 2008; Chowdhury et al., 2011; Crouch et al., 2012), 2) computational fluid dynamics (CFD) simulations (Defraeye et al., 2010; Blocken et al., 2013), 3) linear regression analysis between metabolic cost and external power output and square velocity (Davies, 1980; Capelli et al., 1998), 4) powermeters or force transducers (Grappe et al., 1997; Martin et al., 2006; Edwards & Byrnes, 2007; Lim et al., 2011), 5) tractive resistance or towing experiments (Capelli et al., 1993; De Groot et al., 1995), and 6) deceleration or coasting down tests (De Groot et al., 1995; Hennekam & Govers, 1996; Candau et al., 1999), though some methods may not be sufficiently valid or reliable to estimate the values of the parameters.

The aerodynamic drag, drag area, and drag coefficient in cycling are mostly determined directly in a wind tunnel from the measured forces that act on the rider-bicycle combination. Technically, the wind tunnel for cycling tests is of a closed loop circuit, subsonic type, and controlled by a remote computer with special software and a wind speed transducer. The drag force could be measured by a stain-gauge force transducer, which is mounted on a rectangular plate and attached to the stationary bicycle. The wind tunnel is as reference method to assess air drag due to its validity and reliability (García-López et al., 2008). However, Gross et al. (1983) reasoned that the air drag from wind tunnel

measurements is lower than from field tests because the effect of the air during the rotation of the wheels is not present. Moreover, the air drag due to the lateral movement of the legs that occurs during actual cycling is not present in the wind tunnel (Candau et al., 1999). Moreover, wind tunnel tests are very expensive at between 5,000 and 10,000 Euros per day (Debraux et al., 2011).

Since very recently, computational fluid dynamics (CFD) simulations can be used to determine the aerodynamic drag, drag area, and drag coefficient. In the studies of Defraeye et al. (2010) and Blocken et al. (2013), CFD simulations rely on wind tunnel tests to provide reliable data in order to evaluate the accuracy of CFD simulations. Debraux et al. (2011) reviewed that CFD provided data for the drag which was in good agreement compared with the measurements from wind tunnel tests. Besides, CFD could be a valuable numerical alternative for evaluating the drag of different cyclist positions with high sensitivity. The advantage of this method is that it allows more detailed insight into the flow field around the body of the cyclist.

As an indirect method, the aerodynamic drag has also been estimated from the relationship between the oxygen consumption obtained form the cycling on a treadmill in a wind tunnel against various wind velocities, and from the cycling on a stationary-cycle ergometer against various mechanical power (Davies, 1980) or from the cycling on a track at constant speeds (Capelli et al., 1998). The drag area was determined from the relationship between the constructed curves of oxygen consumption, the square velocity and the mechanical power output. That is, 1) the value of the square velocity and the mechanical power were calculated from the oxygen consumption, 2) the mechanical power was divided by the velocity that was obtained from the total forces opposing the motion, and 3) a slope of linear regression was generated from the relationship between the total forces and the square velocity, which was then used to calculate both the air drag and the rolling resistance (when the velocity approached zero) (Davies, 1980; Capelli et al., 1998). But García-López et al. (2008) commented that this method also has its caveats, such as different environmental and physiological conditions between laboratory and field measurements.

Aerodynamic drag can also be determined in the field by the direct measurement of the total resistances opposing the motion of the cyclist. There are three techniques, namely the force transducers technique, the tractive resistance technique, and the coasting deceleration technique. These techniques can assess both the aerodynamic drag and the rolling friction as resistive forces during actual cycling, which cannot be determined in a wind tunnel. Force transducers are attached to the bicycle crank (SRM®) or the rear-wheel hub (MaxOne® and PowerTap®) through a strain gauge and are used to the measure mechanical power output (powermeter) during cycling. This method must be conducted in the field in order to quantify both the aerodynamic drag and the rolling resistance in different cycling positions, while taking into account the movement of the cyclist while pedalling. Hence, the measurement of aerodynamic drag is undertaken during actual cycling and is easy to implement. Aerodynamic drag and rolling

resistance are determined from the measured total resistances opposing the motion using the fact that the total force is equal to the external mechanical power output divided by the cycling velocity. The average external mechanical power of the cyclist during cycling is measured using the powermeter. Then, the drag area is determined from the slope of the linear regression described by the total forces and the square velocity (Grappe et al., 1997; Martin et al., 2006; Edwards & Byrnes, 2007; Lim et al., 2011).

The tractive resistance technique can also measure both the aerodynamic drag and the rolling resistance opposing the motion while towing a rider-bicycle combination at a constant speed behind a moving car or a motorcycle on level ground. The cyclist is required to keep the defined riding position during the towing test. The cyclist can pedal without the transmission chain to reproduce the same turbulent air patterns as during actual cycling (Capelli et al., 1993). A cable length of 12 m is selected to reduce the air turbulence caused by the moving car (De Groot et al., 1995). The resistive forces are measured from a load cell mounted to the cable. The resistive forces need to be measured at different velocities in order to obtain the relationship between them and the velocity. The air drag and rolling friction are then assessed from a slope of linear regression between the resistive forces and the square of the velocity (Debraux et al., 2011). Nevertheless, some authors discus the problems of the towing experiment, namely that is difficult to perform and that errors can occur because of the air turbulence produced by the vehicle at high speeds. Moreover, the atmospheric conditions can alter the measured values (García-López et al., 2008).

The coasting down technique measures the deceleration of the rider-bicycle combination while freewheeling. This method can be carried out on a flat floor both indoors and outdoors but requires a level surface. After the cyclist reaches the defined velocity, the cyclist stops pedaling (or pedaling without a transmitting force to the rear wheel) prior to reaching the coast-down phase. During freewheeling, the cyclist-bicycle system is slowed down due to the aerodynamic drag and rolling resistance. The velocity-time series is recorded in a systematic manner in order to calculate the resistive forces. The coasting down technique is based on Newton's second law ( $\sum \vec{F} = m \cdot \vec{a}$ ) (Faria et al., 2005; Debraux et al., 2011). That is, the product of the deceleration and the rider-bicycle mass can determined by the resistive forces opposing the motion. Gross et al. (1983) mentioned that the results from the coasting down method compared very well with wind tunnel data. However, some authors mention that the deceleration method in the field might overestimate the aerodynamic drag and its reliability is low (García-López et al., 2008).

Previous studies, such as Candau et al. (1999), determined the drag area in an upright and aero position with the deceleration method. They applied three switches to obtain the measuring velocity as a function of distance in an 80-m indoor hallway with a linoleum surface. The distance between the first and the second switch was 3 meters and the distance between the second and third switch was 20 meters (deceleration phase). All switches were linked to a

chronometer system and then interfaced to a computer for data recording. The total resistive forces were assessed with several trials at different velocities by iterations with a mathematical model that described the deceleration of the trajectory of the cyclist-bicycle system. They resolved the previously mentioned argument for this technique by conducting a large number of coasting down trials under same circumstances, which was possible with high reliability. For performing in the open air under wind-free conditions, Hennekam and Govers (1996) used the freewheeling technique to measure the drag area in a racing position. The decreasing of velocity as a function of time was measured from an electronic recording of electrical pulses, which were generated by an inductive sensor mounted on the front fork of the bicycle. During the rotation of the wheel, the electrical pulses were induced by the magnetic field formed by 28 small magnets, which where attached to the spokes of the wheel. Then, all electrical pulses were detected by a portable audio-recorder and converted to a velocity-over-time diagram in the laboratory. The drag area was determined from the linear regression of the deceleration and the squared velocity, the curve of which is a straight line.

De Groot et al. (1995) investigated the coasting down method to determine the value of the drag area in a crouched position on a straight of 600-m in an indoor flower auction hall with an asphalt surface. Their investigation applied a small infrared light emitter and detector (LED) mounted on the front fork of the bicycle to measure the velocity as a function of time during the deceleration phase. All data was recorded every second and stored on a cassette tape of a small portable audio recorder. The least squares method was used to estimate the parameter of the drag area by using a coasting down model. There is no information concerning the reliability and sensitivity of this approach.

To the best of knowledge, the coasting down method lacks sensitivity testing for the measurements of both the drag area and the drag coefficient in the upright position, the aero position, and the fully dropped position. The sensitivity of the deceleration technique among three cycling positions also needs to be tested for the aerodynamic drag because this has not yet been investigated. Moreover, the use of new technology for measuring the velocity during actual cycling, such as a tachogenerator, and for both transmitting and obtaining accurate data, such as a telemetry system equipped to a bicycle with special software, has yet to be demonstrated.

# CHAPTER 4: METHODS AND MATERIALS

## 4.1 Spiroergometry testing

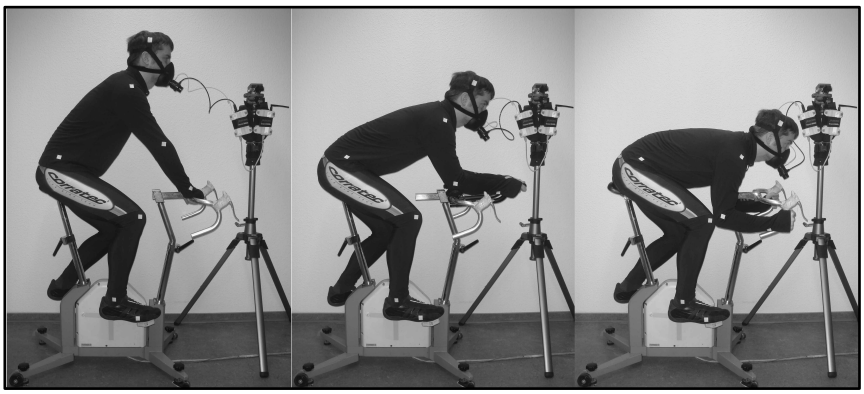

Figure 4.1 Illustrations of upright position (UP), aero position (AP), and fully dropped position (DP) during submaximal spiroergometry testing, using the portable telemetric gas analysis system.

*Participants and Experimental procedure*

Twenty-four recreational male cyclists who were familiar with daily cycling in the upright position (hands grip a handlebar, arms are straight, and torso is vertical with the ground) on a mountain bike, a city bike or a racing bike were recruited. Basic anthropometric data an included mean (± standard deviation) age of 27.1 (± 4.2) years, a height of 179.8 (± 6.5) cm, and a body mass of 76.8 (± 8.0) kg (see Appendix B: Table 2). All participants were non-smokers and did not have any chronic illnesses including asthma, hypertension, diabetes mellitus or heart disease. The tests excluded the participants with physical injuries which could have influenced their performance on the experiment. All participants were informed of the purposes, procedures and prohibitions of the experiment before giving written informed consents to participate.

All experiments were performed under similar environmental conditions at the Biomechanics Laboratory of the Institute of Sports Science at the University of Rostock. Each participant had three separate days of experiment within two weeks, including at least two days of recovery in between each experiment day. All participants were refrained from any stimulants and intense program training for at least twenty-four hours before each session, and had no food intake for at least two hours before the experiment except water. Anthropometric measurements of the participants were required in order to configure their optimal seat height (distance from crank axis to saddle center), handlebar height (distance from stem to saddle center), and handlebar length (distance from stem to saddle center) on a modified bicycle ergometer (Model 380B; Siemens-Elema, Solna, Sweden), which was equipped with a racing style saddle (Dakar ISCA Mod 09, Italy) and a standard racing handlebar (3ttt Mod. Competizione, Italy), mounted with clip-on aerodynamics

handlebars (Easton Aeroforce Mod Bar Mount Kits, USA). The participants performed each bicycling position under the same configuration on this modified bicycle ergometer.

In this study, the three cycling positions (Figure 4.1) consisted of 1) upright position (UP) –hands placed on the top part of the standard racing handlebar and arms extended; 2) aero position (AP) – elbows rested on the bar pads and hands holding the bar extensions of the aerodynamics handlebars; and 3) fully dropped position (DP) – hands placed on the lower part of the standard racing handlebar and the torso bent extremely, so that it is parallel to the ground. In order to eliminate potential side effects, all participants were randomly assigned into six groups of four people (i.e. randomized block design). A sequence of three cycling positions for each group were implemented as follows: Group 1 (UP→DP→AP); Group 2 (UP→AP→DP); Group 3 (AP→DP→UP); Group 4 (AP→UP→DP); Group 5 (DP→UP→AP); and Group 6 (DP→AP→UP) (see Appendix B: Table 2). Each participant spent the same amount of time in the laboratory on the three separate days. The participants began with a 3-min rest phase on the modified bicycle ergometer, followed by a 3-min warm-up at a workload of 60 Watts. After this period, they cycled continuously at three stages of the submaximal bicycle ergometer testing, which consist of 5-min in each of the three workloads of 100, 140, and 180 Watts, respectively. Finally, they cooled down for 5-min at a workload of 60 Watts. Furthermore, during the rest, warm-up and cool-down period, the participants were always in UP, and maintained a pedaling cadence of 80 revolution·min$^{-1}$ throughout the exercise.

*Cardiorespiratory parameter measurements*

Before the experiment, the common lung functions of all participants were evaluated in the sitting upright position: the forced tidal capacity (FVC, L BTPS), the forced expiratory volume in one second (FEV1, L·s$^{-1}$ BTPS), and the maximal voluntary ventilation (MVV, L·min$^{-1}$ BTPS) were measured while they breathed through a tightly fitted mouthpiece. During the submaximal bicycle ergometer tests, the cardiorespiratory parameters that consisted of the heart rate (HR, beats·min$^{-1}$), the oxygen uptake ($\dot{V}O_2$, ml·min$^{-1}$ STPD), the carbon dioxide output ($\dot{V}CO_2$, ml·min$^{-1}$ STPD), the minute ventilation ($\dot{V}_E$, L·min$^{-1}$ BTPS), the breathing frequency (BF, breaths·min$^{-1}$), the tidal volume ($V_T$, L BTPS), and the respiratory exchange rate (RER), were continuously measured directly breath-by-breath through a portable telemetric gas analysis system (Jaeger Oxycon Mobile®, Viasys Healthcare, Hoecberg, Germany). The gas analyzer and turbine were carefully calibrated before each test.

*Statistical analysis*

In order to obtain the accurate parameter values at a steady-state level, the cardiorespiratory values in the last 1-min period of each workload were analyzed. Standard parametric statistics were used throughout the analysis. The mean cardiorespiratory parameters among the cycling positions at various workloads were compared by a one-way repeated measurement analysis of the variance. In addition, Turkey's *post-hoc* test was applied to determine significant differences between the cycling positions with the significant *F*-test. The analyses in this study were accomplished with the Statistical Package for the Social Sciences (SPSS) 16.0. All results in this study are shown as mean values with standard deviations ($\bar{x}$ ± SD). The level of statistical significance was set at $P<0.05$ for all tests.

## 4.2 Coasting down testing

### 4.2.1 Velocity-time functional measurement

Figure 4.2 Illustrations of upright position (UP), aero position (AP), and fully dropped position (DP) during the coasting down test. A tachogenerator, equipped on a distal of the front fork of the bicycle, was used to measure the velocity-time function through a telemetry bicycle, which transmitted a signal at 433.92 MHz to a receiver module.

*Subjects and Experimental procedure*

From the twenty-four recreational male cyclists, who took part in the spiroergometry testing, four subjects - 01-WN, 06-UC, 09-HL, and 15-ES - were selected for the coasting down investigation. Their basic anthropometric data included a mean (± standard deviation) age of 31.5 (± 2.6) years, a body mass of 76.0 (± 3.8) kg, and a body height of

174.5 (± 2.5) cm. All coasting deceleration tests were performed under similar environmental conditions in a 50 m long level indoor sports hall at the University of Rostock on wood flooring. Therefore, the wind velocity with respect to the rider-bicycle was equal to the rider-bicycle velocity with respect to the ground. Each subject was investigated on three consecutive days (1st Day for UP, 2nd Day for AP, and 3rd for DP) and carried out 25 respective trials at two initial velocities of 25 and 15 $km \cdot h^{-1}$ on every test day. Therefore, each subject completed a total of 150 trials (3 positions x 2 velocities x 25 trials). All tests were done with the same classical standard racing bicycle (Peugeot, France) equipped with a telemetry system in the bicycle frame, which is also called a telemetry bicycle. For riding in AP, the telemetry bicycle was additionally equipped with clip-on aerodynamics handlebars (Easton Aeroforce Mod Bar Mount Kits, USA). The front and rear wheels were standard wheels with 32 oval spokes (Mavic®, France). The tires were 28 inch in diameter, had a cross-sectional width of 22 mm (Giro Tubular, Continental®, Germany) and were inflated to a pressure of 8 bars (800 kPa) and always checked before testing. All subjects were similarly dressed with a cycling outfit, helmet, gloves and shoes. Three cycling positions were tested in this study, which are commonly used by racing cyclists (Figure 4.2): 1) upright position (UP) where the torso is upright with the hands placed near the stem of the standard handlebars; 2) aero position (AP) where the torso is forced to crouch by using clip-on aerobar extensions with the elbows resting on pads, the hands extended along the bars and the arms gripping the end of the bars; 3) fully dropped position (DP) where the torso is parallel to the ground with the hands in the drop portion of the standard handlebars and the elbows bent.

The trial began with the subject cycling up to the defined velocity of 25 $km \cdot h^{-1}$ and then stopping the pedaling, keeping the legs still, and remaining in the cycling position before freewheeling. The subject coasted down over a straight lane length of 30 m and width of 1 m and the coasting time was held for 3 seconds. During the coasting down period, the subject needed to control the bicycle motion into a defined straight lane. If the rider-bicycle oscillated too much on the coasting-down lane, the test needed to be done again until the requirements were met. Basically, the subject was slowed down by aerodynamic drag and rolling friction. During the coasting deceleration of the rider-bicycle, the velocity-time function was measured as a data signal by a tachogenerator (or speed sensor), transmitted from the telemetry bicycle to the receiver unit and then interfaced to a computer. Moreover, at the initial and final point of the 30-m coasting-down lane, a light barrier system (DG 2000, Heuser, Germany) was installed to detect the rider-bicycle motion and mark the location parallel to the transmitted velocity-time signal in order to analyze the data. During testing, the ambient temperature and relative humidity were recorded for every trial in order to determine the air density. The costing-down test at an initial velocity of 15 $km \cdot h^{-1}$ was processed in the same way. How the telemetry bicycle measures its deceleration from the velocity-time function $v(t)$ is explained in Chapter 2.2.3 (Telemetry-bicycle system).

*Nonlinear parameter estimation by the least-squares method*

The technique of least squares was used to obtain the estimation of the parameters in this study. The mathematical model, given by Equation (2.26), is the coasting deceleration equation as the tan-function relationship (nonlinear) that includes the initial velocity ( $v_i$ ) and aerodynamic constant divided by mass ( $K_m$ ), which both need to be estimated. From all coasting down trials, the observed values of the decreasing velocity over time (3000 data points per 3 seconds) were fitted with the postulated mathematical model by using the Solver program of Microsoft Excel®. The procedure began by converting the mathematical model from Equation (2.26) to Equation (2.34), which was then entered into the excel spreadsheet, with the values for $v_i$ and $K_m$ being chosen as the target values which achieved the best estimation. The Solver function employed an iterative procedure to interpolate the values of both parameters that were related to the specified values in order to minimize the sum of squared errors. In other words, the Solver program generated a fitted curve on the 3000 data points of velocity-time from the best-parameter values of $v_i$ and $K_m$ that resulted in the smallest value of the sum of squared errors and corresponded to the stipulated model. For each subject, only the best 20 trials were then selected to be analyzed from the total of 25 trials per riding position by considering the values of the initial velocity that best approached the expected velocity of 25 $km \cdot h^{-1}$ (6.94 $m \cdot s^{-1}$). The trials for the expected initial velocity of 15 $km \cdot h^{-1}$ (4.17 $m \cdot s^{-1}$) were processed in the same way. After all velocity-time data from every trial was fitted, the fitted curve of 25 $km \cdot h^{-1}$ was overlapped with the fitted curve of 15 $km \cdot h^{-1}$ for each cycling position of each subject in order to find its true location. The velocity-time data for the initial velocities of 25 $km \cdot h^{-1}$ and 15 $km \cdot h^{-1}$ was then fitted again. The Solver yielded the best-parameter values for $v_i$ and $K_m$ via the least-squares method and generated the fitted curve of velocity with respect to time for the different cycling positions. How the least-squares method is used for the nonlinear parameter estimation in the Solver program, is explained in Chapter 2.3 (Nonlinear parameter estimation).

### 4.2.2 Projected frontal area measurement

After the coasting down tests, the four subjects were photographed in order to measure their projected frontal area ($A$) in each cycling position, which is an important variable for the determination of the drag coefficient ( $C_D$ ). Within a calibration-frame (MEROFORM, Germany) with dimensions of 1 m x 2 m x 2 m (width x length x height), a

telemetry bicycle was mounted on a stationary indoor trainer, leveled, and positioned against a white background prior to all measurements. A calibration square frame of a known area of 1 m x 1 m was located at midway between the front and rear wheels of the bicycle (roughly at the position of the bicycle cranks), and faced the camera. In order to simulate the same coating-down conditions, all subjects wore a similar cycling outfit, helmet, gloves, and shoes, and looked directly into the camera. The projected frontal area *A* was determined in three different cycling positions while the subjects sat on the same telemetry bicycle mounted on a stationary trainer. In addition, the subjects placed their right foot downward (i.e. at a crank position of 180°, with the top center being 0°) and their left foot upward (i.e. at a crank position of 0°) in all positions. Measurements of *A* were determined from digital photographic images taken indoors using a digital camera with a resolution of 21 megapixels (Cannon EOS 5D mark II, Japan), equipped with a telephoto zoom lens (Cannon EF 70-200 mm f/2.8L IS USM, Japan) and a flash attached (Cannon Speedlite 550EX, Japan). Following the recommendations of Olds and Olive (1999), the camera was mounted on a tripod (Titan Professional CT400, CULLMANN®, Germany) that was placed 20 m in front of the subject and 1.1 m above the ground.

For the photographs, the three cycling positions were similar to those in the coasting down investigation: 1) upright position (UP): the torso is upright with the hands placed near the stem of the standard handlebars; 2) aero position (AP): the torso is forced to crouch by using the clip-on aerobar extensions with the elbows resting on the pads, the hands extended along the bars and the arms gripping the end of the bars; and 3) fully dropped position (DP): the torso is parallel to the ground with the hands in the drop portion of the standard handlebars and the elbows bent at 90°. After the four subjects were photographed, all original photographic images were 3744 x 5616 pixels in size and saved in the JPEG format. They were transferred to a computer and analysed by two image-processing packages. For the present investigation, the digitizing method was applied to measure *A* (Heil, 2002; Debraux et al., 2009; Jensen et al., 2010). As a first step, the subject-bicycle and a calibration square frame (1m x1m) was extracted from each original image, leading to an image with a size of 2500 x 4800 pixels in the TIFF format, which was then modified by a computer-based imaging software (Adobe Photoshop CS5 Extended Version 12.0.4 x64, Adobe®, USA). Thereafter, each image was converted into black and white, by darkening for the subject-bicycle combination and by whitening for the calibration square frame before the calculation of *A*. The elliptical marquee tool (crop tool) was used to select between the portion of the image containing the whole subject-bicycle and the background. The magnetic lasso tool was then used to tune the edge of the whole subject-bicycle. The portion of the image containing the background needed to be converted to white. Then, the image of the whole subject-bicycle and the background was converted to a black and grey image by reducing the contrast to minus 100%. Then, the color was tuned until the resulting image contained a representation of *A* by setting the subject-bicycle to black and the background to white. Subsequently, this black-gray image was opened with a computer-based image analysis software application (ImageJ Version 1.48, National institutes

of Health, USA) in order to again obtain a darkened zone for the subject-bicycle and a brightened zone for the background. The measurement of $A$ was obtained by using the "Magic wand" to select the darkened zone and to obtain the area in pixels. The calibration square frame (1m x 1m) image was processed in the same way. Finally, the actual total $A$ of the subject-bicycle in square meters ($m^2$) of each digitized image was determined by dividing the area of the digitized image by the area of the corresponding calibration image and multiplying by the known area of the calibration square frame (1m x 1m), which can be represented by:

$$A = \frac{A_{CP}(\text{pixels}^2) \cdot 1(\text{m}^2)}{A_{CAL}(\text{pixels}^2)} \tag{4.1}$$

where, $A$ is the projected frontal area of the cycling position in $m^2$, $A_{CP}$ is the projected frontal area of the cycling position in $pixels^2$, and $A_{CAL}$ is the projected frontal area of the calibration square frame (1m x1m) in $pixels^2$. For example, Figure 4.3, where $A$ was measured for subject 15-ES in UP, the ImageJ software revealed $A_{CP}$ = 2,246,883 $pixels^2$ and $A_{CAL}$ = 4,544,585 $pixels^2$. Hence, $A$ = 0.49 $m^2$.

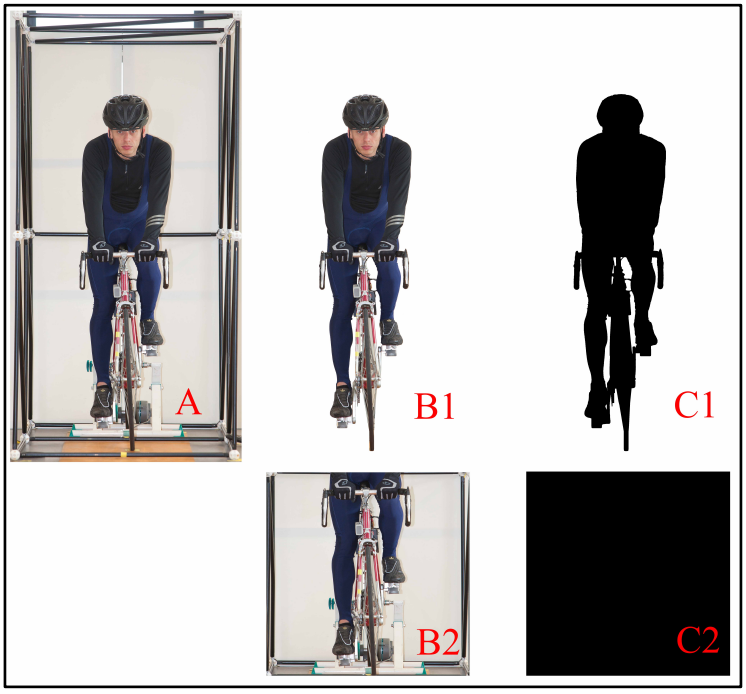


Figure 4.3 Illustrations of a measured sample of the projected frontal area in upright position (UP). To begin from: (A) photograph a cyclist with a determined cycling position and a bicycle, (B1) capture a cross-section area of the cyclist-bicycle combination and (B2) a cross-section area of a calibration square frame (1m x1m), and (C1) convert the whole cyclist-bicycle area and (C2) the calibration square frame to a black but convert the background to a white.

# CHAPTER 5: RESULTS

## 5.1 Effects of cycling positions on cardiorespiratory responses.

This chapter presents the results from statistical analysis for average of cardiorespiratory parameters (i.e. heart rate (HR), oxygen uptake ($\dot{V}O_2$), carbon dioxide output ($\dot{V}CO_2$), respiratory exchange rate (RER), tidal volume ($V_T$), breathing frequency (BF), and minute ventilation ($\dot{V}_E$)) among cycling positions (i.e. upright position (UP), aero position (AP), and fully dropped position (DP)) at various workloads (i.e. 0, 60, 100, 140, and 180 Watts).

The Tables 5.1 to 5.8 summarize all mean and standard deviations ($\bar{x}$ ± SD) and multiple comparison results of cardiorespiratory parameters. Including, the Figure 5.1 to 5.8 illustrate the multiple comparisons in form of bar graphs. Note: UP vs. AP = upright position versus aero position. AP vs. DP = aero position versus fully dropped position. DP vs. UP = fully dropped position versus upright position. *P*-value = probability value. NS = no significant difference between the mean values of those cycling positions at $P>0.05$. Significant difference between the mean values of those cycling positions at: * = $P<0.05$, ** = $P<0.01$, and *** = $P<0.001$. Additionally, because of a lot of the raw data, the online-record graphs for all mean of cardiorespiratory parameters are provided in Appendix A: Figure 13 to 20.

As can be seen in all illustrations of the average data, the cardiorespiratory responses continuously increased with the exercise intensity. All values were averaged over the last 1-min of each exercise bout. According to the statistical tests in this study, the one-way repeated measures analysis of variance (ANOVA) was used to test the effect of among three cycling positions on all the cardiorespiratory parameters at each workload. The results of the *F*-test revealed that, while the participants rested (0 Watts) and warmed-up (60 Watts), no significant differences ($P>0.05$) were found for the mean of all cardiorespiratory parameters among the three cycling positions. Whereas the increased workloads (100, 140, and 180 Watts), there were significant differences ($P<0.05$). Therefore, the multiple comparison by Turkey's *post-hoc* test was used to compare the mean of cardiorespiratory variables between UP versus AP, AP versus DP, and DP versus UP, respectively, in each workload as shown:

# CHAPTER 5: RESULTS

Table 5.1 Results from the statistical analysis for the average of the heart rate (HR) among the three cycling positions at each workload ($\bar{x}$ ± SD; $n$ = 24).

| Cardiorespiratory Parameters | Cycling Positions | Rest | Warm-up | Workloads | | |
|---|---|---|---|---|---|---|
| | | | | Stage 1 | Stage 2 | Stage 3 |
| | | (0 Watts) | (60 Watts) | (100 Watts) | (140 Watts) | (180 Watts) |
| **HR** | **UP** | 75.54 ± 10.73 | 102.15 ± 8.52 | **116.45** ± 9.71 | **134.80** ± 12.77 | **153.52** ± 15.67 |
| (beats·min$^{-1}$) | **AP** | 75.32 ± 8.76 | 102.60 ± 7.35 | **120.83** ± 10.79 | **139.00** ± 13.48 | **157.55** ± 15.01 |
| | **DP** | 75.38 ± 6.70 | 104.14 ± 7.04 | **128.72** ± 10.13 | **145.50** ± 13.16 | **163.77** ± 14.09 |
| | UP vs. AP | NS | NS | ** | ** | ** |
| | *P*-value | 0.900380 | 0.722628 | 0.001660 | 0.003719 | 0.009992 |
| | AP vs. DP | NS | NS | *** | *** | *** |
| | *P*-value | 0.960144 | 0.124914 | 0.000019 | 0.000263 | 0.000343 |
| | DP vs. UP | NS | NS | *** | *** | *** |
| | *P*-value | 0.919992 | 0.083099 | 0.000000 | 0.000000 | 0.000003 |

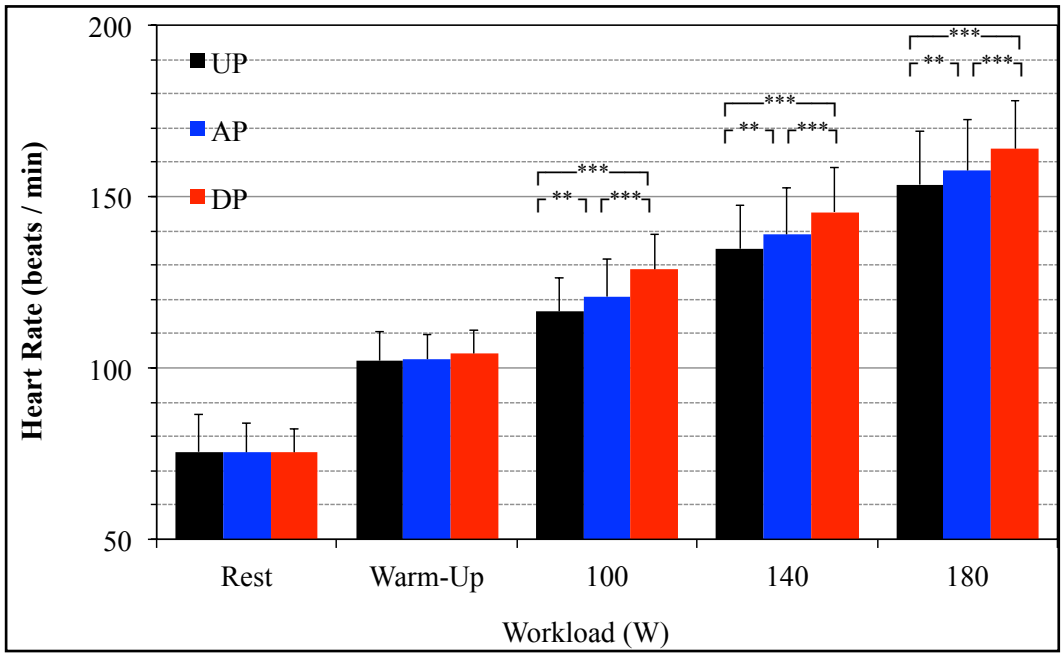


Figure 5.1 Multiple comparisons for the average of the heart rate among the three cycling positions.

Table 5.1 shows the resulting mean values of HR for UP, AP, and DP: at 100 Watts HR was 116.45, 120.83, and 128.72 beats·min$^{-1}$, respectively; at 140 Watts HR was 134.80, 139.00, and 145.50 beats·min$^{-1}$, respectively; and at 180 Watts HR was 153.52, 157.55, and 163.77 beats·min$^{-1}$, respectively. The *post-hoc* analysis revealed that UP yielded a significantly lower mean HR ($P$<0.01) than AP at every level of intensity. Likewise, AP yielded a significantly lower mean HR ($P$<0.001) than DP at every level of intensity. Thus, DP yielded a significantly higher mean HR ($P$<0.001) than UP at every level of intensity.

Table 5.2 Results from the statistical analysis for the average of the oxygen uptake ($\dot{V}O_2$) per body weight among the three cycling positions at each workload ($\bar{x}$ ± SD; $n$ = 24).

| Cardiorespiratory Parameters | Cycling Positions | Rest | Warm-up | Workloads | | |
|---|---|---|---|---|---|---|
| | | | | Stage 1 | Stage 2 | Stage 3 |
| | | (0 Watts) | (60 Watts) | (100 Watts) | (140 Watts) | (180 Watts) |
| $VO_2$ (ml·kg$^{-1}$·min$^{-1}$) | **UP** | 5.63 ± 1.16 | 17.88 ± 1.93 | **23.21** ± 2.49 | **29.30** ± 3.00 | **35.71** ± 3.53 |
| | **AP** | 5.36 ± 0.99 | 17.68 ± 1.28 | **24.18** ± 1.89 | **30.31** ± 2.79 | **37.23** ± 3.36 |
| | **DP** | 5.45 ± 0.88 | 17.91 ± 2.01 | **26.95** ± 1.85 | **32.40** ± 2.32 | **38.75** ± 2.69 |
| | UP vs. AP | NS | NS | ** | ** | ** |
| | *P*-value | 0.234840 | 0.543310 | 0.008790 | 0.005805 | 0.003840 |
| | AP vs. DP | NS | NS | *** | *** | *** |
| | *P*-value | 0.677641 | 0.560509 | 0.000000 | 0.000032 | 0.000502 |
| | DP vs. UP | NS | NS | *** | *** | *** |
| | *P*-value | 0.324063 | 0.930860 | 0.000000 | 0.000003 | 0.000003 |

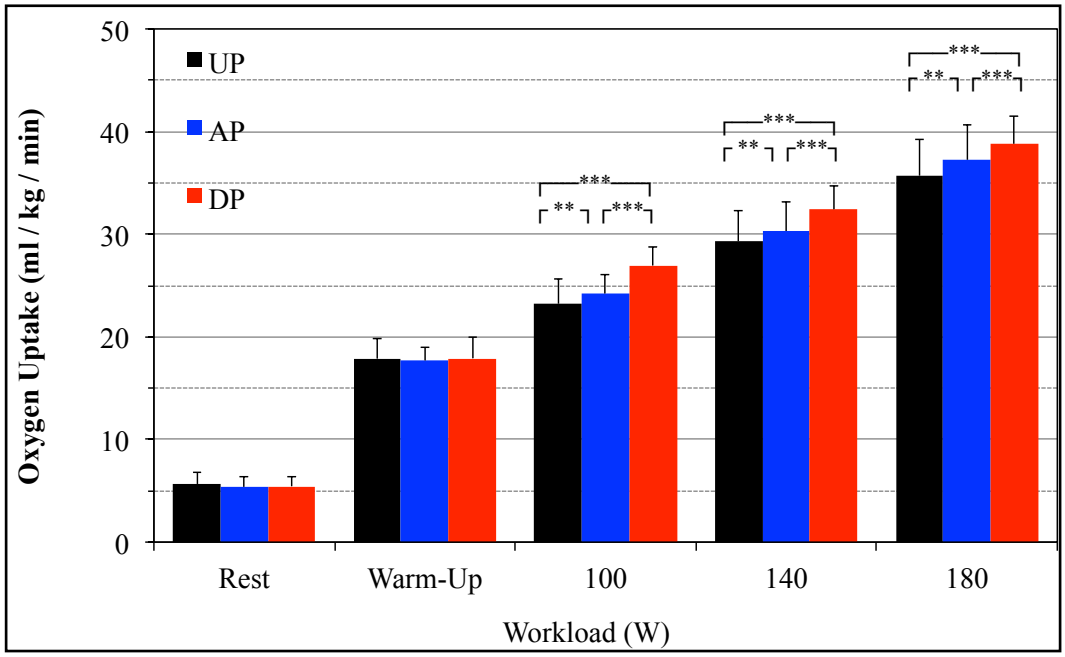


Figure 5.2 Multiple comparisons for the average of the oxygen uptake per body weight among the three positions.

Table 5.2 shows the obtained results that were found for the mean values of $\dot{V}O_2$ per body weight for UP, AP, and DP: at 100 Watts these were 23.21, 24.18, and 26.95 ml·kg$^{-1}$·min$^{-1}$, respectively; at 140 Watts they were 29.30, 30.31, and 32.40 ml·kg$^{-1}$·min$^{-1}$, respectively; and at 180 Watts they were 35.71, 37.23, and 38.75 ml·kg$^{-1}$·min$^{-1}$, respectively. The *post-hoc* analysis revealed that UP yielded a significantly lower mean $\dot{V}O_2$ per body weight ($P$<0.01) than AP at every level of intensity. Likewise, AP yielded a significantly lower mean $\dot{V}O_2$ per body weight ($P$<0.001) than DP at every level of intensity. Thus, DP yielded a significantly higher mean $\dot{V}O_2$ per body weight ($P$<0.001) than UP at every level of intensity.

Table 5.3 Results from the statistical analysis for the average of the oxygen uptake ($\dot{V}O_2$) among the three cycling positions at each workload ($\bar{x}$ ± SD; $n$ = 24).

| Cardiorespiratory Parameters | Cycling Positions | Rest (0 Watts) | Warm-up (60 Watts) | Workloads Stage 1 (100 Watts) | Stage 2 (140 Watts) | Stage 3 (180 Watts) |
|---|---|---|---|---|---|---|
| ***VO₂*** (ml·min$^{-1}$) | **UP** | 428.80 ± 80.73 | 1362.86 ± 112.52 | **1767.42** ± 118.23 | **2229.64** ± 103.58 | **2718.64** ± 135.74 |
| | **AP** | 411.45 ± 88.10 | 1354.87 ± 148.18 | **1847.99** ± 154.88 | **2311.40** ± 151.36 | **2841.13** ± 208.91 |
| | **DP** | 415.48 ± 62.19 | 1356.00 ± 113.97 | **2066.47** ± 232.70 | **2477.15** ± 210.36 | **2962.28** ± 226.01 |
| | UP vs. AP | NS | NS | ** | ** | ** |
| | *P*-value | 0.302481 | 0.737117 | 0.005607 | 0.006438 | 0.002977 |
| | AP vs. DP | NS | NS | *** | *** | *** |
| | *P*-value | 0.816005 | 0.761346 | 0.000000 | 0.000019 | 0.000404 |
| | DP vs. UP | NS | NS | *** | *** | *** |
| | *P*-value | 0.341620 | 0.943611 | 0.000000 | 0.000004 | 0.000003 |

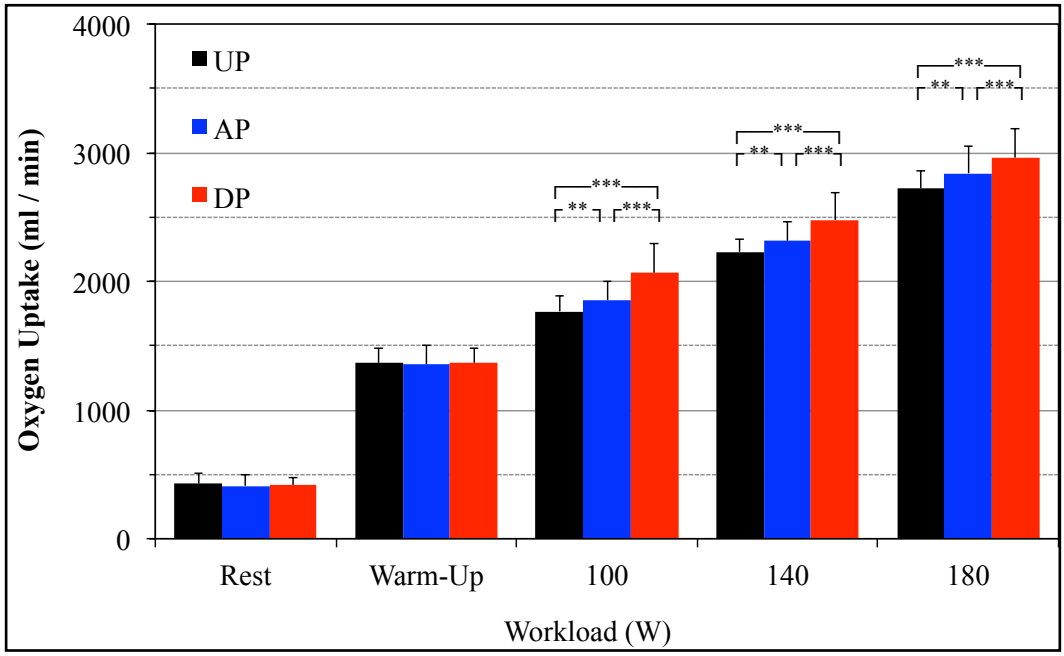


Figure 5.3 Multiple comparisons for the average of the oxygen uptake among the three cycling positions.

Table 5.3 shows the obtained results for the mean values of $\dot{V}O_2$ for UP, AP, and DP: at 100 Watts $\dot{V}O_2$ was 1767.42, 1847.99, and 2066.47 ml·min$^{-1}$, respectively; at 140 Watts the values were 2229.64, 2311.40, and 2477.15 ml·min$^{-1}$, respectively; and at 180 Watts they were 2718.64, 2841.13, and 2962.28 ml·min$^{-1}$, respectively. The *post-hoc* analysis revealed that UP yielded a significantly lower mean $\dot{V}O_2$ ($P$<0.01) than AP at every level of intensity. Likewise, AP yielded a significantly lower mean $\dot{V}O_2$ ($P$<0.001) than DP at every level of intensity. And therefore, DP yielded a significantly higher mean $\dot{V}O_2$ ($P$<0.001) than UP at every level of intensity.

Table 5.4 Results from the statistical analysis for the average of the carbon dioxide output ($\dot{V}CO_2$) among the three cycling positions at each workload ($\bar{x}$ ± SD; $n$ = 24).

| Cardiorespiratory Parameters | Cycling Positions | Rest | Warm-up | Workloads | | |
|---|---|---|---|---|---|---|
| | | | | Stage 1 | Stage 2 | Stage 3 |
| | | (0 Watts) | (60 Watts) | (100 Watts) | (140 Watts) | (180 Watts) |
| ***VCO₂*** | **UP** | 352.02 ± 73.65 | 1096.97 ± 97.82 | **1639.02** ± 134.95 | **2129.35** ± 131.68 | **2685.30** ± 179.93 |
| (ml·min$^{-1}$) | **AP** | 335.12 ± 68.86 | 1099.69 ± 131.41 | **1719.83** ± 167.50 | **2218.13** ± 196.39 | **2856.87** ± 262.68 |
| | **DP** | 346.08 ± 55.24 | 1114.61 ± 116.31 | **1939.67** ± 242.11 | **2362.75** ± 202.17 | **2976.32** ± 277.95 |
| | UP vs. AP | NS | NS | ** | ** | *** |
| | *P*-value | 0.298812 | 0.904952 | 0.008008 | 0.007937 | 0.000206 |
| | AP vs. DP | NS | NS | *** | ** | * |
| | *P*-value | 0.426265 | 0.646191 | 0.000004 | 0.001555 | 0.025985 |
| | DP vs. UP | NS | NS | *** | *** | *** |
| | *P*-value | 0.659855 | 0.549242 | 0.000001 | 0.000020 | 0.000014 |

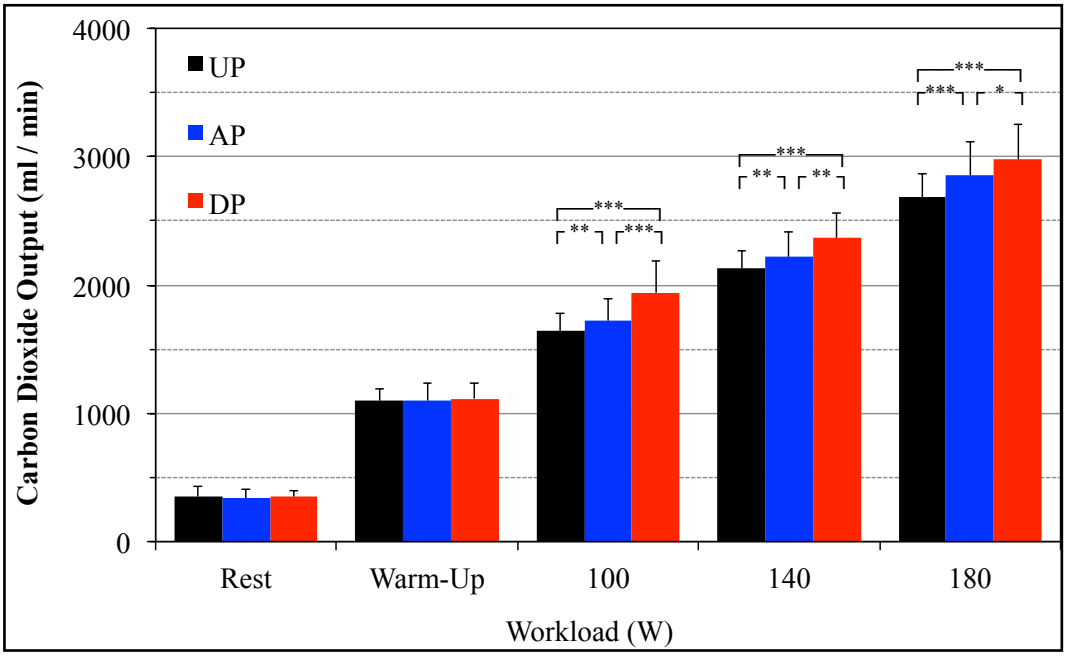


Figure 5.4 Multiple comparisons for the average of the carbon dioxide output among the three cycling positions.

Table 5.4 shows the results that were found for the mean values of $\dot{V}CO_2$ for UP, AP, and DP: at 100 Watts these were 1639.02, 1719.83, and 1939.67 ml·min$^{-1}$, respectively; at 140 Watts they were 2129.35, 2218.13, and 2362.75 ml·min$^{-1}$, respectively; and at 180 Watts they were 2685.30, 2856.87, and 2976.32 ml·min$^{-1}$, respectively. The *post-hoc* analysis revealed that UP yielded a significantly lower mean $\dot{V}CO_2$ than AP ($P$<0.01 at 100 and 140 Watts; $P$<0.001 at 180 Watts). Likewise, AP yielded a significantly lower mean $\dot{V}CO_2$ than DP ($P$<0.001 at 100 Watts; $P$<0.01 at 140 Watts; $P$<0.05 at 180 Watts). And consequently, DP yielded a significantly higher mean $\dot{V}CO_2$ ($P$<0.001) than UP at every level of intensity.

Table 5.5 Results from the statistical analysis for the average of the respiratory exchange rate (RER) among the three cycling positions at each workload ( $\bar{x}$ ± SD; $n$ = 24).

| Cardiorespiratory Parameters | Cycling Positions | Rest | Warm-up | Workloads | | |
|---|---|---|---|---|---|---|
| | | | | Stage 1 | Stage 2 | Stage 3 |
| | | (0 Watts) | (60 Watts) | (100 Watts) | (140 Watts) | (180 Watts) |
| **RER** | **UP** | 0.82 ± 0.05 | 0.81 ± 0.03 | **0.93** ± 0.04 | **0.96** ± 0.04 | **0.99** ± 0.05 |
| (unitless) | **AP** | 0.82 ± 0.06 | 0.81 ± 0.06 | **0.93** ± 0.05 | **0.96** ± 0.06 | **1.01** ± 0.08 |
| | **DP** | 0.83 ± 0.06 | 0.82 ± 0.04 | **0.94** ± 0.05 | **0.95** ± 0.05 | **1.01** ± 0.07 |
| | UP vs. AP | NS | NS | NS | NS | NS |
| | *P*-value | 0.977385 | 0.560181 | 0.666891 | 0.623453 | 0.147811 |
| | AP vs. DP | NS | NS | NS | NS | NS |
| | *P*-value | 0.344937 | 0.815531 | 0.471539 | 0.670711 | 0.925252 |
| | DP vs. UP | NS | NS | NS | NS | NS |
| | *P*-value | 0.297884 | 0.284648 | 0.240708 | 0.963710 | 0.094881 |

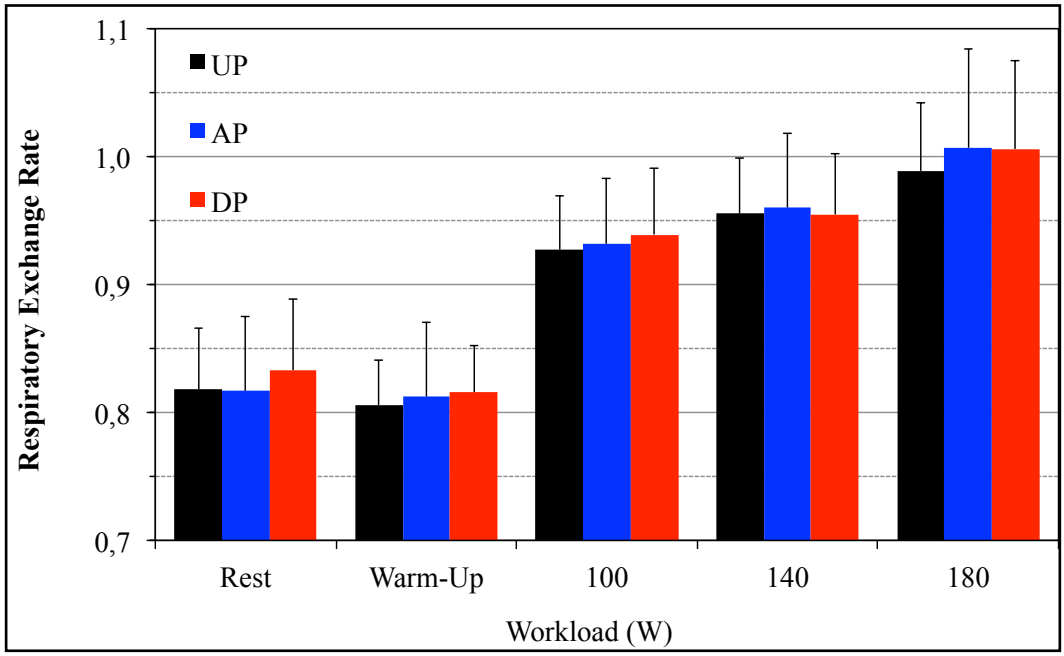


Figure 5.5 Multiple comparisons for the average of the respiratory exchange rate among the three cycling positions.

Table 5.5 shows the results that were found for the mean values of RER for UP, AP, and DP: at 100 Watts these were 0.93, 0.93, and 0.94, respectively; at 140 Watts they were 0.96, 0.96, and 0.95, respectively; and at 180 Watts they were 0.99, 1.01, and 1.01, respectively. In contrast with the other variables, the *post-hoc* analysis revealed that there are no significant differences for the mean RER ($P$>0.05) between UP and AP, AP and DP, and DP and UP, at either level of intensity.

Table 5.6 Results from the statistical analysis for the average of the tidal volume ($V_T$) among the three cycling positions at each workload ($\bar{x}$ ± SD; $n$ = 24).

| Cardiorespiratory Parameters | Cycling Positions | Rest | Warm-up | Workloads | | |
|---|---|---|---|---|---|---|
| | | | | Stage 1 | Stage 2 | Stage 3 |
| | | (0 Watts) | (60 Watts) | (100 Watts) | (140 Watts) | (180 Watts) |
| $V_T$ | **UP** | 0.96 ± 0.32 | 1.60 ± 0.31 | **2.06** ± 0.47 | **2.26** ± 0.40 | **2.58** ± 0.42 |
| (L) | **AP** | 0.93 ± 0.30 | 1.60 ± 0.29 | **1.88** ± 0.33 | **2.16** ± 0.40 | **2.48** ± 0.42 |
| | **DP** | 0.95 ± 0.29 | 1.58 ± 0.27 | **1.91** ± 0.37 | **2.19** ± 0.42 | **2.52** ± 0.54 |
| | UP vs. AP | NS | NS | * | * | * |
| | *P*-value | 0.501421 | 0.871613 | 0.018028 | 0.039668 | 0.046550 |
| | AP vs. DP | NS | NS | NS | NS | NS |
| | *P*-value | 0.403272 | 0.687191 | 0.613119 | 0.562775 | 0.441196 |
| | DP vs. UP | NS | NS | NS | NS | NS |
| | *P*-value | 0.873539 | 0.823110 | 0.105464 | 0.229244 | 0.373110 |

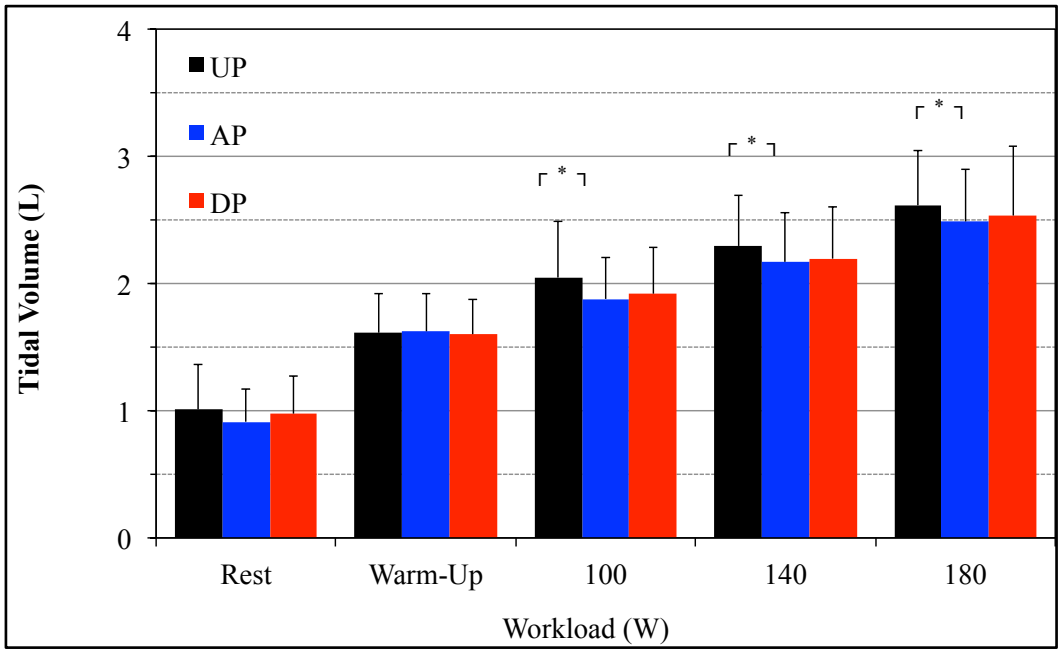


Figure 5.6 Multiple comparisons for the average of the tidal volume among the three cycling positions.

Table 5.6 shows the results that were found for the mean values of $V_T$ for UP, AP, and DP: at 100 Watts they were 2.06, 1.88, and 1.91 L, respectively; at 140 Watts they were 2.26, 2.16, and 2.19 L, respectively; and at 180 Watts they were 2.58, 2.48, and 2.52 L, respectively. The *post-hoc* analysis revealed that only UP yielded a significantly higher mean $V_T$ ($P$<0.05) than AP at every level of intensity. Whereas for AP versus DP and for DP versus UP, no significant difference was found in the mean $V_T$ ($P$>0.05) at either level of intensity. However, it is likely that UP yielded a higher mean $V_T$ than DP and AP, respectively, at every level of intensity.

Table 5.7 Results from the statistical analysis for the average of the breathing frequency (BF) among the three cycling positions at each workload ( $\bar{x}$ ± SD; $n$ = 24).

| Cardiorespiratory Parameters | Cycling Positions | Rest | Warm-up | Workloads | | |
|---|---|---|---|---|---|---|
| | | | | Stage 1 | Stage 2 | Stage 3 |
| | | (0 Watts) | (60 Watts) | (100 Watts) | (140 Watts) | (180 Watts) |
| **BF** | **UP** | 14.34 ± 3.87 | 19.61 ± 5.33 | **21.16** ± 4.75 | **24.39** ± 5.95 | **27.39** ± 10.45 |
| (breaths·min$^{-1}$) | **AP** | 13.63 ± 3.84 | 19.25 ± 4.05 | **24.50** ± 5.99 | **27.14** ± 8.09 | **31.61** ± 11.63 |
| | **DP** | 14.24 ± 4.37 | 20.37 ± 4.23 | **27.95** ± 7.49 | **30.71** ± 10.59 | **35.79** ± 16.33 |
| | UP vs. AP | NS | NS | ** | ** | *** |
| | *P*-value | 0.265294 | 0.678555 | 0.001963 | 0.003002 | 0.000195 |
| | AP vs. DP | NS | NS | *** | ** | * |
| | *P*-value | 0.408003 | 0.071055 | 0.000139 | 0.001884 | 0.014613 |
| | DP vs. UP | NS | NS | *** | *** | *** |
| | *P*-value | 0.890871 | 0.449889 | 0.000009 | 0.000031 | 0.000159 |

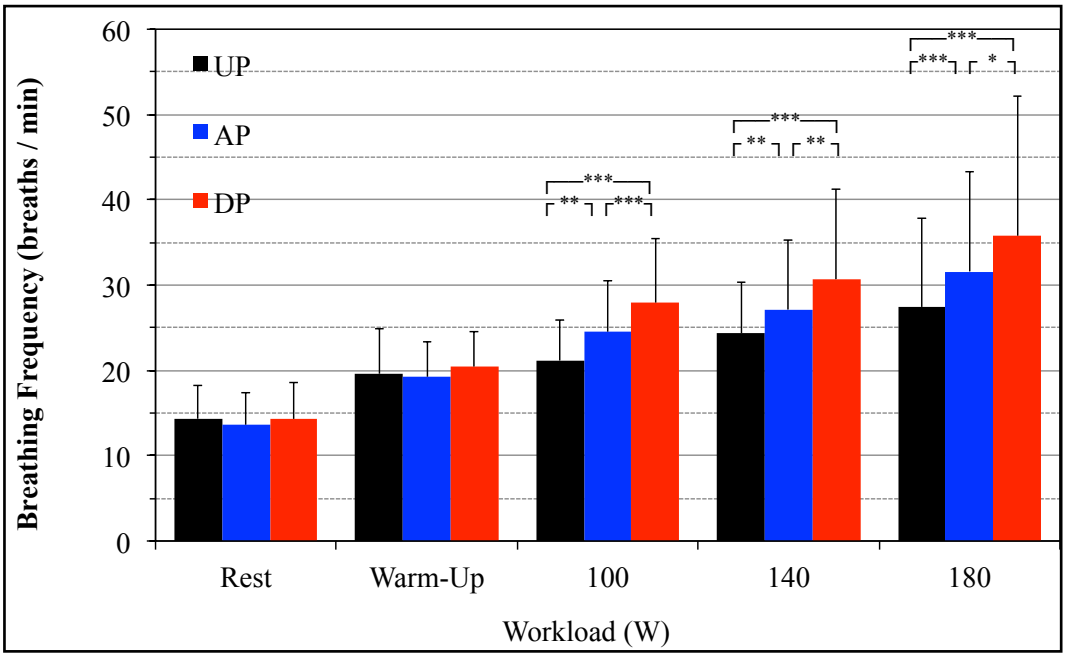


Figure 5.7 Multiple comparisons for the average of the breathing frequency among the three cycling positions.

Table 5.7 shows the results that were found for the mean values of BF for UP, AP, and DP: at 100 Watts they were 21.16, 24.50, and 27.95 breaths·min$^{-1}$, respectively; at 140 Watts they were 24.39, 27.14, and 30.71 breaths·min$^{-1}$, respectively; and at 180 Watts they were 27.39, 31.61, and 35.79 breaths·min$^{-1}$, respectively. The *post-hoc* analysis revealed that UP yielded a significantly lower mean BF than AP ($P$<0.01 at 100 and 140 Watts; $P$<0.001 at 180 Watts). Likewise, AP yielded a significantly lower mean BF than DP ($P$<0.001 at 100 Watts; $P$<0.01 at 140 Watts; $P$<0.05 at 180 Watts;). Consequently, DP yielded a significantly higher mean BF ($P$<0.001) than UP at every level of intensity.

Table 5.8 Results from the statistical analysis for the average of the minute ventilation ($\dot{V}_E$) among the three cycling positions at each workload ($\bar{x}$ ± SD; $n$ = 24).

| Cardiorespiratory Parameters | Cycling Positions | Rest | Warm-up | Workloads | | |
|---|---|---|---|---|---|---|
| | | | | Stage 1 | Stage 2 | Stage 3 |
| | | (0 Watts) | (60 Watts) | (100 Watts) | (140 Watts) | (180 Watts) |
| $V_E$ | **UP** | 12.33 ± 2.60 | 29.22 ± 5.01 | **40.94** ± 5.09 | **52.58** ± 6.98 | **67.09** ± 15.75 |
| (L·min$^{-1}$) | **AP** | 11.43 ± 2.04 | 29.07 ± 4.35 | **43.80** ± 5.56 | **55.55** ± 8.27 | **74.61** ± 16.85 |
| | **DP** | 12.15 ± 1.92 | 30.45 ± 3.58 | **50.75** ± 9.24 | **63.03** ± 11.64 | **83.23** ± 21.07 |
| | UP vs. AP | NS | NS | ** | ** | *** |
| | *P*-value | 0.089100 | 0.844348 | 0.003526 | 0.001705 | 0.000014 |
| | AP vs. DP | NS | NS | *** | *** | *** |
| | *P*-value | 0.126399 | 0.095441 | 0.000002 | 0.000023 | 0.000165 |
| | DP vs. UP | NS | NS | *** | *** | *** |
| | *P*-value | 0.714585 | 0.177706 | 0.000001 | 0.000002 | 0.000002 |

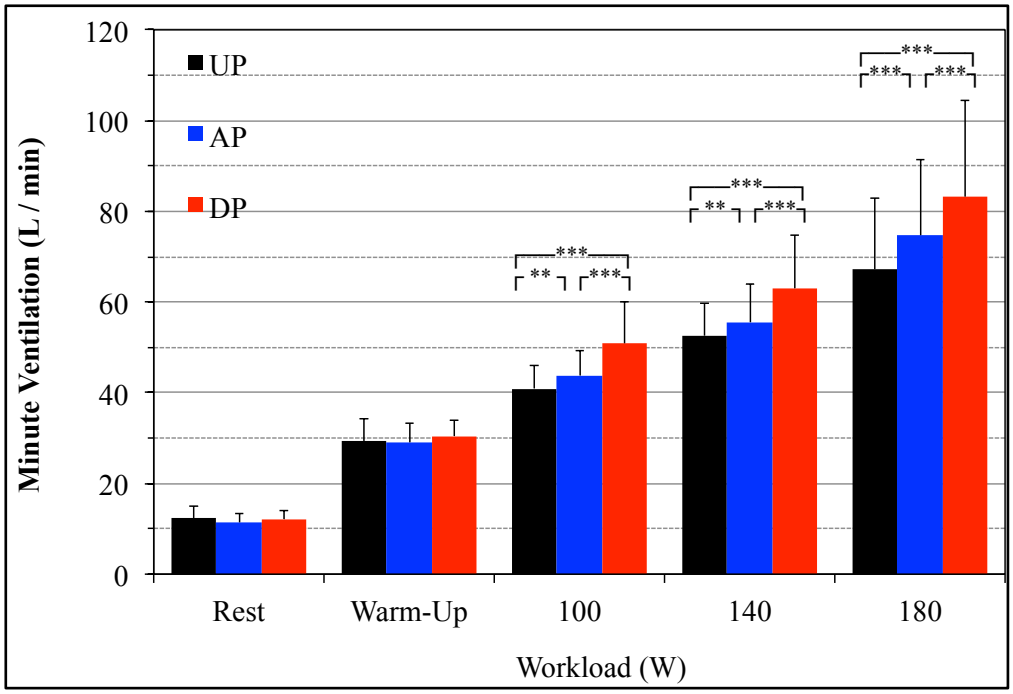


Figure 5.8 Multiple comparisons for the average of the minute ventilation among the three cycling positions.

Table 5.8 shows the results that were found for the mean values of $\dot{V}_E$ for UP, AP, and DP: at 100 Watts they were 40.94, 43.80, and 50.75 L·min$^{-1}$, respectively; at 140 Watts they were 52.58, 55.55, and 63.03 L·min$^{-1}$, respectively; and at 180 Watts they were 67.09, 74.61, and 83.23 L·min$^{-1}$, respectively. The *post-hoc* analysis revealed that UP yielded a significantly lower mean $\dot{V}_E$ than AP ($P$<0.01 at 100 and 140 Watts; $P$<0.001 at 180 Watts). Likewise, AP yielded a significantly lower mean $\dot{V}_E$ ($P$<0.001) than DP at every level of intensity. And thus, DP yielded a significantly higher mean $\dot{V}_E$ ($P$<0.001) than UP at every level of intensity.

In summary, the presented results for statistical comparisons between UP vs. AP, AP vs. DP, and DP vs. UP, show that almost all the mean cardiorespiratory parameters were significantly higher in DP than in AP and UP at the workloads of 100, 140, and 180 Watts, respectively. Especially the mean of HR, $\dot{V}O_2$, and $\dot{V}_E$ during increased workloads, had significantly higher ($P$<0.001) means in DP than in AP and UP, respectively. Furthermore, AP also yielded significantly higher ($P$<0.01 and P<0.001 for $\dot{V}_E$ at 180 Watts) means of HR, $\dot{V}O_2$, and $\dot{V}_E$ than UP. Regarding the mean of BF as well as the mean of $\dot{V}CO_2$ at almost all workloads, DP yielded significant differences ($P$<0.001 for DP vs. UP; $P$<0.01 and $P$<0.001 for AP vs. DP) at higher levels compared to UP and AP. But at a workload of 180 Watts, the mean of BF and $\dot{V}CO_2$ between AP and DP showed a significant difference ($P$<0.05) at a lower level. Moreover, UP compared with AP also yielded a high significant difference ($P$<0.01) at workloads of 100 and 140 Watts, while at 180 Watts an even higher significant difference ($P$<0.001) was yielded. In contrast, the mean of $V_T$ was rather different from the other parameters, as the statistical comparison indicated that there was no statistically significant difference ($P$>0.05) for DP compared with UP and AP at each workload, while the mean of $V_T$ for UP versus AP at workloads of 100, 140 and 180 Watts did yield a significant difference ($P$<0.05). In addition, no significant difference ($P$>0.05) existed for the mean of RER in any workload among the three cycling positions.

5.2 Effects of cycling positions on aerodynamic parameters.

Overall, four participants *(n=4)* were selected from the twenty-four participants *(n=24)* for the coasting down investigation of the three cycling position. As in the sprioergometry testing, the cycling positions consisted of the upright position (UP), the aero position (AP), and the fully dropped position (DP). In order to determine the various aerodynamic parameters leading to the cycling motion models of the three cycling positions, the following important parameters were calculated step by step. The measured velocities from the coasting down tests were fitted by the velocity-time function, which consisted of two main parameters. Given the fitted models, the parameter of the initial velocity ( $v_i$ ) and the parameter of the aerodynamic constant divided by mass ( $K_m$ ) were both obtained from the best-parameter value estimation for the fitting curve by applying the least-squares method with the Solver program in Microsoft Excel® version 2011. As a constant value, the parameter of the acceleration of rolling friction ( $a_{rol}$ ) was obtained from the coefficient of rolling friction ($\mu$) multiplied with the gravitational force ($g$), leading to the calculation

of the rolling friction ( $F_{rol}$ ). Consequently, when the parameters $v_i$, $K_m$ and $a_{rol}$ were known, the cycling motion models of functions such as velocity versus time $v(t)$, displacement versus time $s(t)$, and velocity versus displacement $v(s)$ could be generated.

Moreover, the estimated parameter $K_m$ was also used to calculate the values of the aerodynamic constant (*K*), the drag area ( $C_D \cdot A$ ), and the drag coefficient ( $C_D$ ). The estimated parameter $v_i$ can also be used to calculate the parameter of the aerodynamic drag ( $F_{aer}$ ) and the net force ( $F_{net}$ ). Other factors that needed to be measured for the calculation of coasting down parameters were the air density ($\rho$) in order to determine $C_D \cdot A$, the projected frontal area (*A*) for the calculation of $C_D$ and the rolling friction coefficient ($\mu$) and the total mass of a rider-bicycle (*m*) for the calculation of $F_{rol}$.

Finally, once these parameters were known, the cycling motion models for the net force with respect to velocity $F_{net}(v)$ and the mechanical power with respect to velocity $P(v)$ were created. Regarding the representation of the results from this study, both illustrations of numerical tables (Table 5.9 to 5.22) and graphs (Figure 5.9 to 5.16) are summarized in form of the mean value with standard deviation ( $\bar{x}$ ± SD) of the four subjects (*n=4*). In addition, the values $\bar{x}$ ± SD of each subject and each position in the numerical tables were averaged over twenty trials *(n=20)* of the coasting down test.

In order to understand the image of the graph from the test, Figure 5.9 demonstrates a measured velocity of (A) 6.9 $m \cdot s^{-1}$ (25 $km \cdot h^{-1}$), (B) 4.2 $m \cdot s^{-1}$ (15 $km \cdot h^{-1}$), and (C) both of these measured velocities in a upright position (UP) of a trial from twenty trials with a curve fitting as a functional model of velocity with respect to time $v(t)$ according to Equation 2.26. The Figure 5.9 (A) and (B) are zoomed in on velocity 6 to 8 $m \cdot s^{-1}$ and at time 1 to 3 s, and on velocity 3 to 5 $m \cdot s^{-1}$ and at time 17.523 to 20.523 s. The graphs of the two velocities were recorded once every millisecond (1/1000), which were measured from the tachogenerator (speed sensor), and then were transmitted to the receiver module. The fluctuation of the graphs will depend on the velocity and the cycling position of cyclist and bicycle combination.

As mentioned earlier in Chapter 2.3, the measured data is fitted by using the least-squares method, which allows us to filter experimental error, but still accommodate the unusual responses by maximising the likelihood of the measured data (Draper & Smith, 1998). Using this method we can extract the trends from the measured data rather than prescribing them by fitting the mathematical model.

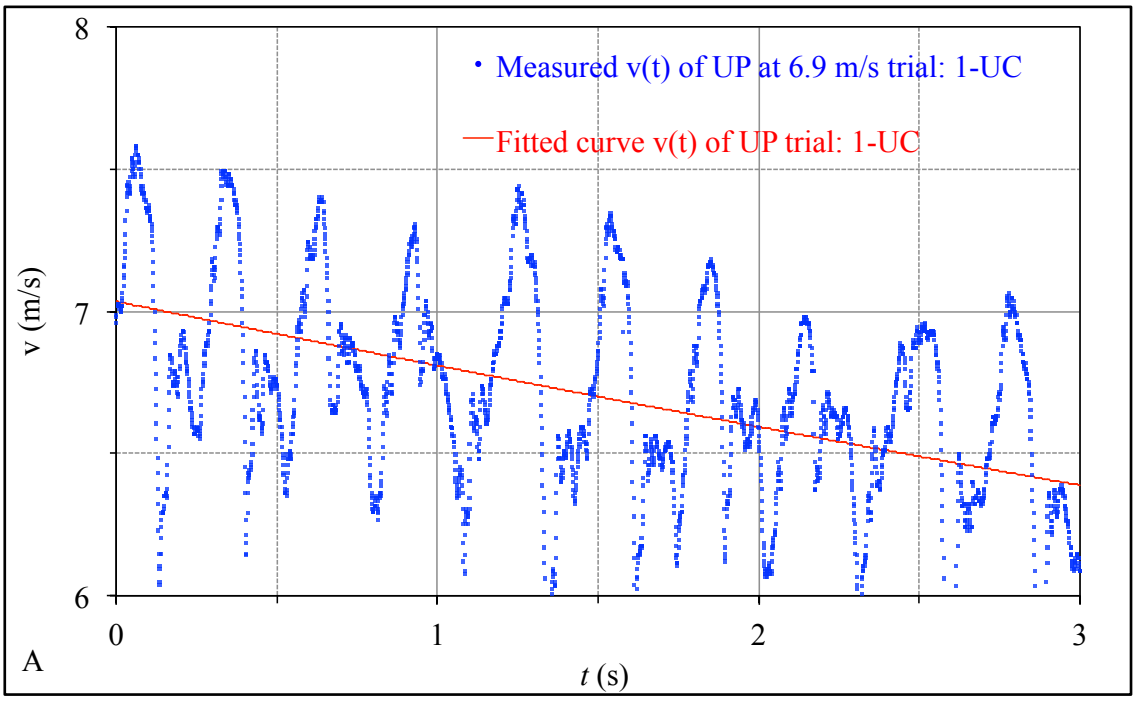
8
7
6
v (m/s)
0
1
2
3
t (s)
Measured v(t) of UP at 6.9 m/s trial: 1-UC
Fitted curve v(t) of UP trial: 1-UC
A

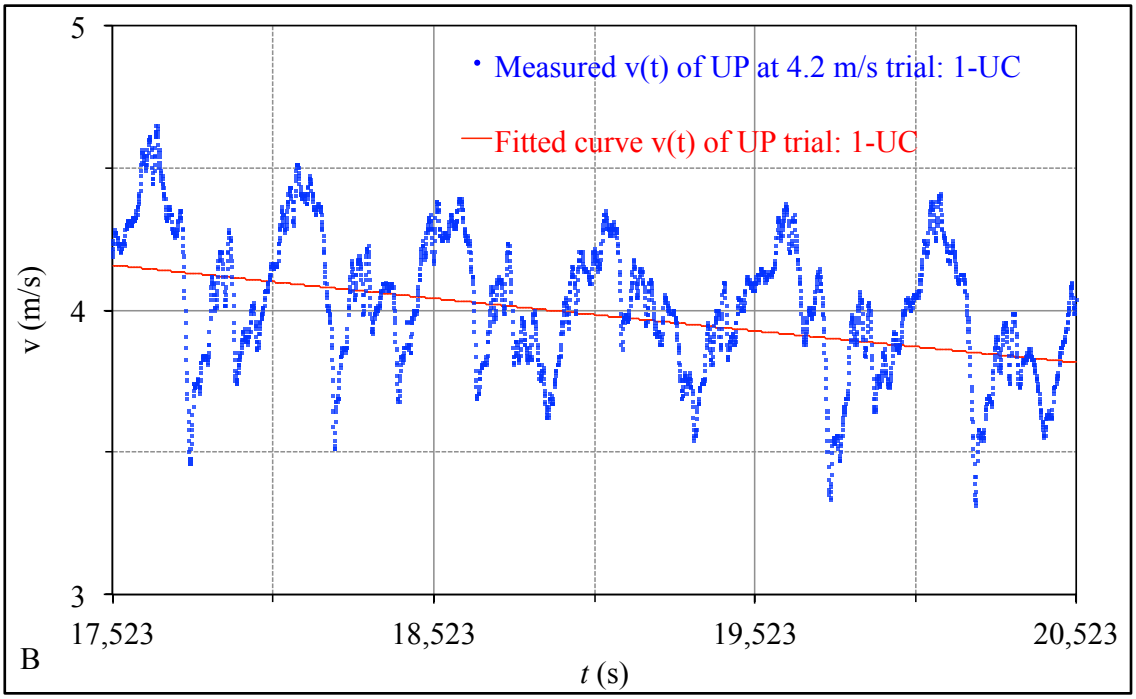
5
4
3
v (m/s)
17,523
18,523
19,523
20,523
t (s)
Measured v(t) of UP at 4.2 m/s trial: 1-UC
Fitted curve v(t) of UP trial: 1-UC
B

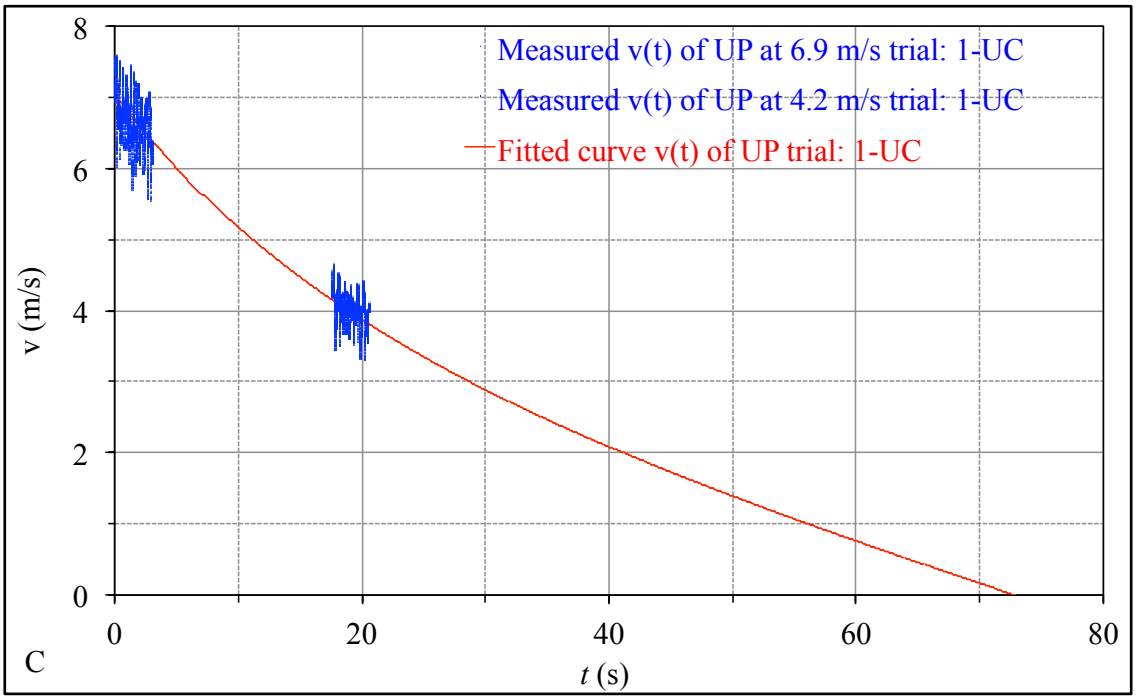


Figure 5.9 An example of two measured velocities: (A) at 6.9 $m \cdot s^{-1}$ (25 $km \cdot h^{-1}$) and (B) at 4.2 $m \cdot s^{-1}$ (15 $km \cdot h^{-1}$) (blue dot) from two coasting down tests in an upright position (UP) is fitted by (C) a curve as a functional model of velocity (v) with respect to time ($t$) (red line).

Table 5.9 Average of the initial velocity ( $v_i$ ) from the parameter estimation with Solver.

| | | $v_i$ ($m \cdot s^{-1}$) | | |
|---|---|---|---|---|
| No. | Code-Subject | **UP** | **AP** | **DP** |
| 1 | 01-WN | 7.06 ± 0.04 | 7.04 ± 0.08 | 6.96 ± 0.16 |
| 2 | 06-UC | 7.02 ± 0.10 | 6.91 ± 0.09 | 7.06 ± 0.16 |
| 3 | 09-HL | 6.97 ± 0.13 | 6.87 ± 0.10 | 6.84 ± 0.18 |
| 4 | 15-ES | 7.08 ± 0.15 | 6.97 ± 0.06 | 7.03 ± 0.07 |
| ($n$=4) | $\bar{x}$ ± SD | **7.03** ± 0.05 | **6.95** ± 0.08 | **6.97** ± 0.10 |

Table 5.10 Average of the aerodynamic constant divided by mass ( $K_m$ ) from the parameter estimation with Solver.

| | | $K_m$ ($m^{-1}$) | | |
|---|---|---|---|---|
| No. | Code-Subject | **UP** | **AP** | **DP** |
| 1 | 01-WN | 0.00389 ± 0.00008 | 0.00219 ± 0.00006 | 0.00123 ± 0.00006 |
| 2 | 06-UC | 0.00334 ± 0.00008 | 0.00210 ± 0.00005 | 0.00118 ± 0.00006 |
| 3 | 09-HL | 0.00303 ± 0.00006 | 0.00202 ± 0.00004 | 0.00112 ± 0.00005 |
| 4 | 15-ES | 0.00308 ± 0.00007 | 0.00200 ± 0.00005 | 0.00115 ± 0.00007 |
| ($n$=4) | $\bar{x}$ ± SD | **0.00333** ± 0.00039 | **0.00208** ± 0.00009 | **0.00117** ± 0.00005 |

After the parameter $v_i$ is estimated from least-squares method, Table 5.9 reveals the mean values of $v_i$ of UP, AP, and DP to be 7.03, 6.95, and 6.97 $m \cdot s^{-1}$, respectively, as estimated by Solver program. In principle, the same velocity is required for all three cycling positions and the estimated mean $v_i$ of the three cycling positions are actually all relatively equal to approximately 25 $km \cdot h^{-1}$ or 6.94 $m \cdot s^{-1}$.

Likewise, Table 5.10 reveals the results for the values of the parameter $K_m$ that were directly estimated by Solver. In descending order, the mean $K_m$ of UP, AP, and DP are 0.00333, 0.00208, and 0.00117 $m^{-1}$, respectively. The estimated parameters show that riding in DP yields a lower value of $K_m$ than AP and UP, respectively. Finally, the mean values of the individual best estimations for $v_i$ (Table 5.9) and $K_m$ (Table 5.10) can be represented in form of the best-fitting curves for the three cycling positions:

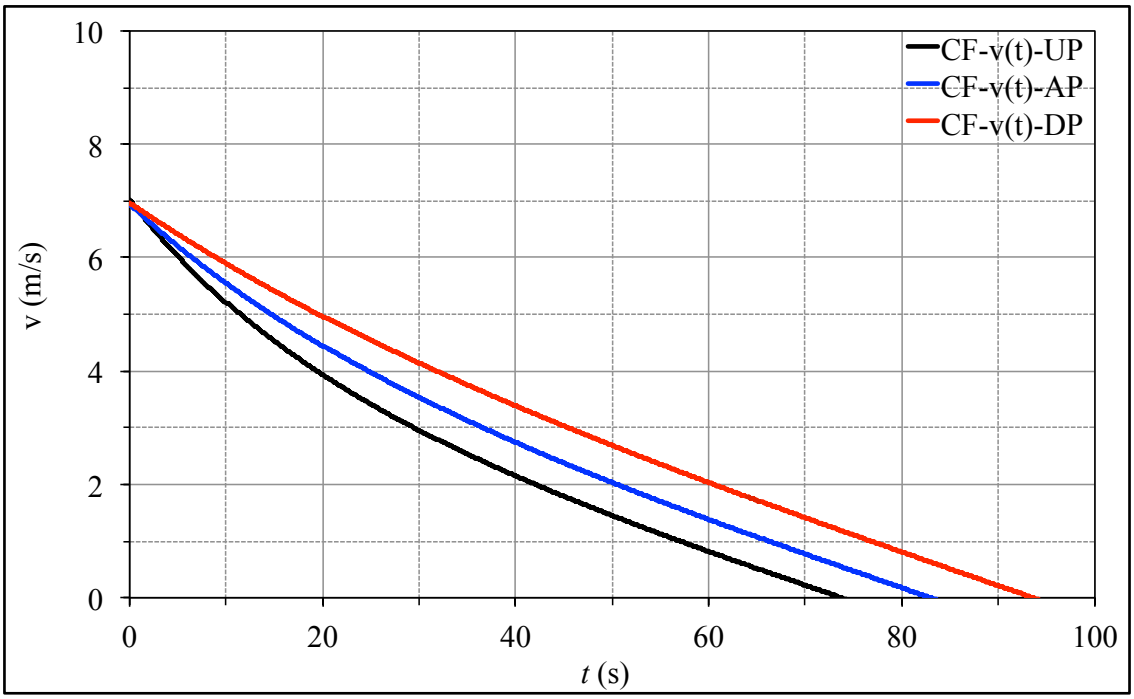


Figure 5.10 Curve fitting (CF) as functional model of velocity (v) with respect to time (*t*) during coasting down cycling motion for UP (black line), AP (blue line), and DP (red line).

Figure 5.10 shows the functional model $v(t)$ or the coasting down fitted curves. It is clear that a longer stopping time is needed for DP than for AP and UP, respectively. The curves depend on the estimated parameters $v_i$ and $K_m$, including the assumed parameter $a_{rol}$. The model curves describe the observed decreasing velocity in form of a fitted

tan-function, according to Equation (2.26). According to Tables 5.9 and 5.10, together with Figure 5.10, the fitted curves are obtained from the following mean values for UP: $v_i$ = 7.03 m·s$^{-1}$ and $K_m$ = 0.00333 m$^{-1}$; for AP: $v_i$ = 6.95 m·s$^{-1}$ and $K_m$ = 0.00208 m$^{-1}$; and for DP: $v_i$ = 6.97 m·s$^{-1}$ and $K_m$ = 0.00117 m$^{-1}$. As a constant value, the parameter $a_{rol}$ is determined from the relationship of rolling friction ($F_{rol}$) for all positions. According to Equation (2.18) and (2.19): $a_{rol} = \frac{F_{rol}}{m} = \frac{\mu \cdot m \cdot g}{m} = \mu \cdot g$, with assuming $\mu$ = 0.006 and $g$ = 9.807 m·s$^{-2}$. Consequently, $a_{rol}$ = 0.059 m·s$^{-2}$. The fact that the curves start from the same point can be explained by the fact that $v_i$ is similar and $a_{rol}$ is constant.

Note that the curve of DP has less curvature than those of AP and UP. That means that at the same $v_i$, the coasting down cycling in DP will stop at a different position. In other words, the coating-down time of DP is more than that of AP and UP, respectively. It is the fact that DP yields a lower value of $K_m$ than AP and UP, respectively, which mainly affects the curvature. Although the cycling motion was not measured until complete standstill, $t_{max}$, or the final time ($t_f$), can be calculated. The functions of $v(t)$ from Figure 5.10 can be used to predict the maximal time ($t_{max}$) or the time at which the final velocity is zero ($v_f$ = 0 m·s$^{-1}$) by substituting the known values of $v_i$, $K_m$, and $a_{rol}$ into Equation (2.27).

Table 5.11 Average of the maximal time ($t_{max}$).

| | | $t_{max}$ (s) | | |
|---|---|---|---|---|
| No. | Code-Subject | **UP** | **AP** | **DP** |
| 1 | 01-WN | 70.56 ± 0.43 | 82.46 ± 0.49 | 92.71 ± 1.65 |
| 2 | 06-UC | 73.62 ± 0.63 | 82.56 ± 0.60 | 94.20 ± 1.20 |
| 3 | 09-HL | 75.38 ± 0.74 | 83.01 ± 0.64 | 93.21 ± 1.70 |
| 4 | 15-ES | 75.61 ± 0.90 | 83.82 ± 0.62 | 94.40 ± 1.14 |
| (*n*=4) | $\bar{x}$ ± SD | **73.79** ± 2.33 | **82.96** ± 0.62 | **93.63** ± 0.80 |

After substitution the parameter values, Table 5.11 reveals the mean values of $t_{max}$ for UP, AP, and DP, which are 73.79, 82.96, and 93.63 s, respectively. The calculated results predict that DP results in a larger value for $t_{max}$ than AP and UP, respectively. Apart from the model function $v(t)$, a model for the function of displacement ($s$) over time ($t$) can be obtained from the known parameters $v_i$, $K_m$, and $a_{rol}$ by entering them into Equation (2.31).

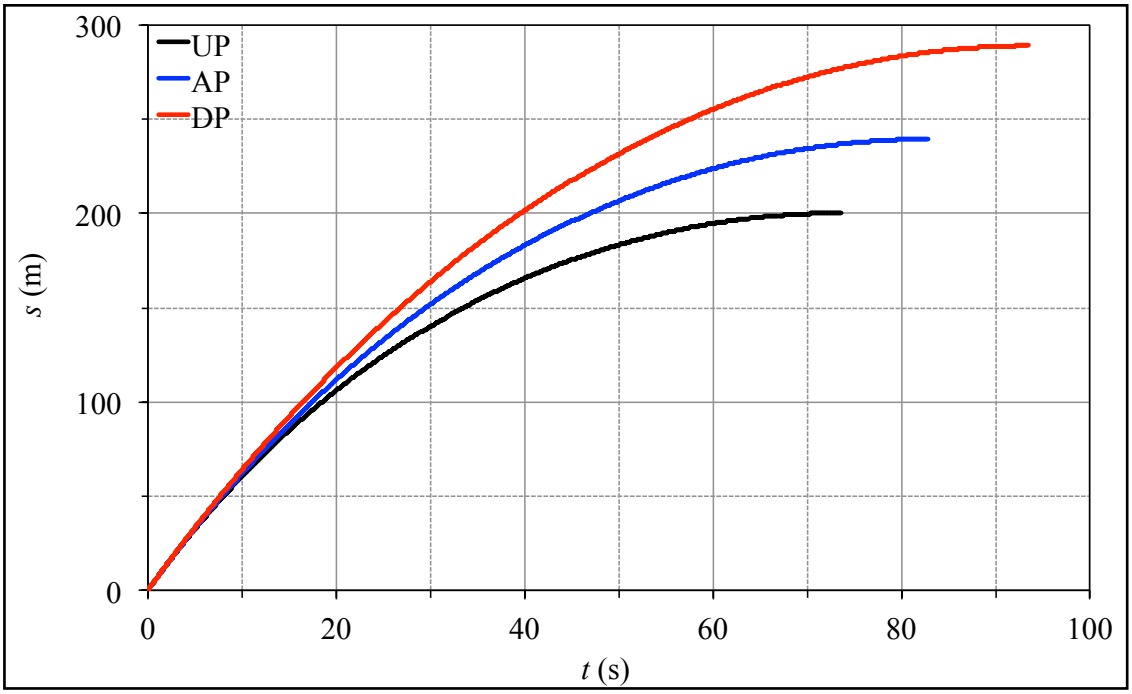


Figure 5.11 Functional model of displacement ($s$) with respect to time ($t$) during the coasting down cycling motion for UP (black line), AP (blue line), and DP (red line).

Figure 5.11 represents the functional model of displacement with respect to time ( $s(t)$ ) during the coasting down cycling motion for UP, AP, and DP. The curves show that the total $s$ in DP is farther than in AP and UP, respectively, as well as that the total time $t$ of DP is greater than that of AP and UP, respectively. The reason for this is that the value of $K_m$ is lower in DP than in AP and UP, respectively. When considering the important factor of Equation (2.31), the curvature of $s(t)$ depends on the values of $v_i$, $a_{rol}$, and, especially, $K_m$. The maximal displacement ( $s_{max}$ ) for the curves of UP, AP, and DP in Figure 5.11 can be found by substituting the value of $t_{max}$ from Table 5.11 into Equation (2.31).

Table 5.12 Average of the maximal displacement ( $s_{max}$ ).

| | | $s_{max}$ (m) | | |
|---|---|---|---|---|
| No. | Code-Subject | **UP** | **AP** | **DP** |
| 1 | 01-WN | 187.42 ± 1.98 | 238.70 ± 2.90 | 284.59 ± 10.73 |
| 2 | 06-UC | 199.74 ± 3.61 | 237.16 ± 3.78 | 293.37 ± 8.23 |
| 3 | 09-HL | 206.61 ± 4.70 | 238.42 ± 4.21 | 284.50 ± 11.20 |
| 4 | 15-ES | 209.10 ± 5.60 | 243.71 ± 3.57 | 293.82 ± 6.37 |
| ($n$=4) | $\bar{x}$ ± SD | **200.72** ± 9.71 | **239.50** ± 2.89 | **289.07** ± 5.23 |

The data in Table 5.12 reveals that the mean values of $s_{max}$ for UP, AP, and DP are 200.72, 239.50, and 289.07 m, respectively. The calculated results predict that DP yields a higher value of $s_{max}$ than AP and UP, respectively, which can also be seen in Figure 5.11. In other words, a further distance can be covered in DP than in AP and UP, respectively.

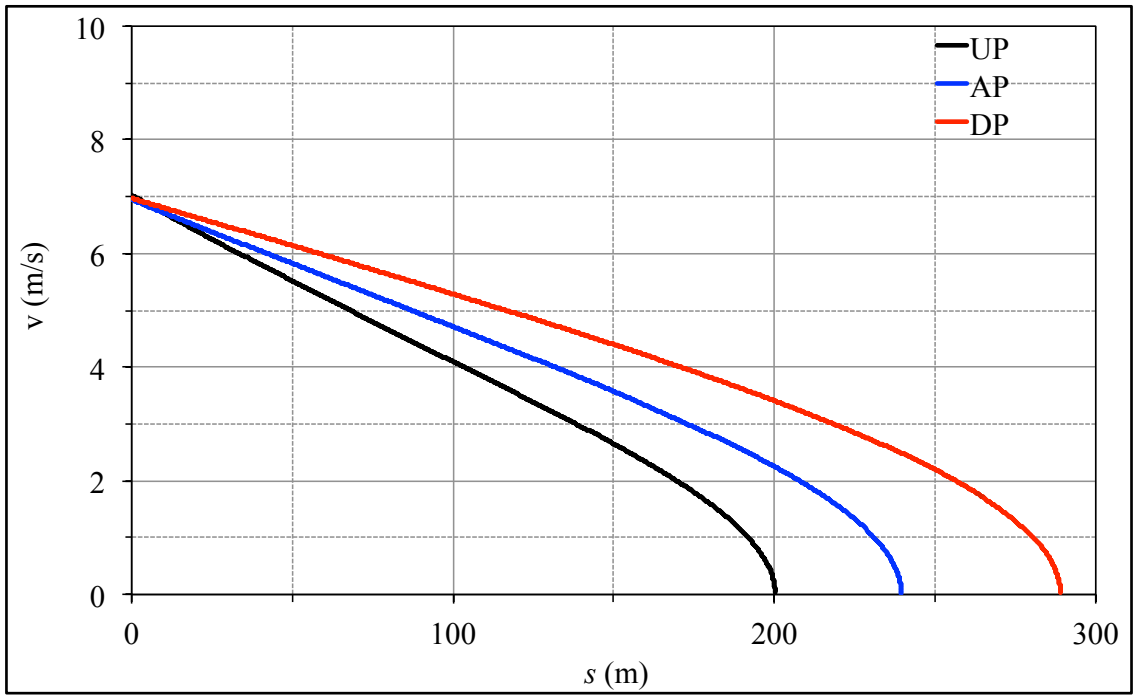


Figure 5.12 Functional model of velocity (v) with respect to displacement ($s$) during the coasting down cycling motion for UP (black line), AP (blue line), and DP (red line).

Furthermore, entering the known parameters $v_i$, $K_m$, and $a_{rol}$ into Equation (2.32), yields the function of velocity over displacement $v(s)$, as shown in Figure 5.12. The graphs show that, when starting from the same $v_i$ in each riding position, DP is coasted down farther than AP and UP, respectively, because the value of $K_m$ is lower for DP than for the others. That is, at the final velocity of zero ($v_f = 0$ m·s$^{-1}$), for UP $s$ = 200.72 m, for AP $s$ = 239.50 m, and for DP $s$ = 289.07 m. In other words, at the same distance or position, the velocity is higher in DP than in AP and UP, respectively.

The next step is to calculate various important aerodynamic parameters for the three cycling positions, with the known aerodynamic constant divided by mass ($K_m$), which is defined as: $K_m = \frac{K}{m} = \frac{0.5 \cdot \rho \cdot C_D \cdot A}{m}$. With the

estimated parameter $K_m$, firstly, one can calculate the values of the aerodynamic constant (*K*) by multiplying this parameter with the total mass, which is a combination of the cyclist's mass and the bicycle mass.

Table 5.13 Average of the total mass ( $m$ ) of the cyclist ( $m_C$ ), bicycle ( $m_B$ ), and aero handlebars ( $m_A$ ).

| | | $m_C$ (kg) | $m_B$ (kg) | $m_A$ (kg) | $m$ (kg) | | |
|---|---|---|---|---|---|---|---|
| No. | Code-Subject | | | | **UP** | **AP** | **DP** |
| 1 | 01-WN | 80.0 | 16.6 | 0.6 | 96.6 | 97.2 | 96.6 |
| 2 | 06-UC | 77.5 | 16.6 | 0.6 | 94.1 | 94.7 | 94.1 |
| 3 | 09-HL | 75.5 | 16.6 | 0.6 | 92.1 | 92.7 | 92.1 |
| 4 | 15-ES | 71.0 | 16.6 | 0.6 | 87.6 | 88.2 | 87.6 |
| (*n*=4) | $\bar{x}$ ± SD | **76.0** ± 3.8 | | | **92.6** ± 3.8 | **93.2** ± 3.8 | **92.6** ± 3.8 |

Before the coasting down trials in each cycling position, all subjects were weighed. Table 5.13 shows the total mass as a measured value: $m = m_C + m_B$ . *Note*: for AP, the aero handlebar mass is 0.6 kg which leads to a little more added mass. Thus, the mean values of *m* for UP and DP are 92.6 kg (76.0 kg + 16.6 kg), and the mean value of *m* for AP is 93.2 kg (76.0 kg + 16.6 kg + 0.6 kg), whereas both values are rather similar. The *m* is an important parameter, which is needed for the calculation of the aerodynamic constant (*K*).

Table 5.14 Average of the aerodynamic constant (*K*).

| | | *K* (kg·m$^{-1}$) | | |
|---|---|---|---|---|
| No. | Code-Subject | **UP** | **AP** | **DP** |
| 1 | 01-WN | 0.376 ± 0.007 | 0.213 ± 0.006 | 0.119 ± 0.006 |
| 2 | 06-UC | 0.314 ± 0.007 | 0.198 ± 0.005 | 0.111 ± 0.006 |
| 3 | 09-HL | 0.279 ± 0.005 | 0.187 ± 0.004 | 0.103 ± 0.005 |
| 4 | 15-ES | 0.269 ± 0.006 | 0.177 ± 0.004 | 0.101 ± 0.006 |
| (*n*=4) | $\bar{x}$ ± SD | **0.310** ± 0.048 | **0.194** ± 0.016 | **0.108** ± 0.008 |

The parameter *K* in Table 5.14 is determined from: $K = K_m \cdot m = \frac{K}{m} \cdot m$ , where the values for $K_m$ are given in Table 5.10 and the values for *m* are given in Table 5.13. As a result, Table 5.14 reveals the mean values of *K* for UP, AP and DP to be 0.310, 0.194, and 0.108 kg·m$^{-1}$, respectively. The calculated results indicate that DP results in lower values of *K* than AP and UP, respectively.

In the next step, the parameter *K* is used to calculate the drag area ( $C_D \cdot A$ ), for which the value of the air density ( $\rho$ ) also needs to be known. According to the theory, the air density is mass divided by unit volume of the Earth's atmosphere, which varies with the temperature (T) and relative humidity (RH), and decreases with increasing altitude. Accordingly, while the coasting down tests were being performed in each cycling position, the temperature and

the relative humidity were measured and recorded in order to calculate the value of the air density ( $\rho$ ) by using an online air density calculator (www.denysschen.com/catalogue/density.aspx).

Table 5.15 Average of the temperature (T), the relative humidity (RH), and the air density ( $\rho$ ).

| | | T (°C) | | | RH (%) | | |
|---|---|---|---|---|---|---|---|
| No. | Code-Subject | **UP** | **AP** | **DP** | **UP** | **AP** | **DP** |
| 1 | 01-WN | 22.0 ± 0.3 | 22.0 ± 0.3 | 25.0 ± 0.3 | 43.2 ± 1.7 | 38.2 ± 0.9 | 50.0 ± 1.6 |
| 2 | 06-UC | 22.4 ± 0.2 | 20.9 ± 0.4 | 23.5 ± 0.2 | 43.9 ± 0.2 | 52.3 ± 0.5 | 42.7 ± 0.3 |
| 3 | 09-HL | 24.7 ± 0.2 | 23.6 ± 0.2 | 26.7 ± 0.3 | 43.6 ± 0.3 | 53.7 ± 0.3 | 39.0 ± 0.3 |
| 4 | 15-ES | 23.8 ± 0.3 | 23.1 ± 0.3 | 22.4 ± 0.4 | 41.7 ± 1.4 | 47.2 ± 0.3 | 45.8 ± 1.0 |
| (*n*=4) | $\bar{x}$ ± SD | **23.2** ± 1.3 | **22.4** ± 1.2 | **24.4** ± 1.9 | **43.1** ± 1.0 | **47.9** ± 7.0 | **44.4** ± 4.7 |

| | | $\rho$ (kg·m$^{-3}$) | | |
|---|---|---|---|---|
| No. | Code-Subject | **UP** | **AP** | **DP** |
| 1 | 01-WN | 1.186 ± 0.002 | 1.186 ± 0.002 | 1.172 ± 0.002 |
| 2 | 06-UC | 1.184 ± 0.001 | 1.190 ± 0.001 | 1.179 ± 0.001 |
| 3 | 09-HL | 1.174 ± 0.001 | 1.178 ± 0.001 | 1.166 ± 0.001 |
| 4 | 15-ES | 1.178 ± 0.001 | 1.181 ± 0.001 | 1.183 ± 0.002 |
| (*n*=4) | $\bar{x}$ ± SD | **1.181** ± 0.005 | **1.184** ± 0.005 | **1.175** ± 0.008 |

Table 5.15 reveals the mean values of T for UP, AP, and DP to be 23.2, 22.4, and 24.4 °C, respectively; the mean values of RH for UP, AP, and DP to be 43.1, 47.9, and 44.4 %, respectively; and the consequent mean values of $\rho$ for UP, AP, and DP to be 1.181, 1.184, and 1.175 kg·m$^{-3}$, respectively. The $\rho$ is an important parameter, which is needed for the calculation of the drag area ( $C_D \cdot A$ ).

Table 5.16 Average of the drag area ( $C_D \cdot A$ ).

| | | $C_D \cdot A$ (m$^2$) | | |
|---|---|---|---|---|
| No. | Code-Subject | **UP** | **AP** | **DP** |
| 1 | 01-WN | 0.633 ± 0.012 | 0.360 ± 0.009 | 0.203 ± 0.009 |
| 2 | 06-UC | 0.530 ± 0.013 | 0.334 ± 0.008 | 0.188 ± 0.009 |
| 3 | 09-HL | 0.475 ± 0.009 | 0.317 ± 0.006 | 0.176 ± 0.008 |
| 4 | 15-ES | 0.458 ± 0.011 | 0.299 ± 0.007 | 0.171 ± 0.010 |
| (*n*=4) | $\bar{x}$ ± SD | **0.524** ± 0.079 | **0.327** ± 0.026 | **0.184** ± 0.014 |

The values of $C_D \cdot A$ in Table 5.16 are calculated from: $C_D \cdot A = \frac{2 \cdot K}{\rho}$, where the values for *K* are taken from Table 5.14 and the values for $\rho$ are taken from Table 5.15. As a result, Table 5.16 reveals the mean values of $C_D \cdot A$ for UP, AP, and DP to be 0.524, 0.327, and 0.184 m$^2$, respectively. The calculated results indicate that DP yields lower

values for $C_D \cdot A$ than AP and UP, respectively. In the next step, the parameter $C_D \cdot A$ is used to calculate the drag coefficient ($C_D$), for which the value of the projected frontal area ($A$) is needed.

Table 5.17 Average of the projected frontal area ($A$).

| | | $A$ (m$^2$) | | |
|---|---|---|---|---|
| No. | Code-Subject | **UP** | **AP** | **DP** |
| 1 | 01-WN | 0.544 | 0.466 | 0.439 |
| 2 | 06-UC | 0.517 | 0.447 | 0.422 |
| 3 | 09-HL | 0.496 | 0.429 | 0.413 |
| 4 | 15-ES | 0.494 | 0.424 | 0.412 |
| ($n$=4) | $\overline{x}$ ± SD | **0.513** ± 0.023 | **0.441** ± 0.019 | **0.421** ± 0.013 |

All cycling positions were photographed with a calibration frame of a known area. The actual total $A$ of the subject-bicycle in square meters (m$^2$) of each digitized image was determined by dividing the area of the digitized image by the area of the corresponding calibration image and multiplying by the known area of the calibration square frame. Table 5.17 reveals the mean values of $A$ for UP, AP, and DP to be 0.513, 0.441, and 0.421 m$^2$, respectively. As expected, the $A$ of DP is less than that of AP and UP, respectively. As the values of $A$ are now known, the drag coefficient ($C_D$) can be determined.

Table 5.18 Average of the drag coefficient ($C_D$).

| | | $C_D$ | | |
|---|---|---|---|---|
| No. | Code-Subject | **UP** | **AP** | **DP** |
| 1 | 01-WN | 1.165 ± 0.023 | 0.772 ± 0.020 | 0.462 ± 0.021 |
| 2 | 06-UC | 1.024 ± 0.024 | 0.745 ± 0.018 | 0.447 ± 0.022 |
| 3 | 09-HL | 0.958 ± 0.018 | 0.740 ± 0.015 | 0.426 ± 0.021 |
| 4 | 15-ES | 0.925 ± 0.022 | 0.706 ± 0.017 | 0.414 ± 0.023 |
| ($n$=4) | $\overline{x}$ ± SD | **1.018** ± 0.106 | **0.741** ± 0.027 | **0.437** ± 0.021 |

The values of $C_D$ in Table 5.18 are calculated from: $C_D = \frac{C_D \cdot A}{A}$, where the values for $C_D \cdot A$ are taken from Table 5.16 and the values for $A$ are taken from Table 5.17. As a result, Table 5.18 reveals the mean values of $C_D$ for UP, AP, and DP to be 1.018, 0.741, and 0.437 (dimensionless), respectively. The calculated results indicate that DP yields lower values of $C_D$ than AP and UP, respectively.

The next step is to model various important forces during cycling for the three cycling positions, which need to rely the known above calculated mean values.

Table 5.19 Average of the rolling friction ( $F_{rol}$ ).

| | | $F_{rol}$ (N) | | |
|---|---|---|---|---|
| No. | Code-Subject | **UP** | **AP** | **DP** |
| 1 | 01-WN | 5.68 | 5.72 | 5.68 |
| 2 | 06-UC | 5.54 | 5.57 | 5.54 |
| 3 | 09-HL | 5.42 | 5.45 | 5.42 |
| 4 | 15-ES | 5.15 | 5.19 | 5.15 |
| (*n*=4) | $\bar{x}$ ± SD | **5.45** ± 0.22 | **5.48** ± 0.22 | **5.45** ± 0.22 |

As a constant value for the entire coasting down test, the rolling friction ( $F_{rol}$ ) can be determined by: $F_{rol} = a_{rol} \cdot m$ , where the values for m are taken from Table 5.13. According to Equation (2.20), $a_{rol}$ is calculated as: $a_{rol} = \mu \cdot g = 0.059$ m·s$^{-2}$, where $\mu$ = 0.006 (dimensionless) and $g$ = 9.807 m·s$^{-2}$. Thus, Table 5.19 reveals that the mean value of $F_{rol}$ for UP and DP is 5.45 N, and the mean value of $F_{rol}$ for AP is 5.48 N.

Table 5.20 Average of the aerodynamic drag ( $F_{aer}$ ).

| | | $F_{aer}$ (N) | | |
|---|---|---|---|---|
| No. | Code-Subject | **UP** | **AP** | **DP** |
| 1 | 01-WN | 18.73 ± 0.46 | 10.58 ± 0.45 | 5.77 ± 0.36 |
| 2 | 06-UC | 15.47 ± 0.63 | 9.48 ± 0.40 | 5.54 ± 0.46 |
| 3 | 09-HL | 13.55 ± 0.57 | 8.81 ± 0.35 | 4.80 ± 0.35 |
| 4 | 15-ES | 13.51 ± 0.60 | 8.58 ± 0.25 | 4.99 ± 0.30 |
| (*n*=4) | $\bar{x}$ ± SD | **15.31** ± 2.45 | **9.36** ± 0.90 | **5.28** ± 0.45 |

At a velocity of 25 km·h$^{-1}$, the values of $F_{aer}$ can be determined by: $F_{aer} = K \cdot \mathrm{v}^2$ , where the values for *K* are taken from Table 5.14 and the values for $\mathrm{v} = \mathrm{v}_i$ are taken from Table 5.9. Thus, Table 5.20 reveals the mean values of $F_{aer}$ for UP, AP, and DP to be 15.31, 9.36, and 5.28 N, respectively. The calculated results indicate that DP yields a lower value of $F_{aer}$ than AP and UP, respectively.

Table 5.21 Average of the net force ( $F_{net}$ ).

| | | $F_{net}$ (N) | | |
|---|---|---|---|---|
| No. | Code-Subject | **UP** | **AP** | **DP** |
| 1 | 01-WN | 24.42 ± 0.46 | 16.30 ± 0.45 | 11.45 ± 0.36 |
| 2 | 06-UC | 21.00 ± 0.63 | 15.05 ± 0.40 | 11.08 ± 0.46 |
| 3 | 09-HL | 18.97 ± 0.57 | 14.27 ± 0.35 | 10.22 ± 0.35 |
| 4 | 15-ES | 18.66 ± 0.60 | 13.77 ± 0,25 | 10.15 ± 0.30 |
| (*n*=4) | $\bar{x}$ ± SD | **20.76** ± 2.65 | **14.85** ± 1.10 | **10.72** ± 0.64 |

At a velocity of 25 km·h$^{-1}$, the values of the net force ( $F_{net}$ ) can be determined by: $F_{net} = F_{rol} + F_{aer}$ , where the values for $F_{rol}$ are taken from Table 5.19 and the values for $F_{aer}$ are taken from Table 5.20. Thus, Table 5.21 reveals the mean values of $F_{net}$ for UP, AP, and DP to be 20.76, 14.85, and 10.72 N, respectively. The calculated results indicate that DP yields a lower value of $F_{net}$ than AP and UP, respectively.

The above calculated mean values were obtained from the coasting down tests at a velocity of 25 and 15 km·h$^{-1}$. The $F_{aer}$ is calculated from $F_{aer} = K \cdot v^2$ , with the value of *K* as obtained through the value estimation of $K_m$ , and also the known v ( $= v_i$ ). The $F_{rol}$ as constant value is assumed from $F_{rol} = a_{rol} \cdot m$ , with the known values of $\mu$ , *g*, and *m*. Finally, the estimated parameter of *K* and the assumed constant parameter $F_{rol}$ were used to model the function of the net force with respect to velocity as: $F_{net} = F_{rol} + K \cdot v^2$ , which is shown following:

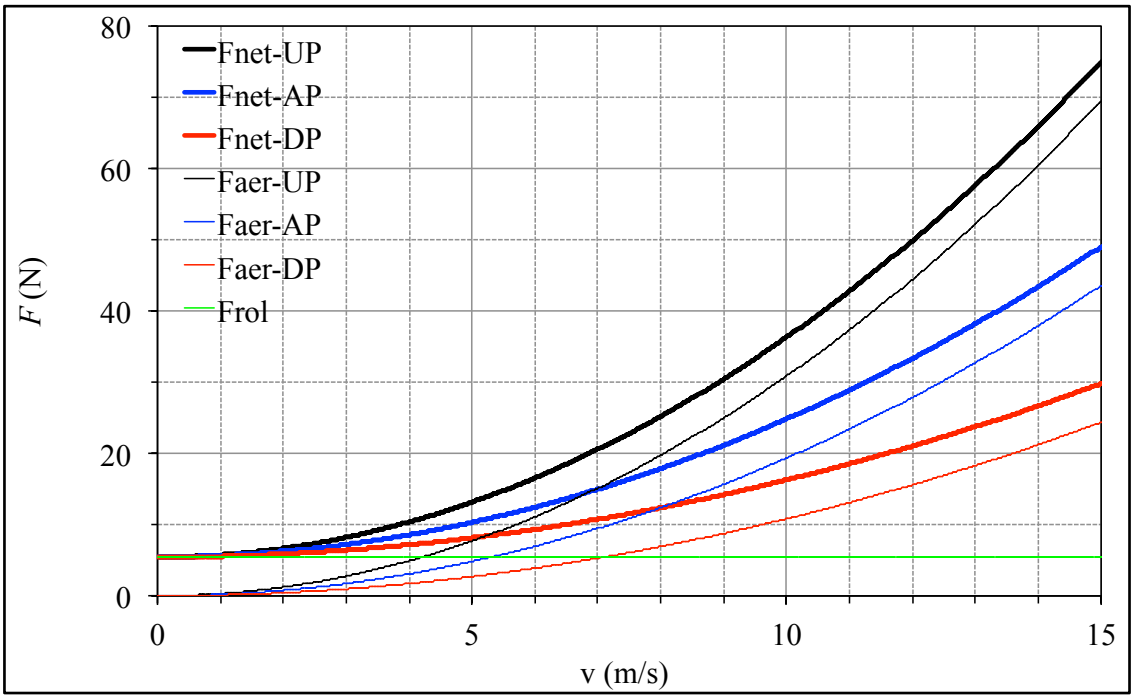


Figure 5.13 Functional models of the net force ( $F_{net}$ ) with respect to velocity (v) during cycling in UP, AP, and DP.

The models in Figure 5.13 represent the functions of net force and increased velocity for the three cycling positions that result from the summation of rolling resistance and air drag: $F_{net} = F_{rol} + K \cdot v^2$ , where $F_{rol} = \mu \cdot g \cdot m$

and $K = 0.5 \cdot \rho \cdot C_D \cdot A$ . Figure 5.13 consists of the functional models of $F_{rol}(\mathrm{v})$ , $F_{aer}(\mathrm{v})$ , and $F_{net}(\mathrm{v})$ . The graphical lines of $F_{aer}$ for UP (thin black line), AP (thin blue line), and DP (thin red line) vary extremely with the velocity as $\mathrm{v}^2$ , whereas the $F_{rol}$ (horizontal thin green line) is always a constant value that does not depend on v. As a result, $F_{aer}(\mathrm{v})$ will cause the graphical lines of $F_{net}$ for UP (solid black line), AP (solid blue line), and DP (solid red line) to also vary with v. As can be seen, the model indicates that DP yields lower values of $F_{aer}$ and $F_{net}$ than AP and UP, respectively.

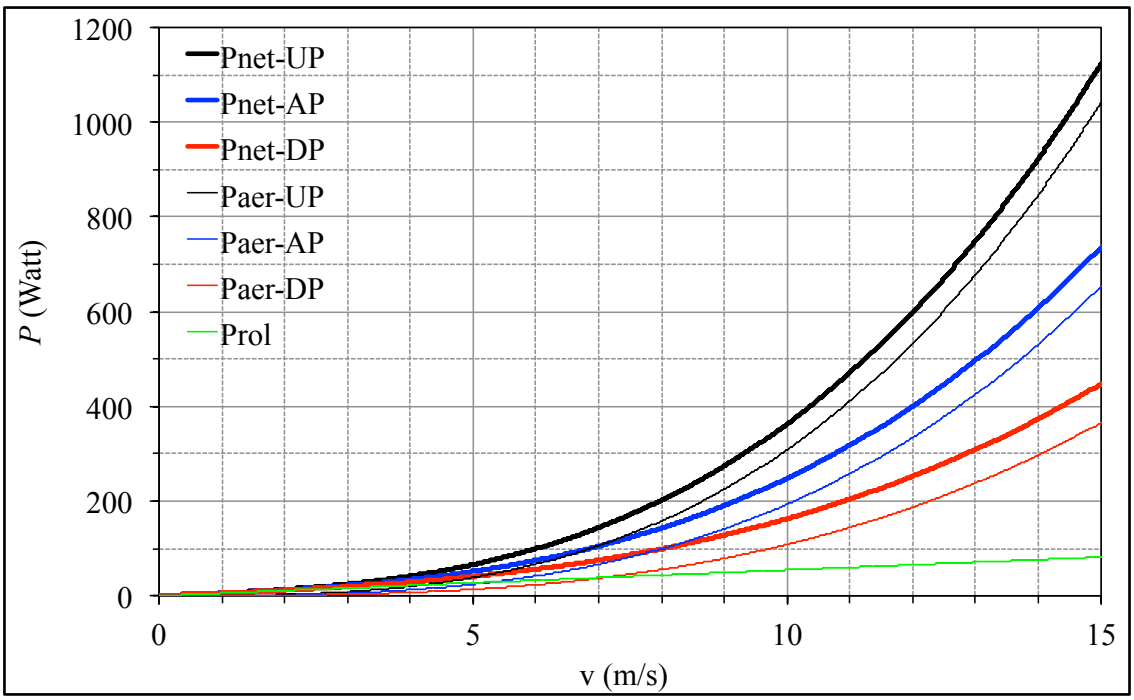


Figure 5.14 Functional models of mechanical power (*P*) with respect to velocity (v) during cycling in UP, AP, and DP.

The models in Figure 5.14 are calculated by: $P_{net} = F_{net} \cdot \mathrm{v} = (F_{rol} + F_{aer}) \cdot \mathrm{v} = F_{rol} \cdot \mathrm{v} + K \cdot \mathrm{v}^3$ . Figure 5.14 consists of the functional models of $P_{rol}(\mathrm{v})$ , $P_{aer}(\mathrm{v})$, and $P_{net}(\mathrm{v})$ . The models show that the magnitude of the mechanical power of the rolling resistance ( $P_{rol} = F_{rol} \cdot \mathrm{v}$ ) (thin green line) is very small when compared to the mechanical power of the aerodynamic drag ( $P_{aer} = F_{aer} \cdot \mathrm{v}$ ) for UP (thin black line), AP (thin blue line), and DP (thin red line). As a result, both $P_{rol}$ and $P_{aer}$ will cause the graphical lines of $P_{net}$ for UP (solid black line), AP (solid blue

line), and DP (solid red line) to also vary with v. The $P_{rol}$ increases linearly with v from $v = 0$, whereas $P_{aer}$ increases with v on a parabolic line. The model indicates that DP yields lower values of $P_{aer}$ and $P_{net}$ than AP and UP, respectively.

5.3 Relationship of energy expenditure during cycling.

Table 5.22 Average oxygen consumption ($\dot{V}O_2$) of the four subjects at three workloads for the three cycling positions during spiroergometry testing.

| | | $\dot{V}O_2$ (ml/min) | | | | | | | | |
|---|---|---|---|---|---|---|---|---|---|---|
| | | **UP** | | | **AP** | | | **DP** | | |
| No. | Code-Subject | **100** Watts | **140** Watts | **180** Watts | **100** Watts | **140** Watts | **180** Watts | **100** Watts | **140** Watts | **180** Watts |
| 1 | 01-WN | 1522.53 | 1950.42 | 2391.03 | 1697.50 | 2083.15 | 2536.07 | 2040.40 | 2521.48 | 2993.22 |
| 2 | 06-UC | 1561.20 | 2041.45 | 2474.33 | 1678.80 | 2141.93 | 2572.15 | 1837.85 | 2243.43 | 2665.97 |
| 3 | 09-HL | 1769.08 | 2223.03 | 2656.55 | 1932.70 | 2369.02 | 2864.55 | 1991.57 | 2547.65 | 2964.00 |
| 4 | 15-ES | 1778.58 | 2208.68 | 2671.85 | 1902.13 | 2338.18 | 2806.70 | 1984.07 | 2493.55 | 2939.17 |
| (*n*=4) | $\bar{x}$ | **1657.80** | **2105.90** | **2548.44** | **1802.78** | **2233.07** | **2694.87** | **1963.47** | **2451.53** | **2890.59** |
| | ± SD | ± 134.91 | ± 132.43 | ± 138.07 | ± 133.17 | ± 141.79 | ± 164.90 | ± 87.39 | ± 140.48 | ± 151.37 |

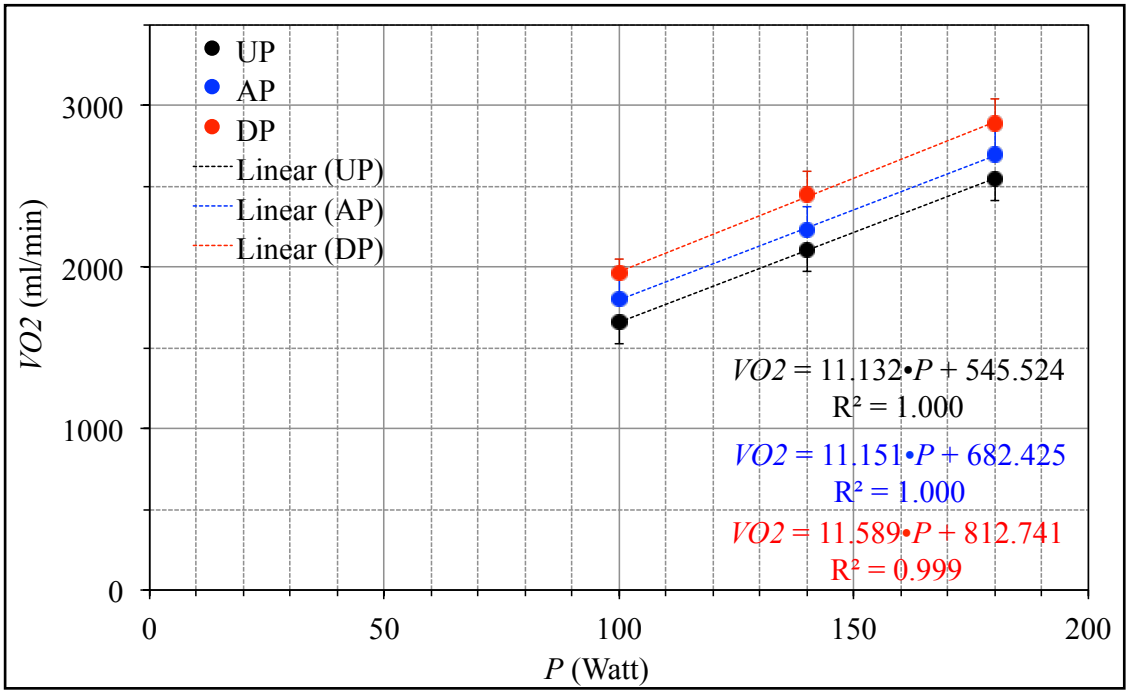


Figure 5.15 Linear regression between the average oxygen consumption ($\dot{V}O_2$) of four subjects and the three mechanical powers (*P*) for UP (black dot), AP (blue dot) and DP (red dot).

Table 5.22 shows the value of oxygen consumption ($\dot{V}O_2$) of the four subjects that was obtained from the spiroergometry testing at the three workloads, given by the mechanical power (*P*), for the three cycling positions. The mean values were then used to find the linear correlation between $\dot{V}O_2$ and *P* at 100, 140, and 180 Watts for UP, AP, and DP. The equation of linear regression can be described by:

$$y = m \cdot x + c \tag{5.1}$$

where, *y* is the dependent variable, *x* is the independent or explanatory variable, *m* is the slope of the linear relationship and *c* is a constant value given by the value of *y* when *x* = 0. Additionally, $R^2$ is the square correlation coefficient, which is a measure of the correlation between *x* and *y* (Draper & Smith, 1998). Hence, assuming the independent variable is *x* = *P,* as given by the workloads, and the dependent variable is *y* = $\dot{V}O_2$, Equation (5.1) becomes:

$$\dot{V}O_2 = m \cdot P + c \tag{5.2}$$

Figure 5.15 is created by the average oxygen consumption ($\dot{V}O_2$) at three workloads or mechanical powers (*P*) in Table 5.22, and demonstrates the results of the linear regressions between $\dot{V}O_2$ and *P* of three cycling positions, which found that

for UP: $\dot{V}O_2 = 11.132 \cdot P + 545.524$, $R^2$ = 1.000,

for AP: $\dot{V}O_2 = 11.151 \cdot P + 682.425$, $R^2$ = 1.000, and

for DP: $\dot{V}O_2 = 11.589 \cdot P + 812.741$, $R^2$ = 0.999.

Considering that $R^2$ = 1.00 for all positions, it can be said that *P* (= *x*) and $\dot{V}O_2$ (= *y*) are perfectly correlated. In the next step, the estimated parameter $P = F_{rol} \cdot \mathrm{v} + K \cdot \mathrm{v}^3$ is inserted into Equation (5.2), given that the value of *K* was determined from the coasting down experiment:

$$\dot{V}O_2 = m \cdot P + c = m \cdot (F_{rol} \cdot \mathrm{v} + K \cdot \mathrm{v}^3) + c \tag{5.3}$$

Equation (5.3) can be used to model the relationship between $\dot{V}O_2$ and v for the three cycling positions, as shown in Figure 5.16. This model is created by using the value of $\dot{V}O_2$ that is measured during the spiroergometry test and the value of *K* that is calculated through the estimated parameter $K_m$ from the coasting down test.

The model in Figure 5.16 can be explained by dividing it into the three important parts, i.e. before the interception point, at the interception point and after the interception point. The graphical lines show that the

interception point of the three cycling positions is at approximately 5 $m \cdot s^{-1}$ or 18 $km \cdot h^{-1}$. At a velocity of this magnitude, the values of $\dot{V}O_2$ for UP, AP, and DP are equal. Once the velocity exceeds 5 $m \cdot s^{-1}$, riding in DP clearly yields a lower value of $\dot{V}O_2$ than riding in AP and UP, respectively, whereas, at velocities smaller than that of the interception point, i.e. below 5 $m \cdot s^{-1}$, riding in DP yields a slightly larger value of $\dot{V}O_2$ than riding in AP and UP, respectively.

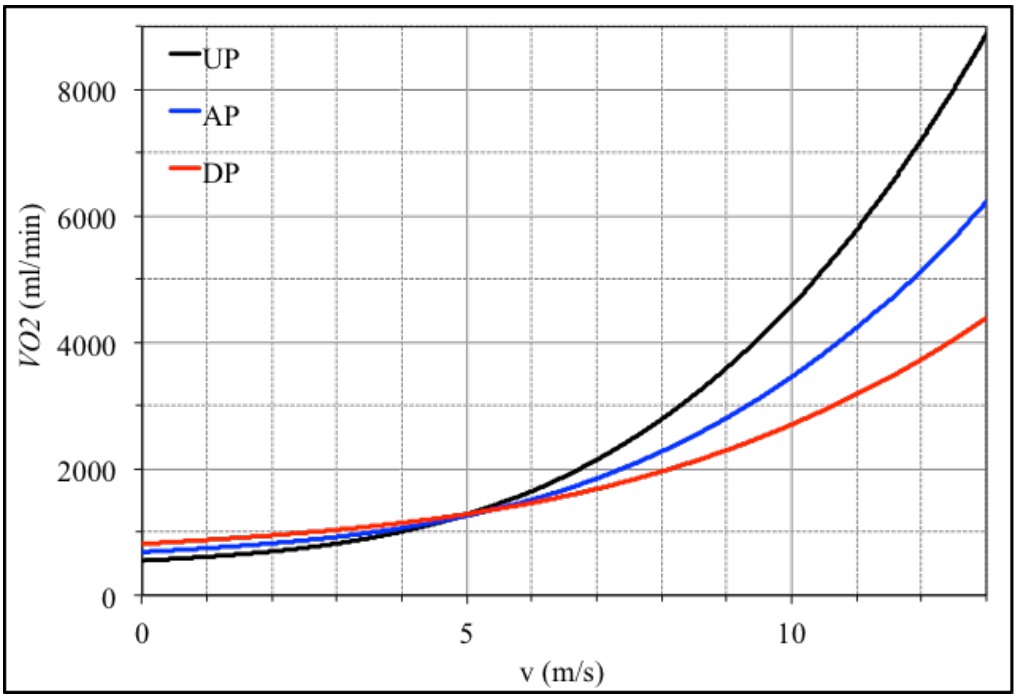


Figure 5.16 Functional model of the oxygen consumption ($\dot{V}O_2$) with respect to velocity (v) while cycling in UP (black line), AP (blue line) and DP (red line).

# CHAPTER 6: DISCUSSIONS

## 6.1 Effects of cycling positions on cardiorespiratory responses

The primary purpose of this present investigation was to compare the cardiorespiratory responses among three cycling position, namely, the upright position (UP) versus the aero position (AP), the upright position (UP) versus the fully dropped position (DP), and the aero position (AP) versus the fully dropped position (DP). The investigation was conducted with twenty-four recreational male cyclists (who have experience with riding in the UP) by cycling on the modified bicycle ergometer. All tests were performed under the same laboratory conditions without any air resistance. They were designed to measure the cardiorespiratory functions while cycling on aerobic power production. Therefore, intensities of 100, 140, and 180 Watts were selected to provide a sufficient mechanical work rate in the submaximal range for the participants in order to enable stable rates of aerobic and minimal rates of anaerobic power production.

The cycling positions in this study were in part alike (i.e. UP and AP) and in part unlike (i.e. DP) the riding positions from previous investigations. That is, the DP for the participants had to bend the torso and flex the arms parallel to the ground (fully crouched) throughout the three submaximal intensities. This differed from the DP in previous studies, where it was required that the elbows remained extended (Franke et al., 1994; Sheel et al., 1996; Gnehm et al., 1997; Grappe et al., 1998; Dorel et al., 2009). The study focused on the fully DP because it is commonly used at high speeds, in particular during the last competitive period, where the cyclists reaching the finish line need to crouch in order to increase their aerodynamics effectiveness. As aforementioned, the previous results have shown conflicts of significant differences between some pairs of cycling positions on the cardiorespiratory responses. Especially, for example, DP versus AP was significant ($P$<0.001) in study of Gnehm et al. (1997) but not significant ($P$>0.05) of Franke et al. (1994), Sheel et al. (1996), and Grappe et al. (1998), and DP versus UP was significant ($P$<0.01) in study of Grappe et al. (1998) but not significant ($P$>0.05) of Franke et al. (1994), Sheel et al. (1996), and Gnehm et al. (1997).

Overall, the statistical analysis, as given in Tables 5.1 to 5.8, revealed that most parameters (e.g. heart rate (HR), oxygen uptake ($\dot{V}O_2$), carbon dioxide output ($\dot{V}CO_2$), minute ventilation ($\dot{V}_E$), and breathing frequency (BF)) yielded a significantly higher mean ($P$<0.001) in DP than in AP and UP, respectively. On the other hand, the value of tidal volume ($V_T$) was significantly higher ($P$<0.05) in UP than in both DP and AP, which were the assumed crouched position in this study. Although the value of respiratory exchange rate (RER) lacked significant differences ($P$>0.05) among the three positions, it was found that the mean RER in the crouched positions was slightly higher than in UP at the same absolute workloads. This may indicate that the participants worked harder in the crouched positions, in particular in the fully DP, than in UP.

6.1.1 Upright position (UP) versus aero position (AP)

The results revealed that all mean values of the cardiorespiratory parameters, except that of RER, showed highly significant differences ($P$<0.01) between UP and AP. Previous studies (Gnehm et al., 1997; Ashe et al., 2003; Peveler et al., 2005) also compared the cardiorespiratory responses in UP to those in AP and yielded similar results for some variables. That is, $\dot{V}O_2$ was studied by Peveler et al. (2005) who examined the metabolic economy with cyclists that trained only in UP and triathletes that trained only in AP. Similarly, the study of Ashe et al. (2003) examined the cardiorespiratory variables for untrained cyclists during a steady-state submaximal exercise at 50, 100, and 150 Watts, as did the study of Gnehm et al. (1997). They found that the mean value of $\dot{V}O_2$ in AP was significantly higher ($P$<0.05) than in UP, and concluded that riding in the AP yielded a higher increase in the metabolic cost than UP during a submaximal test.

In contrast to the investigation of Hubenig et al. (2011) examined the cardiorespiratory parameters and the power output at two ventilatory threshold levels with female cyclists/triathletes, and Jobson et al. (2008) conducted 40.23-km time-trials on a cycling ergometer with male cyclists in order to compare the physiological demands. In addition to the investigation of Berry et al. (1994) measured the response of ventilation, pulmonary function and gas exchange to prolonged cycling at 80% of the maximal oxygen uptake ($\dot{V}O_{2max}$) with trained cyclists, and Origenes et al. (1993) measured the difference of the ventilatory responses between UP and AP at both submaximal and maximal exercise with moderately trained cyclists. Their results revealed no significant differences ($P$>0.05) for the mean values of HR, $\dot{V}O_2$, $\dot{V}_E$, BF, and $V_T$ between UP and AP exist. Likewise, investigations among three cycling positions (UP versus AP versus DP), such as those of Franke et al. (1994), Grappe et al. (1998), and Dorel et al. (2009), also found no significant differences ($P$>0.05) for the mean values of the ventilatory variables when comparing UP to AP. In contrast, some studies, that performed field tests at a constant velocity of 30 km·h$^{-1}$ around a 400 m asphalt track (Sheel et al., 1996) or 40 km·h$^{-1}$ on a flat 4 km course (Richardson & Johnson, 1994) revealed lower mean values of HR, $\dot{V}O_2$, $\dot{V}_E$, and RER in AP than in UP. They summarized that the AP yielded an energy expenditure saving that is effective in maintaining higher velocities for a longer period of time. Interestingly, Origenes et al. (1993) hypothesized that AP should yield a smaller $V_T$ but a higher BF and therefore result in a higher $\dot{V}_E$ than UP, caused by a possible constraint enforced by the low-crouched AP. Ashe et al. (2003) believed that AP may decrease the ability to increase $V_T$, which is followed by an increased BF, which leads to an earlier termination of the exercise when compared to UP; furthermore,

they speculated that AP may restrict the inspiratory flow and increase the energy cost and that the subsequent resulting fatigue outweighs any cardiorespiratory advantages for participants who were unfamiliar with aerobars.

### 6.1.2 Upright position (UP) versus fully dropped position (DP)

Likewise, regarding UP versus DP, the results showed highly significant differences ($P$<0.001) in the mean values of HR, $\dot{V}O_2$, $\dot{V}CO_2$, $\dot{V}_E$, and BF, but not ($P$>0.05) for $V_T$ and RER. Consistently, the study of Faria et al. (1978) found significant differences ($P$<0.05) in the mean values of $\dot{V}O_2$ and $\dot{V}_E$ when comparing UP to DP, whereas the mean HR was not significantly different ($P$>0.05). In addition, Grappe et al. (1998) revealed that the mean $\dot{V}_E$ and RER were significantly higher ($P$<0.01) in DP than in UP. They described that the increased respiratory mechanics could be caused by the hip flexion (or trunk forward flexion) altering the alignment of the upper respiratory tract.

However, there were no significant differences ($P$>0.05) in the mean HR and $\dot{V}O_2$ between UP and DP in the study of Grappe et al. (1998), as well as in the study of Ryschon and Stray-Gundersen (1991) who measured the energy expenditure while cycling up a 4% incline on a motor-driven treadmill. In addition, the study of Welbergen and Clijsen (1990), who conducted the supra-maximal test with healthy men, found no difference in the mean $\dot{V}O_{2max}$ parameter between UP and DP. Moreover, regarding the mean ventilatory parameters, Grappe et al. (1998) found that there were no significant differences ($P$>0.05) in both the mean $V_T$ and the mean BF between UP and DP, whereas significantly higher values ($P$<0.01) of $\dot{V}_E$ and RER were yielded in DP than in UP. These reason for the contradictory results between their study and the current results may be the fact that the elbows were slightly extended in their DP, compared to the DP in this study, where both elbows were always flexed and the torso was bent downwards. In addition, the cyclists in this study were unfamiliar with cycling in DP, whereas the participants in the study of Grappe et al. (1998) were familiar with the cycling position. Consequently, these differences could have influenced the cardiorespiratory variables.

### 6.1.3 Aero position (AP) versus fully dropped position (DP)

There have been quite a few investigations between AP and DP that are both crouched positions. The present results showed significant differences ($P$<0.001) in the mean values of HR, $\dot{V}O_2$, $\dot{V}CO_2$, $\dot{V}_E$, and BF, respectively, for

this pair; nevertheless, there was no significant difference ($P$>0.05) in the mean $V_T$ and RER. Specifically, the mean HR, $\dot{V}O_2$, and RER variables are similar only to the results from the study by Gnehm et al. (1997), who investigated the metabolic consequences of different racing positions at 70% of $\dot{V}O_{2max}$ with elite cyclists.

The present findings differ from the previous studies of Dorel et al. (2009) which compared gas exchange/ventilatory parameters and also measured an electromyography (EMG) at the ventilatory threshold (VT+Δ20%) and respiratory compensation point (RCP) with twelve male triathletes. In addition, sport scientists investigated the performance of trained cyclists during a submaximal exercise at 70% of $\dot{V}O_{2max}$ (Evangelisti et al., 1995; Grappe et al., 1998), during a graded maximal bicycle ergometry exercise (Franke et al., 1994), and during a field submaximal cycling test at a constant velocity of 30 km·h$^{-1}$ (Sheel et al., 1996). They found no significant differences ($P$>0.05) in the mean values of HR, $\dot{V}O_2$, $\dot{V}_E$, BF, and $V_T$ between AP and DP. As there were also no significant differences ($P$>0.05) in these variables when comparing UP to DP, it may be possible that the reason for this is the different DP that was used. Overall, the current findings demonstrate that DP seems to generally be more strenuous than AP, given the significantly higher values ($P$<0.001) of the mean HR, $\dot{V}O_2$, $\dot{V}_E$, and BF.

### 6.1.4 Crouched position versus upright position

The 15-min observations clearly demonstrated that the crouched positions (i.e. AP and fully DP) directly lead to increased cardiorespiratory functions when compared with UP due to the bending of the torso. The study showed that the trunk forward flexion of the crouched positions certainly affected the breathing mechanics, especially in the fully DP. It was speculated that during inhalation the crouched position might cause an increased thoracic and abdominal pressure because when the diaphragm moves downwards, it encroaches on the abdominal cavity, which will in turn obstruct the movement of the diaphragm and cause its negative impact on the respiratory muscle mechanics. The assumption may be consistent with the investigation of breathing patterns of Lucía et al. (1999, 2001), which indicated that cycling positions that are characterized by inclination of the torso, cause the thoracic cavity to be compressed by the abdominal viscera, which makes it hard for the respiratory muscles to work. Consequently, it is believed that the requirement of increased work for breathing (pressure times volume) in the crouched position could be explained by either an increase in the energy expenditure of the respiratory muscle or by a decrease in efficiency of the ventilation.

The effect of increased pressure might alter the inspiration/expiration mechanics; hence, the results showed that for both UP versus AP and UP versus DP, the ventilatory responses in UP tended to be more efficient than in AP and

DP for $\dot{V}_E$, which is reflected by a lower BF and a larger $V_T$. This meant that the oxygen consumption through inhalation into the lungs was optimal while cycling in UP because the lungs were fully expanded. In contrast, for the crouched positions, the increased amount of $\dot{V}_E$ which resulted in a higher BF and a smaller $V_T$, indicated that the air breathed into the lungs was reduced for the oxygen consumption because the lung volumes were decreased due to the encroachment on the visceral organ; thus, the breathing had to be accelerated to inhale more air into the lungs and increase the oxygen consumption in order to match the energy requirements during cycling. As a general principle, the increased minute ventilation (tidal volume times breathing frequency) in the crouched positions may be explained by the fact that if $V_T$ is smaller due to the bending of the torso, this will be compensated by the increase of BF, which yields higher values of $\dot{V}_E$. According to this assumption, the decreased $V_T$ is compensated by a higher BF and $\dot{V}_E$, respectively. From this standpoint, therefore, it is believed that during cycling in the crouched positions, $\dot{V}_E$ was smaller but BF was higher than in UP because the decreased $V_T$ was compensated by the increased BF, which consequently induced a higher $\dot{V}_E$. Namely, the respiratory musculature of the crouched positions demands the energy for work of breathing more than in UP.

It is also interesting to compare $V_T$ between the crouched positions, although no significant difference ($P$>0.05) was found. Nevertheless, the mean $V_T$ in AP was slightly smaller than in DP, which may have been due to the fact that the biomechanical properties in the lung were limited in AP. This assumption could be explained by the fact that in AP the elbows were placed on the pads of the aerobars, which resulted in a narrower width of the shoulders than in DP and may have limited the $V_T$. However, the mean BF was slightly higher in DP than in AP. This may have been caused by the fact that the torso was bent down lower in DP than in AP, which induced an increase in pressure due to the decreased volume for the lung function, in addition to reducing the lung's ability to aid in the inspiratory/expiratory phase of the breathing cycle.

There have been a few empirical studies that have compared the pulmonary function between UP and a rowing position which, for a certain rowing stroke (the catch), is similar to the crouched position (Cunningham et al., 1975; Bouckaert et al., 1983; Szal & Schoene, 1989). They found that the $\dot{V}_E$ and BF of the rowing position were higher than in UP, but that the $V_T$ was lower. While the body is cramped or in the catch position, Cunningham et al. (1975) predicted that the abdominal viscera might constrict the movement of the diaphragm during inhalation. Moreover, Szal and Schoene (1989) explained that the lung volume is limited because the abdominal contents are pressed against the

diaphragm while catching. Hence, they summarized that a trunk-flexion exercise will cause hyperventilation with a higher BF and a lower $V_T$ because the sensory input from the muscle mechanoreceptor to the respiratory center may be stimulated, leading to an increased respiratory drive and ventilatory result. Their assumptions may also help to support the disadvantage for cycling in the crouched positions in this study.

In terms of a streamline shape, AP looks like a streamlined position more than DP because the upper body is characterized by the outstretched arms over the aerobars, and the torso is bent low and almost parallel to the ground. This suggests that AP is a more comfortable position than DP because the elbows are supported by the elbow-pads that help distribute the upper body weight; this may therefore have contributed to the fact that the mean cardiorespiratory responses for AP were lower than for DP. For DP, however, it was observed that the muscle groups of the shoulders, arms, and hands appeared to be more active in order to maintain the stabilization of the upper body throughout the 15-min test. That is, these muscle groups functioned as static muscular contraction through the shoulder and elbow flexion. This also shows in the increased values of HR and $\dot{V}O_2$ in DP when compared to AP, which are the best indicators in the current study. Furthermore, after the submaximal exercise testing in DP, the participants in this investigation complained about this position. They commented that the control of DP is very hard and uncomfortable because the abdomen was compressed more than in AP and because of the pain in the arms due to the shoulder and elbow flexion.

Moreover, it is possible that gravitational force might also affect the respiratory function, particularly in the crouched positions, more than in UP. Cabello and Mancebo (2006) reviewed that the pleural pressure is influenced by gravity and that this pressure can be modified by the posture and by the weight of the thoracic content. For this reason, it is speculated that while cycling in a crouched or horizontal position, the thoracic cavity may be compressed by the upper body weight due to the influence of gravity, which limits the expansion of the lungs while inhaling. In comparison, in UP the advantage of the gravity may help the diaphragm muscle expand easily along the longitudinal axis (neck to abdomen). This assumption can be supported by the study of Behrakis et al. (1983), who measured the lung compliance when shifting from a sitting to a horizontal posture. They explained that gravitational effects will change the shape of the diaphragm (towards the head or anterior section or called the cephalad displacement) due to the increased abdominal pressure in the horizontal posture. Their results showed that the vital capacity and expiratory reserve volume decreased, but that the flow-resistance increased in the horizontal posture due to the closure of small airways and the increased pulmonary blood volume. As a result, the blood pressure increased around the chest, which was also seen in the results of Evangelisti et al. (1995), who reported that the mean blood pressure (both systolic and diastolic) increased in the fully DP. Besides, for a change from the upright to the crouched position, the gravitational effect could also influence the blood flow into the atrium and out of the ventricle, which would directly influence the

cardiac function. It must be recognized that, theoretically, the cardiac output ( $\dot{Q}$ ) is the stroke volume (SV) multiplied with the heart rate (HR). Previously studies, such as the results of Franke et al. (1994), also showed that while resting the SV in the crouched position (i.e. AP) was larger than in UP, but slightly less than in a supine position. Similarly, Rohdin et al. (2003) measured the differences in the cardiopulmonary function between the supine (face-up) and the prone (face-down) posture, the latter of which is similar to the crouched postures (AP and DP), while exposed to 1 and 5 times normal gravity (1G, 5G). The results revealed that during resting in the prone posture, the SV was decreased, but $\dot{Q}$ and HR were increased. It is possible though that exercising in the lying position may produce a higher SV compared to UP because of the reduced of gravitational force in this position and an increased preloading (Peveler et al., 2005). In addition, the gravity may influence the hydrostatic pressure (Egana et al. 2006). In order to understand this, one should take into account that for the exercise in the crouched position under gravity there may be more blood in the lower extremities and consequently a reduction in the venous return to the heart when compared to the exercise in UP. As a result, SV would decrease, whereas HR should increase in order to maintain sufficient $\dot{Q}$ ; furthermore, the effect of the elbow and hip flexion in the crouched position could also obstruct the venous return flow back to the right atrium.

Apart from the fact that the abdominal cavity is compressed by the visceral organ and that gravity has an effect on the internal organs in the thoracic cavity, which can lead to increased cardiorespiratory work while crouching, it is also believed that the increased energy expenditure in the crouched position might be related to increased dynamic muscular activity around the hip joints, leading to increased metabolic requirements. Because the hip angle changes between various cycling positions, the power production of muscles crossing at the hip joints will also be affected (Welbergen & Clijsen, 1990; Reiser et al., 2002). This was further evidenced by Savelberg et al. (2003), which revealed that the electromyography (EMG) activity of the *gluteus maximus* increased when changing from UP to a crouched position, as a cause of increased $\dot{V}O_2$ , $\dot{V}_E$ , and RER (Dorel et al., 2009). The disadvantage of the crouched position, as Dorel et al. (2009) hypothesized, is that the *gluteus maximus* is stretched more which may induce passive resistance; whereas the *rectus femoris* is shortened which may affect its ability to generate force. Therefore, it is noteworthy that in the crouched position the hip joint will flex most at a crank position of 0° (12 o'clock). Gnehm et al. (1997) speculated that this position may cause increased adductor activation and consequently a higher metabolic cost in order to keep the lower limb cycling; furthermore, its position may also alter the flow resistance in the iliac and femoral vessels, and hence it may cause a higher cardiac energy expenditure. In order to optimize the effectiveness for riding in the crouched position (in AP), the effects of various angles of the frame geometry on cardiorespiratory responses have previously

been investigated in studies of Heil et al. (1995, 1997) and Heil (1997). They found that the values of HR, $\dot{V}O_2$, and $\dot{V}_E$ certainly depend on the hip angles as a consequence of the seat-tube and torso angles. Consistently, Price and Donne (1997) reported that HR and $\dot{V}O_2$ decreased significantly ($P$<0.001) with increased seat-tube angles of 68, 74, and 80°, respectively. They summarized that decreasing the seat-tube angle resulted in decreasing hip angle (i.e. more torso bent forward), which increased the cardiorespiratory responses, including alterations in the muscle force-length relationship for power output (Ricard et al., 2006). Furthermore, Too (1990, 1991) concluded that changes of cycling positions will clearly alter the joint angles, muscle lengths and muscle moment arm lengths, thus affecting the tension-length, the force-velocity-power relationship of multi-joint muscles and the effectiveness of force production.

## 6.2 Effects of cycling positions on aerodynamic parameters

The aerodynamic drag ($F_{aer}$) in cycling positions can be measured both directly and indirectly with several different methods. To the best of knowledge, the aerodynamic parameters such as the drag area ($C_D \cdot A$) or only the drag coefficient ($C_D$) can be determined from: 1) the wind tunnel (Martin et al., 1998; García-López et al., 2008; Gibertini et al., 2008; Chowdhury et al., 2011; Crouch et al., 2012), 2) the towing experiment (Capelli et al., 1993; De Groot et al., 1995), 3) the force transducers (Grappe et al., 1997; Martin et al., 2006; Edwards & Byrnes, 2007; Lim et al., 2011), and 4) the computational fluid dynamics (CFD) (Defraeye et al., 2010; Blocken et al., 2013). Apart from these methods, coasting deceleration or coasting down method is a technique that can determine $C_D \cdot A$, as well as $C_D$. The coasting-down test with either one or two cycling positions has been reviewed in the studies of De Groot et al. (1995), Hennekam and Govers (1996), and Candau et al. (1999) and was found to be an effective way.

### 6.2.1 Simplified coasting down method

As a good method, the technique of coasting down is a simple and economical approach for obtaining the values of the aerodynamic drag force and the rolling friction as the main resistive forces. The most important result of the present study was the fact that the coasting-down technique could perform this investigation. The technique has sufficient accuracy to detect the change in the drag force due to a change of the cycling position. This is given by the accurate values of the resistive forces that were determined from many measurements of velocity-time values under similar circumstances, which is imperative for the cycling coasting deceleration. For such a study, well-controlled

experiments are necessary. In order to obtain most of the data, the velocity-time curves were fitted by the cycling coasting deceleration equation, given by Equation (2.26). Furthermore, the best-fit parameters for the cycling models were obtained from the least-squares method.

The coasting deceleration technique represents an alternative to wind tunnel testing that can offer some advantages because this technique allows the investigation of both the air drag ( $F_{aer}$ ) and the rolling friction ( $F_{rol}$ ) (De Groot et al., 1995; Hennekam & Govers, 1996; Candau et al., 1999). This method should be performed under real and constant conditions that cannot be achieved in a laboratory. During coasting-down cycling in a sports hall, there is no side-wind drag interaction with the rider-bicycle motion, which is also the case in a wind tunnel. Moreover, the dynamical drag linked to the spokes, the wheel rotation and the position of the lower-limbs can be considered with this technique, as well as during wind tunnel testing. The method can also be a useful technique to improve cycling performance. For instance, a considerable improvement in coasted-down time only due to a change in the rider position could be detected by this technique. Candau et al. (1999) indicated that the coasting-down technique is also suitable to detect the $F_{rol}$ by including small alternations in the vertical force through external loading. Indeed, from the direct results of Martin et al. (1998), Gibertini et al. (2008), García-López et al. (2008), Chowdhury et al. (2011), and Crouch et al. (2012), it seems that the reproducibility of tests in a wind tunnel by using the fixed plate technique is better than or equivalent to that of the simplified coasting deceleration technique indoors. The results of the present investigation indicate that the coasting-down technique is a good method for measuring $F_{aer}$, and can equally be used instead of wind tunnel measurements.

Small errors for the estimation of the aerodynamic constant divided by mass ( $K_m$ ) might be caused by the difficulty in keeping the positioning control stable while coasting down, which might also have a minimal impact on the calculated $C_D$ . This error was minimized by using a large number of trials in the present investigation, which could be an indicator for the high reproducibility of the coasting down of a rider-bicycle combination over a sports hall floor. In addition to the control of stable conditions for this study, the good reproducibility was also given by the accuracy of the tachogenerator (speed sensor) and the telemetry-bicycle system and also by the many trials of the coasting-down motion. All coasting-down experiments were carried out with a Peugeot racing bicycle with an installed telemetry system. To the best of knowledge, no previous study had used a telemetry-bicycle system and a tachogenerator for the coasting-down method. The accuracy values were gained by recording the velocity once every millisecond and by performing 20 coasting-down trials per velocity and cycling position. The reproducibility of the costing-down technique could also be further enhanced by performing more trials. Nevertheless, the reproducibility of the results of the coasting

deceleration method is supported by the fact that previous authors found comparable results (De Groot et al., 1995; Hennekam & Govers, 1996; Candau et al., 1999).

In the present study, the technique of coasting down was used to offer a useful approach for the determination of aerodynamic parameters acting on different rider positions. The coasting-down technique is not very complex and as it only requires a short distance (20 m long for accelerating phase and 30 m long for freewheeling phase) in a sports hall, it can be readily examined. Both $F_{aer}$ and $F_{rol}$ can be quantified simultaneously with the coasting-down technique, whereas $F_{rol}$ cannot be determined through drag testing in a wind tunnel. On the other hand, the coasting-down technique requires multiple trials and is time consuming compared to the air drag testing in wind tunnel. However, the coasting-down method also requires the generation of relatively high speeds, which may be physically demanding for the subject. Namely, the high initial speed is a requirement for aerodynamic parameter estimation on different cycling positions. Surely though, professional cyclists can reach higher initial speeds (> 50 km·h$^{-1}$) with using this technique.

The rolling resistance accounts for the smallest proportion of resistive forces opposing the forward progression of a bicycle at racing speeds, whereas the impact of air drag is relatively high under these conditions. From a theoretical point of view, Whitt and Wilson (1982) determined that the $F_{rol}$ during cycling should depend on the wheel diameter, the type of tire, the inflation pressure, the friction of surface, the friction in the bicycle's machinery and the mass distribution. In this study, the magnitude of the coefficient of rolling ($\mu$) was not examined. The $\mu$ was assumed to be constant at 0.006, which is the value that was also used in the calculation of $F_{rol}$. Kyle (1996) found that the different $\mu$ between the wheels and the road is primarily a function of tire and caster type, and ground property type as well. The value of $\mu$ = 0.006 that was selected in this study was also in agreement with the range of values that were reported by Grappe et al. (1999b), Chua et al. (2010) and Henchoz et al. (2010). For the rolling resistance, as determined with the coasting-down technique, Candau et al. (1999) yielded $F_{rol}$ = 3.53 N and $\mu$ = 0.00563 (inflation pressure = 6 bar), Hennekam and Govers (1996) yielded $F_{rol}$ = 2.3 N and $\mu$ = 0.005 (7-8 bar) and De Groot et al. (1995) yielded $F_{rol}$ = 3.4 N and $\mu$ = 0.0038 (6-6.5 bar). These authors determined the $\mu$ from $\mu = a_{rol} / g$, with the value of $a_{rol}$ being obtained by parameter estimation, as given by Equation (2.20). This indicates that $\mu$ is a velocity-independent component and consequently, as was also in Figure 5.13, the $F_{rol}$ is also a velocity-independent component. The value of $\mu$ was not investigated in this study because the used distance was too short, there was a bump on the floor surface and there was a problem with the balance control at very low speeds. Thus, $\mu$ = 0.006 was assumed because the trials were coasted down on a sports hall floor. Another reason for using a constant value for $\mu$ was the need to reduce the

number of parameters from three ( $v_i$ , $K_m$ , and $a_{rol}$ ) to two (without $a_{rol}$ because it is a constant value according to the theory) in order to avoid errors in the parameter estimation by the least-squares principle.

An example is given in Figure 5.9, where, in order to fit the best curve on the measured velocity (raw data), one tested riding position used the two velocities of 25 and 15 km·h$^{-1}$ for twenty trials each, which enhanced the accuracy. Thus, all estimated values for $v_i$ (Table 5.9) and $K_m$ (Table 5.10) were in good mutual agreement. Analysing the velocity with respect to time for twenty trials enhanced the accuracy of determining the values for $v_i$ and $K_m$ , which was performed by the least-squares method with the Solver program. Furthermore, a graphical sample, given by the vertical lines in Figure 5.9, was obtained for each test. The best-fitted curve suggested a tendency of rider-bicycle movement to oscillate with respect to the theoretical curve. As the signal of the velocity-time graph (oscillatory graph) was transmitted from the telemetry bicycle to a receiver unit, this oscillatory behaviour (up and down line) could probably be ascribed to the sensitivity of the tachogenerator (speed sensor) and the vibration of the rider-bicycle while coasting down. The oscillatory graph at the velocity of 25 km·h$^{-1}$ shows that there is more fluctuation than at 15 km·h$^{-1}$. This could be simultaneously influenced by the resistive force and vibration of the system. According to observation in this study, the test velocities influence the behaviour of oscillatory graph (the more speed, the more vibration). Moreover, the different cycling positions and the flooring type can also influence the oscillatory graph as the $F_{aer}$ and the $F_{rol}$ . The oscillatory behaviour should not be caused by the $F_{aer}$ greater than the $F_{rol}$ in the sports hall though because it is important to recognize that $F_{aer} > F_{rol}$ . Although small environmental effects (i.e. temperature and relative humidity) could not be stably controlled during the coasting-down tests, they only account for a small proportion of the resistive forces opposing the motion.

The values of the drag area ( $C_D \cdot A$ ), the coefficient of drag ( $C_D$ ) and the projected frontal area ($A$) from the present study are compared to those found by previous authors and shown in Table 6.1, where the main cycling positions, namely the upright position (UP), the aero position (AP) and the fully dropped position (DP), are considered.

Table 6.1 Comparison of drag area ( $C_D \cdot A$ ), coefficient of drag ( $C_D$ ), and projected frontal area ($A$) from this study with other experimental studies of cycling positions over the last two decades.

| Researcher | Technique | Riding Posture | $C_D \cdot A$ ($m^2$) | $C_D$ | $A$ ($m^2$) | v | $n$ |
|---|---|---|---|---|---|---|---|
| Blocken et al. (2013) | CFD | Upright[a] | 0.213[o] | 0.520[n,o] | 0.41 | 15 m/s | 1 |
| | | Dropped[b] | 0.173[o] | 0.468[n,o] | 0.37 | (54 km/h) | |
| | | Time-trial[d] | 0.135[o] | 0.397[n,o] | 0.34 | | |
| Crouch et al. (2012) | Wind tunnel | Time-trial[d] | 0.200 to 0.234[m] | 0.49 to 0.56[m] | 0.410 to 0.419[m] | 16 m/s | 1[l] |
| | | | | | | (57.6 km/h) | |
| Chowdhury et al. | Wind tunnel | Upright[a] | 0.451[n] | 1.1[m] | 0.410 | 20-70 km/h | 1 |
| (2011) | | Dropped[b] | 0.405[n] | 1.0[m] | 0.405 | (5.6-19.4 m/s) | |
| | | Time-trial[d] | 0.342[n] | 0.9[m] | 0.380 | | |
| Lim et al. (2011) | Force | Hoods[f] | 0.3633 ± 0.0557 | | | Used power | 8 |
| | transducers[p,q] | Dropped[b] | 0.3238 ± 0.0510 | | | | |
| Defraeye et al. (2010) | CFD | Upright[a] | 0.219[o] | 0.534[n,o] | 0.41 | 10 m/s | 1 |
| | | Dropped[b] | 0.179[o] | 0.484[n,o] | 0.37 | (36 km/h) | |
| | | Time-trial[d] | 0.150[o] | 0.441[n,o] | 0.34 | | |
| Defraeye et al. (2010) | Wind tunnel | Upright[a] | 0.270 | 0.659[n] | 0.41 | 10 m/s | 1 |
| | | Dropped[b] | 0.243 | 0.657[n] | 0.37 | (36 km/h) | |
| | | Time-trial[d] | 0.211 | 0.621[n] | 0.34 | | |
| García-López et al. | Wind tunnel | Hoods[g] | 0.481 ± 0.017 | 1.33 ± 0.07 | 0.364 ± 0.012 | 15 m/s | 5 |
| (2008) | | Time-trial[d] | 0.293 ± 0.003 | 0.96 ± 0.03 | 0.305 ± 0.008 | (54 km/h) | |
| Gibertini et al. (2008) | Wind tunnel | Dropped[b] | 0.275 | | | 50 km/h | 1 |
| | | Time-trial[d] | 0.223 | | | (13.9 m/s) | |
| Edwards & Byrnes | Force | Dropped[b] | 0.309 ± 0.034[n] | 0.768 ± 0.066[n] | 0.438 ± 0.113[n] | 25-45 km/h | 13 |
| (2007) | transducers[q] | | | | | (6.9-12.5 m/s) | |
| Martin et al. (2006) | Force | Standing[a] | 0.304 ± 0.055 | | | 6-16 m/s | 3 |
| | transducers[p] | Seated[e] | 0.245 ± 0.044 | | | (21.6-57.6km/h) | |
| Candau et al. (1999) | Coast-down | Upright[a] | 0.355 | | | 2.5-12.8 m/s | 1 |
| | | Standard-aero[e] | 0.333 | | | (9-46.1 km/h) | |
| | | Racing-aero[i,j] | 0.304[i], 0.262[j] | | | | |
| Martin et al. (1998) | Wind tunnel | Time-trial[d] | 0.269 ± 0.006 | | | 13.4 m/s | 6 |
| | | | | | | (48.2 km/h) | |
| Grappe et al. (1997) | Force | Upright[a] | 0.299 | | | 5.5-11.0 m/s | 1 |
| | transducers[r] | Dropped[b] | 0.276 | | | (19.8-39.6km/h) | |
| | | Aero[e] | 0.262 | | | | |
| | | Obree[h] | 0.216 | | | | |
| Hennekam & Govers | Coast-down | Racing[k] | 0.342[n] | | | 5-55 km/h | 1 |
| (1996) | | | | | | (1.4-15.3 m/s) | |
| De Groot et al. (1995) | Coast-down | Hoods[g] | 0.318 ± 0.035[n] | 0.829 ± 0.104[n] | 0.39 ± 0.03[n] | 10-15 m/s | 7 |
| | | | | | | (36-54 km/h) | |
| Capelli et al. (1993) | Towing | Dropped[b] | 0.255[n] | 0.645 | 0.395 | 8.6-14.6 m/s | 1 |
| | | | | | | (31-52.6 km/h) | |
| Present study | Coast-down | Upright[a] | 0.524 ± 0.079 | 1.018 ± 0.106 | 0.513 ± 0.023 | 25, 15 km/h | 4 |
| | | Aero[e] | 0.327 ± 0.026 | 0.741 ± 0.027 | 0.441 ± 0.019 | (6.9, 4.2 m/s) | |
| | | Fully dropped[c] | 0.184 ± 0.014 | 0.437 ± 0.021 | 0.421 ± 0.013 | | |

[a] Hands on upper parts of standard handlebar with straight arms. [b] Hands on lower parts of standard handlebar with straight arms. [c] Hands on lower parts of standard handlebar with crouching torso. [d] Hands on end portions and arms on elbow pads of time-trial handlebars. [e] Hands on end portions and arms on elbow pads of aero handlebars that are mounted to the standard handlebars. [f] Hands on brake-hood parts of standard handlebar with straight arms. [g] Hands on brake-hood parts of standard handlebar with crouching torso. [h] Hands on small bar under chest with forearms pressed against the upper arms, and torso tilted forward. [i] Similar to aero posture with torso and head up. [j] Similar to aero posture with head in torso line. [k] Posture is not characterized. [l] Used a cyclist model. [m] Approximated from the existing curves. [n] Calculated from the existing values. [o] Only cyclist body without bicycle. [p] Used SRM®. [q] Used PowerTap®. [r] Used MaxOne®.

6.2.2 Drag area ( $C_D \cdot A$ )

From a theoretical perspective, the drag area ( $C_D \cdot A$ ) is expressed as the drag coefficient ( $C_D$ ) which represents the shape of the object under concern and how streamlined it is, multiplied with the projected frontal area (*A*) which is a representative area of the object (Debraux et al., 2011). In other words, usually, the $C_D \cdot A$ of a body will be used to describe the effective size and shape of the body position as it is seen by the air flowing around it. The $C_D \cdot A$ is also contained in the nonlinear relationship between the aerodynamic drag force ( $F_{aer}$ ) and the velocity (v) (Faria et al., 2005). Figure 5.13 shows the quadratic relationship between $F_{aer}$ and v, which the $F_{aer}$ is increased with $v^2$ (parabolic curve); and the concomitant linear relationship between $F_{rol}$ and v, which the $F_{rol}$ is the same constant value from every cycling positions. The $C_D \cdot A$ is an important factor that induces the increased drag, namely, a higher value of $C_D \cdot A$ can also raise the value of $F_{aer}$. Therefore, the curvature of the fitted curve for the function $v(t)$ can be controlled by $C_D \cdot A$ according to Equation (2.26). The discrepancy between the values of $C_D \cdot A$ in same position (i.e. UP and AP or time trial) obtained in this present study and those obtained from previous authors (Grappe et al., 1997; Candau et al., 1999; Defraeye et al., 2010; Chowdhury et al., 2011) can be seen in Table 6.1. This is probably due to the difference in the shape of subject, the bicycle and the accessories, and particularly the tested velocities. Namely, the determined value of $C_D \cdot A$ may vary with velocity. For example, a study of De Groot et al. (1995), who investigated a skiing position, found that the value of $C_D \cdot A$ was relatively high at low speeds, whereas the value decreased at higher speeds. Although the competitive speed is usually relatively high at an average speed of more than 50 $km \cdot h^{-1}$, the speed of 25 $km \cdot h^{-1}$, which was used in this study with the coasting-down method, could explain the difference in the obtained value of $C_D \cdot A$ .

Comparing the present results with those from previous coasting-down methods in Table 6.1 shows that while in this investigation the mean value of $C_D \cdot A$ for UP was 0.524 (± 0.079) $m^2$, this is slightly higher than the value obtained in an upright position (0.355 $m^2$) in the study of Candau et al. (1999), whereas the mean value of $C_D \cdot A$ for AP was 0.327 (± 0.026) $m^2$, which is similar to that of a standard-aero posture (0.333 $m^2$). Moreover, the mean value of $C_D \cdot A$ for DP was 0.184 (± 0.014) $m^2$ and is thus less than that of the racing-aero posture (0.262 $m^2$) of Candau et al. (1999), where the head and torso were in line and at an angle of 10 degrees with respect to the ground. For a racing

position (which is similar to the dropped position with straight arms), Hennekam and Govers (1996) found a mean $C_D \cdot A$ of 0.342 m$^2$, which is quite similar to the mean $C_D \cdot A$ for AP obtained in the present study. De Groot et al. (1995) determined the $C_D \cdot A$ of a hoods position (crouched with hands on the brake hoods), which yielded a value of 0.318 (± 0.035) m$^2$, which is also similar to the mean $C_D \cdot A$ for AP obtained in this study. Regarding the various measuring systems, the investigation of Candau et al. (1999) applied a chronometer system with an accuracy of 30 μs, which was connected to a computer in order to obtain the data. Hennekam and Govers (1996) obtained their measuring data by an electric recording of electrical pulses that were generated in an inductive sensor mounted on the front fork of the bicycle. The study of De Groot et al. (1995) used a small infrared light emitter and detector mounted on the front fork of the bicycle.

The present results can further be compared with previous wind tunnel tests in Table 6.1. Chowdhury et al. (2011) tested with a velocity range from 20 to 70 km·h$^{-1}$ in the upright position and obtained a $C_D \cdot A$ value of approximately 0.451 m$^2$, which is somewhat different compared to the mean $C_D \cdot A$ of 0.524 (± 0.079) m$^2$ obtained for UP in this study. An entirely different value was found in the study of Defraeye et al. (2010), who obtained a $C_D \cdot A$ of 0.270 m$^2$ at a velocity of 10 m·s$^{-1}$ in the upright position. As for measuring the $C_D \cdot A$ value in the dropped position with straight arms, Chowdhury et al. (2011), Defraeye et al. (2010), and Gibertini et al. (2008) (tested at a velocity of 50 km·h$^{-1}$) and yielded values of 0.405 m$^2$, 0.243 m$^2$, and 0.275 m$^2$, respectively. Their values were different from the mean $C_D \cdot A$ of 0.184 (± 0.014) m$^2$ obtained in this study for DP, because of the torso of the DP, must be crouched parallel to the ground with the hands on the lower part of the standard handlebar (fully dropped). Whereas a comparison of the mean $C_D \cdot A$ of 0.327 (± 0.026) m$^2$ for AP in this study with the time-trial position, which is the same as AP, revealed similar results with a value of 0.342 m$^2$ obtained by Chowdhury et al. (2011), and a value of 0.293 (± 0.003) m$^2$ obtained by García-López et al. (2008) (tested at a velocity of 15 m·s$^{-1}$). However, these values are all somewhat different from those obtained by the investigations of Defraeye et al. (2010) $C_D \cdot A$ = 0.211 m$^2$, Gibertini et al. (2008) $C_D \cdot A$ = 0.223 m$^2$, and Martin et al. (1998) $C_D \cdot A$ = 0.269 (± 0.006) m$^2$, tested at a velocity of 13.4 m·s$^{-1}$. Interestingly, Crouch et al. (2012) recently used a cyclist model instead of a subject to measure the $C_D \cdot A$ in time-trial postures with different leg positions and found values within a range of 0.200 to 0.234 m$^2$ at a velocity of 16 m·s$^{-1}$. Furthermore, for a hoods posture with the hands gripping the brake hoods and slight crouching, García-López et al. (2008) obtained a $C_D \cdot A$ of 0.481 (± 0.017) m$^2$, which is the closest value to the mean $C_D \cdot A$ for UP in the current

investigation. More recently, the $C_D \cdot A$ for cycling positions can also be determined by computational fluid dynamics (CFD) simulations, which relies on reliable data from a closed-circuit wind tunnel as a reference. Defraeye et al. (2010) revealed that the values for $C_D \cdot A$ (without a bicycle) obtained from CFD simulations for the upright, dropped, and time-trial posture were 0.219, 0.179, and 0.150 $m^2$, respectively. Similar results of $C_D \cdot A$ (without a bicycle) were obtained from CFD simulations by Blocken et al. (2013), who found that the upright, dropped, and time-trial posture yielded values of 0.213, 0.173, and 0.135 $m^2$, respectively.

The present results can also be compared with the force transducer technique through powermeters (i.e. SRM®, PowerTap®, and MaxOne®) in Table 6.1. For the upright position, Grappe et al. (1997) applied a MaxOne® to evaluate the $C_D \cdot A$ value, which was equal to 0.299 $m^2$. This value was similar to that obtained in a study of Martin et al. (2006) that used a SRM® to measure the $C_D \cdot A$ of a standing position (as similar as possible to the UP of the present study) at a velocity range of 6 to 16 $m \cdot s^{-1}$ and yielded a value of 0.304 (± 0.055) $m^2$. In contrast, an investigation of Lim et al. (2011) used both a SRM® and a PowerTap® to assess the $C_D \cdot A$ of the hoods position (hands on the brake hoods with straight arms), which gave a value of 0.3633 (± 0.0557) $m^2$. Their values are obviously different to the mean $C_D \cdot A$ of 0.524 (± 0.079) $m^2$ obtained for UP in this study. The $C_D \cdot A$ of the dropped position was assessed in the studies of Lim et al. (2011), Edwards and Byrnes (2007) that used the PowerTap® to test with a velocity range of 25 to 45 $km \cdot h^{-1}$, and Grappe et al. (1997). The obtained $C_D \cdot A$ values were revealed to be 0.3238 (± 0.0510) $m^2$, 0.309 (± 0.034) $m^2$, and 0.276 $m^2$, respectively. As expected, the $C_D \cdot A$ values of their dropped posture are clearly greater than the mean $C_D \cdot A$ of 0.184 (± 0.014) $m^2$ obtained for DP in this study due to the difference in the arm and torso angle. For the aero position, Grappe et al. (1997) measured a value for $C_D \cdot A$ of 0.262 $m^2$. Martin et al. (2006) revealed a mean $C_D \cdot A$ of 0.245 (± 0.044) $m^2$ in the seated position (possibly similar to AP). Interestingly, for the Obree's position, which is characterized by the arms bent below the chest and thus an extremely streamlined posture, Grappe et al. (1997) obtained a value of $C_D \cdot A$ = 0.216 $m^2$. In comparison, the mean $C_D \cdot A$ of 0.327 (± 0.026) $m^2$ obtained for AP in the present investigation is quite higher than the results from previous authors. Furthermore, Table 6.1 also shows the results of a towing experiment of Capelli et al. (1993) with a speed range of 8.6 to 14.6 $m \cdot s^{-1}$. For this, the $C_D \cdot A$ of the dropped position (straight arms) was found to be 0.255 $m^2$, which is dissimilar to the mean $C_D \cdot A$ of 0.184 (± 0.014) $m^2$ which was obtained for DP in this study.

The present results for UP reveal that the $C_D \cdot A$ value of UP is considerably higher than would be due to the fact that the cyclist must grip near the centre of the stem of the standard handlebar, which causes the torso angle to be more extended than in other positions. Likewise, the $C_D \cdot A$ value of DP is considerably lower than would be expected due to the fact that the cyclist must grip the lower part of the standard handlebar and the torso must crouch in a horizontal line. Generally, time-trial events are carried out in AP and for final period of the long distance events is carried out in DP, whereas both postures are characteristic streamlined cycling postures which reduce $F_{aer}$ at high speeds. The individual different values of $C_D \cdot A$ that were found in this study compared to the same cycling positions (UP and AP) in the previous studies, are possibly due to either different rider shapes or the bicycle. It is possible that the body shape of the subject is smaller and used the better bicycle that aerodynamic design. Finally, the coasting-down technique can perfectly distinguish between the $C_D \cdot A$ values among the individual subjects because their values were evidently different. It is also important to keep in mind that the different $C_D \cdot A$ values for each subject cannot have been a result of the effect of the cycling clothing, helmet or bicycle, because these were identical for all subjects in the present investigation.

### 6.2.3 Drag coefficient ( $C_D$ )

The value of the drag coefficient ( $C_D$ ) indicates the numerical efficiency of an object or body shape with which it moves through the air. The coasting-down technique has sufficient sensitivity to measure the changes of the three cycling positions, which revealed the obvious differences in $C_D$ . With this technique, Candau et al. (1999) concluded that the variability of $C_D$ was lower than 1%. In addition, the testing of the sensitivity showed that the $C_D$ can be determined with sufficient accuracy to identify slight control changes in $F_{aer}$. From a theoretical perspective, it could not be rejected that the $C_D$ can be found to be dependent on the Reynolds number that refers to the critical velocity at the point where the laminar flow becomes turbulent (Whitt & Wilson, 1982). The value of the Reynolds number depends on the object diameter and velocity and, consequently, the value of $C_D$ decreases as a function of velocity when the Reynolds number is in the critical range between laminar and turbulent flow (Janna, 1993). Regarding the Reynolds number in cycling science, the factors affecting the values of $C_D$ , $A$ and v are reviewed by Kyle and Weaver

(2004), Lukes et al. (2005), Martin et al. (2007), and Debraux et al. (2011). The value of $C_D$ for each riding posture of the study of Chowdhury et al. (2011) seems to be constant for velocities from 20 to 70 km·h$^{-1}$ under same conditions. This might be ascribed to the fact that this velocity range is too small and might therefore not be enough to vary the value of $C_D$. In other words, this speed range might not be reached the magnitude of $C_D$ that should be decreased with increased velocity. To the best of knowledge, previous authors in the last two decades mostly studied the value of $C_D \cdot A$ instead of $C_D$. The values of $C_D$ were determined by the coasting-down method and have been shown to be comparable to reference methods such as wind tunnel testing. From Table 6.1, comparing the $C_D$ values from the present study to the previous coasting-down method from De Groot et al. (1995) showed that the value of $C_D$ for the hoods posture was 0.829 (± 0.104), which is between the mean $C_D$ of 1.018 (± 0.106) obtained for UP and 0.741 (± 0.027) obtained for AP and higher than the mean $C_D$ of 0.437 (± 0.021) obtained for DP in the present investigation.

The $C_D$ values can further be compared between previous wind tunnel testing and the present results in Table 6.1. Chowdhury et al. (2011) reported a $C_D$ of 1.1 for the upright posture, which is most similar to the mean $C_D$ of 1.018 (± 0.106) for UP in the present study, whereas it is very different from the $C_D$ of 0.659 obtained in the study of Defraeye et al. (2010). The values of $C_D$ for the dropped posture in the studies of Chowdhury et al. (2011) and Defraeye et al. (2010) were found to be 1.0 and 0.657, respectively, which is greater than the mean $C_D$ of 0.437 (± 0.021) that was found for DP in the present investigation. The cycling posture that is most popular in wind tunnel testing is a time-trial posture, which is the same as AP in the present study. From Table 6.1, the $C_D$ for the time-trial posture was revealed to be 0.9 (Chowdhury et al., 2011) and 0.96 (± 0.03) (García-López et al., 2008); whereas these values are somewhat higher than the $C_D$ of 0.621 obtained by Defraeye et al. (2010). It seems that the mean $C_D$ of 0.741 (± 0.027) obtained for AP in this study is closest to the results of Defraeye et al. (2010). Furthermore, Crouch et al. (2012) reported that the lowest value of $C_D$ in the time-trial posture varied from 0.49 to 0.56, where the subject was a cyclist model. As for the highest value of $C_D$ for the various postures in Table 6.1, however, the hoods posture in the study of García-López et al. (2008) revealed the highest value of $C_D$ to be 1.33 (± 0.07).

The results of the CFD simulations of Blocken et al. (2013) found that the $C_D$ of the upright, dropped and time-trial position was 0.520, 0.468, and 0.397, respectively. Likewise, the CFD simulations of Defraeye et al. (2010)

revealed the $C_D$ of the upright, dropped, and time-trial position to be 0.534, 0.484, and 0.441, respectively. The $C_D$ values from the CFD simulations are lower than the $C_D$ values from this study and other author's results. However, one has to recognize that in both cases, the $C_D$ values were only simulated for the body surface of the subject without the bicycle. Additionally, in comparing the values of $C_D$ of previous force transducer methods and the present results from Table 6.1, there is only one investigation of Edwards and Byrnes (2007) that revealed the $C_D$ value of the dropped position to be 0.768 (± 0.066). The towing experiment of Capelli et al. (1993) showed that the value of $C_D$ for the dropped position was found to be 0.645. Their values are different from the mean $C_D$ of 0.437 (± 0.021) that was obtained for DP in this study.

From reviewing the previous findings, it can be summarized that the various aerodynamic factors for the upright position are higher than for the dropped position (with straight arms) and the time-trial (or aero) position, respectively. The comparison between the present results and previous studies revealed that only the mean $C_D$ of 1.018 (± 0.106) in UP is found to be very similar to the study of Chowdhury et al. (2011), which reported a values of $C_D$ = 1.1. This value was obtained in the same range of velocities between 20 and 70 km·h$^{-1}$ as that which was used to determine the values in the wind tunnel test. In contrast, the value of $C_D$ for DP (fully crouched and flexed arms), which was 0.437 (± 0.021) in the present study, was revealed to be entirely different to the values of $C_D$ obtained for the dropped position (with straight arms) in previous studies: the wind tunnel tests revealed $C_D$ = 1.0 (Chowdhury et al., 2011), and $C_D$ = 0.657 (Defraeye et al., 2010), the test with force transducers yielded $C_D$ = 0.768 (± 0.066) (Edwards & Byrnes, 2007), and the towing experiment revealed $C_D$ = 0.645 (Capelli et al., 1993). Regarding AP, which is the same as the time-trial position, the value of $C_D$ was found to be 0.741 (± 0.027). Although the experimental patterns differed from those of previous studies of $C_D$ in the aero position, it seems that the results of Defraeye et al. (2010) revealed the closest value of $C_D$, namely 0.621, which was obtained in a wind tunnel. For UP, it is possible that there is more turbulent airflow, which not only increases the air friction, but also reduces the capacity of the body surface that flows through the air. This is in contrast to AP or fully DP, where both postures seem to be more streamlined shapes. Although all rider positions were coasted down at 25 km·h$^{-1}$, which is not such a high speed, the $C_D$ values of the cycling positions are different for UP, AP, and DP at 1.018 (± 0.106), 0.741 (± 0.027), and 0.437 (± 0.021) respectively.

Consequently, the value of $F_{aer}$ would be expected to be different for all cycling positions. That means, the different $C_D$ values of UP, AP, and DP are adequately explained with the resistive forces model (Figure 5.13), the mechanical power model (Figure 5.14), and the energy expenditure model (Figure 5.16).

The present values of $C_D$ for the three cycling positions seem to be consistent with previous results in Table 6.1, where the value of $C_D$ depended on the shape and the tested velocity. As expected, the value of $C_D$ for DP is less than that of the dropped posture of previous authors because in the DP in the present study the upper body is fully crouched and the overall posture is therefore lower than in the previous studies. This low-crouched position causes a decrease of the frontal area and drag coefficient. In contrast with the value of $C_D$ for UP in the present study was found to be higher than that obtained in previous studies, because the hands grasped near the stem of the standard handlebars, causing the torso to straighten and leading to an increased frontal area.

### 6.2.4 Projected frontal area (*A*)

Table 6.2 Comparison of projected frontal area (*A*) with other technical measurements for cycling positions over the last two decades.

| Researcher | Technique | *n* | *A* ($m^2$) | | | | | |
|---|---|---|---|---|---|---|---|---|
| | | | Upright (Stem) | Hoods (Brakes) | dropped with Straight arms | Fully dropped (Traditional aero) | Aero | Time trial |
| Crouch et al. (2012) | Counting Photo-Pixels | 1 | | | | | | 0.410 to 0.419 |
| Chowdhury et al. (2011) | Digitalization | 1 | 0.410 | | 0.405 | | | 0.380 |
| Jensen et al. (2010) | Digitalization | 8 | | | | | 0.385 to 0.389 | |
| Debraux et al. (2009) | CAD | 9 | 0.565 ± 0.037 | | | 0.450 ± 0.040 | | |
| García-López et al. (2008) | Weighting Photographs | 5 | | 0.364 ± 0.012 | | | | 0.305 ± 0.008 |
| Edwards & Byrnes (2007) | Digitalization | 13 | | | 0.438 ± 0.113 | | | |
| Heil (2002) | Digitalization | 21 | 0.525 ± 0.010 | 0.562 ± 0.008 | 0.531 ± 0.008 | 0.460 ± 0.009 | | |
| Heil (2001) | Digitalization | 21 | | | | | 0.286 to 0.352 | |
| Olds & Olive (1999) | Planimetry | 17 | | 0.605 ± 0.069 | 0.563 ± 0.071 | | 0.493 ± 0.057 | |
| De Groot et al. (1995) | Planimetry | 7 | | 0.39 ± 0.03 | | | | |
| Capelli et al. (1993) | Weighting Photographs | 2 | | | 0.394 ± 0.013 | | | |
| Present study | Digitalization | 4 | 0.513 ± 0.023 | | | 0.421 ± 0.013 | 0.441 ± 0.019 | |

# CHAPTER 6: DISCUSSIONS

As expected, the mean $A$ of 0.513 (± 0.023) $m^2$ which was identified for UP in the present investigation is completely different to the values obtained for the other riding postures. The present results indicate that the value of $A$ for UP is similar to the values obtained by previous authors. For example, using Computer Aided Design (CAD) the study of Debraux et al. (2009) demonstrated a higher value of $A$ for an upright position ($A$ = 0.565 (± 0.037) $m^2$) than for a traditional aero position. Likewise, Heil (2002) used the digitizing method to find a value of 0.525 (± 0.010) $m^2$ for $A$ for a stem (upright) position, which was more than for other rider positions. Moreover, the hoods position is also similar to the upright posture apart from the fact that the rider grips the standard handlebar. Heil (2002) also measured the $A$ of the hoods posture and obtained a value of 0.562 (± 0.008) $m^2$, which was rather less than the value of 0.605 (± 0.069) $m^2$ which was obtained by use of the planimetry technique of Olds and Olive (1999). In fact, the UP yielded the highest value because the hands grasped near the stem of the standard handlebar causing the straight torso and increased frontal area. Nevertheless, the investigation of Heil (2002) revealed that the value of $A$ for the hoods posture is slightly greater than that for UP.

A review of scientific literature revealed that very little has been published so far regarding the comparison of $A$ between fully DP and other different cycling positions. To the best of knowledge, only two publications presented values of $A$ for a traditional-aero position, which is identical to DP: a value of 0.450 (± 0.040) $m^2$ was found in the study of Debraux et al. (2009) and a value of 0.460 (± 0.009) $m^2$ was obtained by Heil (2002). Hence, their values are similar to the mean $A$ of 0.421 (± 0.013) $m^2$ which was found for DP in the current study. Regarding the dropped posture with straight arms, Heil (2002) measured a value 0.531 (± 0.008) $m^2$ for $A$, which is similar to the value of 0.563 (± 0.071) $m^2$ found by Olds and Olive (1999).

Likewise, the value of $A$ for AP has also received little previous attention in scientific literature. It is interesting to compare the present results for the mean of $A$ for AP ( $A$ = 0.441 (± 0.019) $m^2$) with a very similar value of reporting by Debraux et al. (2009), namely $A$ = 0.450 (± 0.040) $m^2$, though it is slightly different to the measurements of Olds and Olive (1999), who obtained a value of 0.493 (± 0.057) $m^2$. Furthermore, Heil (2001) applied the digitalization method to determine the value of $A$ for the aero posture with different seat-tube angles of the bicycle and torso angles of the cyclist and found values between 0.286 to 0.352 $m^2$. These values are consistent with the digitizing method of Jensen et al. (2010), which found values between 0.385 to 0.389 $m^2$.

As aforementioned, both the aero and time-trial positions are popular cycling positions and are both the same riding position apart from the different use of the handlebar. By definition, the aero position uses an aero-bar mounted to the upper part of the standard handlebar, while the time-trial position uses a time-trial bar (tri-bars), because both handlebars will force the upper body, hands, and arms into a streamlined shape. When viewed from the outside, the

time-trial bar seems to be more aerodynamically efficient than the standard handlebar mounted to the aerobars. From Table 6.1, the *A* of the time-trial posture was mostly measured in the wind tunnel, which yielded lower values of *A* than for AP. For example, the measurements of Blocken et al. (2013) and Defraeye et al. (2010) found a value of 0.34 $m^2$, which is little different to the value of 0.380 $m^2$ reported by Chowdhury et al. (2011). The results of Crouch et al. (2012) revealed values between 0.410 to 0.419 $m^2$, which are most similar to the present results. In contrast to the present findings, García-López et al. (2008) reported a value of 0.305 (± 0.008) $m^2$ for *A* in the time-trial posture, which is lower than the value of *A* that was determined in the present investigation for AP and lower than that of various comparable positions, which may be due to the different handlebar.

## 6.3 Cycling models

### 6.3.1 Resistive forces model

The cycling model in Figure 5.13 is used to explain the resistive forces or $F_{net}$, which consists of a velocity-dependent force, $F_{aer}$ (parabolic lines), and a velocity-independent force, $F_{rol}$ (constant line), of the three cycling positions. The models of the function for $F_{net}$ with respect to v in each rider position can be rearranged according to a mathematical formula as: $y = a + b \cdot x^2 = F_{net} = F_{rol} + K \cdot \mathrm{v}^2$. Consequently, the rearranged resistive forces models are

for UP: $F_{net} = 5.449 + 0.310 \cdot \mathrm{v}^2$,

for AP: $F_{net} = 5.484 + 0.194 \cdot \mathrm{v}^2$, and

for DP: $F_{net} = 5.449 + 0.108 \cdot \mathrm{v}^2$.

The resistive forces were modeled from these equations for each cycling position. With regard to the $F_{rol}$, a value of 0.006 was assumed for $\mu$; thus, a mean $F_{rol}$ of 5.449 N was yielded for UP and DP and of 5.484 N for AP for all tests. Regarding Figure 5.13 with two tested initial velocities for the costing-down tests, the values of $F_{aer}$ for UP, AP, and DP were approximated as follows: 14.8, 9.2, and 5.1 N, respectively, at 6.9 $m \cdot s^{-1}$ (25 $km \cdot h^{-1}$); and 5.5, 3.4, and 1.9 N, respectively, at 4.2 $m \cdot s^{-1}$ (15 $km \cdot h^{-1}$). Thus, the values of $F_{net}$ for UP, AP, and DP at 6.9 $m \cdot s^{-1}$ are 20.2, 14.7, and 10.6 N, respectively, and at 4.2 $m \cdot s^{-1}$ they are 10.9, 8.9, and 7.4 N, respectively. The model shows that at very high

velocities the value of $F_{rol}$ is much smaller than the value of $F_{aer}$: $0.310 \cdot v^2$ N for UP, $0.194 \cdot v^2$ N for AP, and $0.108 \cdot v^2$ N for DP.

However, from calculations it was also found that, at a velocity of 4.19 m·s$^{-1}$ (15.10 km·h$^{-1}$) for UP, 5.32 m·s$^{-1}$ (19.14 km·h$^{-1}$) for AP, and 7.10 m·s$^{-1}$ (25.57 km·h$^{-1}$) for DP, a constant $F_{rol}$ curve intersects with these $F_{aer}$ curves. In other words, the value of $F_{aer}$ in each position is then equal to the constant $F_{rol}$ value. The value of $K \cdot v^2 = 0.194 \cdot v^2$ for AP in this investigation is similar to the value that was found in the study of De Groot et al. (1995), who reported a value of $K \cdot v^2 = 0.19 \cdot v^2$ in the hoods posture (crouched and hands gripping the break-hood parts).

### 6.3.2 Mechanical power model

The mathematical model in Figure 5.13, when multiplied with the velocity, becomes $P_{net} = F_{net} \cdot v$, which is used to explain a mechanical power model, as shown in Figure 5.14 for the three cycling positions. Actually, it consists of the mechanical power of aerodynamic drag, given by $P_{aer} = F_{aer} \cdot v = K \cdot v^2 \cdot v$, which is the parabolic line, and the mechanical power of rolling friction, given by $P_{rol} = F_{rol} \cdot v$, which is an oblique straight line. The functional model of the mechanical power with respect to velocity $P(v)$ can be rearranged according to a mathematical form for each rider position: $y = a \cdot x + b \cdot x^3 = P_{net} = F_{rol} \cdot v + K \cdot v^3$. Consequently, the rearranged cycling mechanical power models are

for UP: $P_{net} = 5.449 \cdot v + 0.310 \cdot v^3$,

for AP: $P_{net} = 5.484 \cdot v + 0.194 \cdot v^3$, and

for DP: $P_{net} = 5.449 \cdot v + 0.108 \cdot v^3$.

The mechanical power was modeled from these equations for each cycling position. Considering Figure 5.14 at very high velocities shows that the value of $P_{rol}$ is considerably smaller than the value of $P_{aer}$: $0.310 \cdot v^3$ Watts for UP, $0.194 \cdot v^3$ Watts for AP, and $0.108 \cdot v^3$ Watts for DP. This demonstrates that the factor $v^3$ of the aerodynamic term is a very important factor that increases the mechanical power and is related to the energy requirement of cyclists. In other words, the aerobic cost at high speeds becomes a significant contributor to generate the mechanical power in order to overcome the resistive forces. There has been a model regarding the energy cost requirements was presented in the study of Candau et al. (1999), which showed that the upright position required slightly more energy than the aero

position. Furthermore, Figure 5.15 represents the linear regression between *P* and $\dot{V}O_2$ for the three cycling positions. It was found that at all workloads energy cost in DP was higher than in AP and UP, respectively, due to the high oxygen uptake requirement, which was described in the first part of the discussion.

Recently, a technique arose which can directly measure the mechanical power versus the velocity which is needed to overcome the resistive forces opposing the motion during real cycling. This technique is called the force transducer technique (García-López et al., 2008) and uses a crank dynamometer or a powermeter (SRM®, MaxOne®, and PowerTap®); however, the accurate ones are expensive. How the mechanical power is determined from the force transducer method is reviewed in the literature by Grappe et al. (1997), Martin et al. (2006), Edwards and Byrnes (2007) and Lim et al. (2011). Thus, the coasting-down technique was presented and proved to be an interesting alternative method. This technique is also suitable for the prediction of the cycling energy cost.

### 6.3.3 Energy expenditure model

While cycling, both the production and use of mechanical power are dissipated to overcome the resistive forces, which can be determined by the net force multiplied with the instantaneous velocity: $P = F_{net} \cdot \mathrm{v}$ . Given the mechanical power, the cycling performance can also be predicted. The effectively produced mechanical power must be covered by the metabolic power, which eventually determines the cycling performance. From the present study, the factors of the drag coefficient ( $C_D$ ) and the projected frontal area (*A*) or drag area ( $C_D \cdot A$ ) all clearly indicated that the effect of the rider position on the mechanical power cannot be neglected. Consequently, the energy expenditure and performance will also be affected. As a matter of fact, in order to compare the energy cost, the direct quantification of the energy measurement should be obtained from the expired-gas collection during real cycling in the various positions. This method of expired-gas collection actually affects the air drag leading to energy expenditure, especially at high speeds.

However, this is associated with the methodological complexity of measuring $\dot{V}O_2$ during real cycling in various rider positions (especially in crouched postures), because the subject needs to attach the measuring devices to his or her face, which is not particularly comfortable during testing. As an alternative option, the coasting deceleration technique (used to determine $C_D$ ) and the spiroergometry testing (used to measure $\dot{V}O_2$ ) were combined to approximate and predict the energy cost of various rider positions in the present study.

The description of the energy expenditure will begin from the model of Figure 5.13, which is used to describe the resistive forces ( $F_{aer}$ and $F_{rol}$ ) opposed to the cycling motion and is based on the initial assumption that $C_D$ , *A*,

and $\mu$ are constant over the increasing velocity. In order to understand the present results, the mechanical power ($P$) was calculated, as shown in Figure 5.14, and the function of oxygen consumption ($\dot{V}O_2$) with respect to velocity (v) was estimated. Both were modeled for the three cycling positions under the same conditions. The individual average oxygen consumption, shown in Table 5.22, was taken to calculate the linear correlation between $\dot{V}O_2$ and $P$ in each position for the tested intensities of 100, 140, and 180 Watts (Figure 5.15). For these intensities, the workloads from the ergometer can be assumed to be the mechanical power. The curves of $\dot{V}O_2$, obtained from the spiroergometry test, were averaged over four subjects. Then, Equations (5.1) to (5.3) are used to obtain model for $\dot{V}O_2$ and $P$, which is represented in Figure 5.16. The mechanical power was modeled by $\dot{V}O_2 = m \cdot P + c = m \cdot (F_{rol} \cdot \mathrm{v} + K \cdot \mathrm{v}^3) + c$ for each cycling position. Hence, the rearranged mechanical power models are

for UP: $\dot{V}O_2 = 11.132 \cdot (5.449 \cdot \mathrm{v} + 0.310 \cdot \mathrm{v}^3) + 545.524$,

for AP: $\dot{V}O_2 = 11.151 \cdot (5.484 \cdot \mathrm{v} + 0.194 \cdot \mathrm{v}^3) + 682.425$, and

for DP: $\dot{V}O_2 = 11.589 \cdot (5.449 \cdot \mathrm{v} + 0.108 \cdot \mathrm{v}^3) + 812.741$.

As a result of this relationship, the models can explain the effect of the cycling positions on the predicted energy expenditure and, especially, estimate the value of $\dot{V}O_2$ at increasing velocity in the different positions. The mathematical models show that both the estimated mechanical power and the metabolic demands indicate that the $C_D \cdot A$ value is the most important variable, which results in the different curves. The model of Figures 5.14 and 5.16 demonstrates that the estimated $P$ and $\dot{V}O_2$ for UP are higher than for AP and DP, respectively. This can be caused by the higher value of $C_D$ and $A$ in UP than in AP and DP, respectively.

However, before the intersection point of all curves in Figure 5.16 at a velocity of approximately 5 $\mathrm{m \cdot s^{-1}}$ (or 18 $\mathrm{km \cdot h^{-1}}$), it seems that the $\dot{V}O_2$ of DP is greater than for the other positions. At this intersection point, it is apparent that the consumed $\dot{V}O_2$ at each rider position is equal at approximately 1200 $\mathrm{ml \cdot min^{-1}}$. As a matter of fact, before the velocity of approximately 5 $\mathrm{m \cdot s^{-1}}$, the curve of $\dot{V}O_2$ should be either equal or nearly equal for all positions, but in this study the $\dot{V}O_2$ of DP yielded a higher value than the other positions. It is possible that at low speeds, up until 5 $\mathrm{m \cdot s^{-1}}$, the upper muscle is recruited more in DP than in the other positions due to stabilising of the posture while cycling. This indicates that at low speeds the aerodynamic drag plays a less important role than the influence of $\dot{V}O_2$.

It is interesting to note that after approximately velocity 5 $m \cdot s^{-1}$ (or 18 $km \cdot h^{-1}$), the $\dot{V}O_2$ for UP increases more with v along a parabolic curve than for AP and DP. In other words, at the same $\dot{V}O_2$, for instance at 2000 $ml \cdot min^{-1}$, the DP can be utilized to produce the speed better than AP and UP. The estimated $\dot{V}O_2$ values with respect to the increasing v show that this present technique can be used to determine the aerodynamic parameters. It is demonstrated that changing the rider position and speed can result in an increase in the energy cost. Concerning the mechanical efficiency of the various rider positions, riding in DP seems to produce the best results. Furthermore, under similar speed conditions it is indicated that the $\dot{V}O_2$ curve increases more with v for UP than for the other positions, because riding in UP yields larger values of $C_D$ and $A$ or $C_D \cdot A$, causing greater values of $F_{aer}$ which then induces greater energy costs, denoted by the higher values of $\dot{V}O_2$.

## 6.4. Limitations and Recommendations

### 6.4.1 Spiroergometry testing

Based on the findings of this study, the following limitations are explained. Firstly, twenty-four subjects were recruited from the recreational male cyclists. They were familiar with daily cycling in the upright position with racing bike, mountain bike, and city bike. Therefore, the limitations in the study are that, subjects had no or less the cycling experience in aero and dropped position and training program was different affecting the physical fitness. Secondly, the comparisons were based on three test intensities (i.e. 100, 140, and 180 Watts) and seven cardiorespiratory variables (i.e. heart rate, oxygen uptake, carbon dioxide output, respiratory exchange rate, minute ventilation, tidal volume, and breathing frequency). Thirdly, laboratory measurements under similarly controlled conditions such as range of humidity, temperature, and air pressure were considered to be the first validation step for the Oxycon Mobile® portable metabolic system. However, the gradient temperature in laboratory in each day could not be equally controlled, especially, testing in the summer season period.

The main aim of this study was to highlight the importance of methodological research in measuring the response of cardiorespiratory parameters. On the basis of the results presented here, the future study should be made the following recommendations. A study should be conducted with well-trained cyclists who have the experience of using both standard and aero handlebars (aero and dropped position). This may exclude the variability experienced in this study from individual subjects and give more practical and significant results. An interesting study would involve

bending of the elbows in fully dropped position to attain similar aerodynamic cross section to the streamlined position. It is hypothesized that this would involve greater upper body muscular effort for the fully dropped position and may show the significant differences of electromyography (EMG). This approach to the study may be of greater practical value as it may give additional answers available from the usage of fully dropped position in the real situation. Therefore, the future study should be shown the need for a more in-depth examination of the correlation between cardiorespiratory functions and EMG analysis in each cycling position.

### 6.4.2 Coasting down testing

This investigation was performed in the sports hall and limited following major and minor importance. Firstly, four subjects were selected from the part of submaximal spiroergometry testing. They were of varying geometry, weight, and height, resulting to difference of value of aerodynamic and rolling parameters. Moreover, subjects also had less experience with their aero position and fully dropped position. Secondly, the greatest limitation to this investigation was the initial velocity that used for the determination of aerodynamic and rolling parameters. Because of the distance of coasting-down tests consisted of three parts: 20 m long for accelerating phase, 30 m long for freewheeling phase, and 20 m long for breaking phase (outside of the sports hall). Thirdly, the floor in sports hall was made of the plywood, which would result the movement as wave due to its softness while coasting down; consequently, this will affect to the parameter estimation of the rolling coefficient value. Fourthly, the gradient temperature and relative humidity in sports hall could not be equally controlled in each day of summer season, which influence to the value of air density.

There are numbers of improvement that could be made to the coasting down experiment to increase its efficiency and accuracy. Based on the findings of this investigation; therefore, the following recommendations should be additionally performed. In the future, a more in-depth investigation of the coasting deceleration method in addition to the conditions in this experiment such as using the higher initial speed, the longer distance, and the harder floor, could give more insight into the value of aerodynamic and rolling parameters, and provide better information for cycling sport scientists.

The first thing that could be improved for the coasting-down technique should increase the distance of every phase. The increased distance for accelerating phase could sufficiently speed up for the defined initial high velocity by subjects. Unless this technique wants to freewheel until standing still, requires to increasing distance depends on initial speed. However, unless this technique coasts down in the short distance with initial high speed, also requires a longer breaking phase distance for safely stop. Because the distance during breaking phase was too short, the rider would be concerned. Increasing of long distance for freewheeling phase until standing still will help to examine the velocity

respect to the time with the mathematical model of coasting down. To do this, the coasting down technique requires the well-trained cyclist to control the bicycle from start point to final point. Using this conditional experiment, an accurate value would be obtained without the least error.

As noted by author, the oscillatory graphs could be influenced from the floor in sports hall because it made of the plywood. Therefore, this should be improved by testing on a harder floor, which the oscillatory graphs would be smaller than testing on a plywood floor. Moreover, this could also relate to the rolling coefficient. The value of rolling coefficient could not be accurately determined unless a cyclist-bicycle system could not approach to the final velocity. If access to a stopping point of rider and bicycle were possible, this value could be more accurately calculated according to the relationship of cycling motion: $F_{res} = F_{rol} + F_{aer} = F_{rol} + K \cdot \mathrm{v}^2$ the value of $F_{res} = F_{rol}$ when the final velocity $\mathrm{v}_f = 0$. However, this concerns just theoretical idea which the fact would be hard to solve. Namely, the control of bicycle would be oscillatory while going to stop resulting to the non-stationary graph of $\mathrm{v}(t)$. An in-depth investigation into the value of rolling coefficient to cycling with upright, aero, and dropped position should be conducted and closely assessed the responses at various levels of added weight.

Another testing to improve validity with the coasting down technique would be a test on the real road without wind and calm day. The telemetry-bicycle system that was used in this study could be directly taken to actual cycling, and data collection could transmit to a receive unit on an automobile. Furthermore, a future work for determination of the projected frontal area in each cycling position suggests that it should be photographed during actual coasting down phase.

As a result, the upright position, the aero position, and the fully dropped position were used in this investigation were significantly different in cardiorespiratory responses, and also represented the different aerodynamic parameters. Therefore, a future study should conduct physiological responses to real situation in upright, aero, and dropped position with using a portable telemetric gas analysis system to measure energy expenditure at various constant speeds. It is hypothesized that this would involve the projected frontal area of upright position may show the significant differences of energy cost greater than aero and dropped position. This may be possible to calculate the aerodynamic variables from energy expenditure obtaining from real situation. The study should be conducted with well-trained cyclists which familiar to both standard and aero handlebars.

# CHAPTER 7: CONCLUSIONS

The present study indicates that the crouched positions (aero position and fully dropped position) lead to a higher metabolic cost, including greater exhaustion at submaximal intensities, than the upright position, with the focus being on participants who were unfamiliar with riding in the crouched positions. Therefore, the author concludes that reducing the torso angle from the upright position to the crouched positions induces an increase in breathing mechanics, cardiac functions, and muscular actions. This can be explained by the following factors. Firstly, the diaphragm movement in the crouched positions are impeded by the internal organs, i.e. by the fact that the abdominal and thoracic cavity are decreased, thus resulting in an increased internal and blood pressure. Secondly, the crouched positions as seem to be an exercise in prone posture (face-down), the gravitational force may increase the difficulty of inhalation because the thorax is compressed; and this force may induce the increased stroke volume due to increased preloading. Thirdly, the crouched positions alter the main group of muscles around the hip by increasing the dynamic muscular contraction; in addition, the static muscle contraction of the upper limb must be recruited in order to support the upper body mass, particularly in the fully dropped position.

As mentioned above, for cyclists who are inexperienced in training in the crouched positions, these leading to an increase in the negative cardiorespiratory functions, as supported by the significantly increased cardiorespiratory variables in present results. In order to benefit from the aerodynamic advantages of these positions, though, the cyclists need to train in the crouched positions for physiological adaptations and familiarity. This can help reduce the disadvantage of the trunk forward flexion on the cardiorespiratory effects. To the best of knowledge, the evidence points in the direction that there is a tendency toward adaptation to a training position, as has been well documented in the literatures (Berry et al., 1994; Dorel et al., 2009; Hubenig et al., 2011; Origenes et al., 1993; Peveler et al., 2005). It appears that there are no significant differences in the cardiorespiratory responses for studies in which the participants were either trained cyclists or triathletes.

Apart from the examination of the cardiorespiratory responses, the aerodynamic parameters (air drag, drag area and drag coefficient) in the three cycling positions were also investigated by the coasting down method. It was concluded that the aerodynamic parameters of the individual subjects could easily be obtained from the coasting down technique. The technique was performed in the short-distance sports-hall because the wind flow, the ambient temperature, and the ground level could be controlled and stable environmental variables were required for the present investigation. Due to this, the resistive or net forces in the still airflow could be accurately determined by the aerodynamic drag, which depended on the square velocity, and a constant rolling resistance. In other words, the fact that the motion of the rider-bicycle combination was always coasted down under the same circumstances ensured good reproducibility of the investigations. Moreover, the coasting down method relies on the precision of the tachogenerator or speed sensor for measuring the velocity-time function and of the telemetry system for transmittance.

# CHAPTER 7: CONCLUSIONS

The cycling positions that were selected to be investigated included an upright position and two crouched positions, namely the aero position and the fully dropped position. As expected, the results showed that the crouched positions yielded lower values for the aerodynamic parameters than the upright position. This confirms that the calculated values from the coasting down test agree well with those found in wind tunnel tests (García-López et al., 2008; Gibertini et al., 2008; Defraeye et al., 2010; Chowdhury et al., 2011; Crouch et al., 2012) and are also comparable to the results of other previous investigations using other methods (Martin et al., 2006; Edwards & Byrnes, 2007; Lim et al., 2011; Blocken et al., 2013). From a physical point of view, the aero posture and fully dropped posture generate a smooth airflow over the head and the horizontal, flat back, which results in the airflow being attached to the crouched upper body for as long as possible. The results of the fully dropped posture were especially interesting and useful in this investigation because it yielded lowest numerical value of the drag coefficient. This is due to the upper body shape of the fully dropped posture, which induces the smallest projected frontal area. On the other hand, the measurements of the upright posture, with the back being rather vertical with respect to the ground, showed an increased projected frontal area leading to the highest drag coefficient.

Finally, it can be said that the present study was able to demonstrate the advantages, the feasibility, and the sensibility of the coasting-down technique for determining the differences of the three cycling positions with respect to the aerodynamic drag, the drag area and the drag coefficient, and that the technique provides an alternative method for aerodynamic studies in cycling.

# REFERENCES


Ashe, M.C., Scroop, G.C., Frisken, P.I., Amery, C.A., Wilkins, M.A. & Khan, K.M. (2003). Body position affects performance in untrained cyclists. *British Journal of Sports Medicine*, *37*, 441-444.

Atkinson, G., Davison, R., Jeukendrup, A. & Passfield, L. (2003). Science and cycling: current knowledge and future directions for research. *Journal of sports sciences*, *21*(9), 767-787.

Atkinson, G., Peacock, O. & Passfield, L. (2007). Variable versus constant power strategies during cycling time-trials: prediction of time savings using an up-to-date mathematical model. *Journal of sports sciences*, *25*(9), 1001-1009.

Bartlett, R. (1997). *Introduction to Sports Biomechanics*. London and New York: Routledge, Taylor & Francis Group.

Behrakis, P.K., Baydur, A., Jaeger, M.J. & Milic-Emili, J. (1983). Lung mechanics in sitting and horizontal body positions. *Chest*, *83*, 643-646.

Berry, M.J., Pollock, W.E., van Nieuwenhuizen, K. & Brubaker, P.H. (1994). A comparison between aero and standard racing handlebars during prolonged exercise. *International Journal of Sports Medicine*, *15*, 16-20.

Billo, E.J. (2007). *Excel for Scientists and Engineers: Numerical Methods*. Hoboken, New Jersey: John Wiley & Sons, Inc.

Blocken, B., Defraeye, T., Koninckx, E., Carmeliet, J. & Hespel, P. (2013). CFD simulations of the aerodynamic drag of two drafting cyclists. *Computers & Fluids*, *71*, 435-445.

Bouckaert, J., Pannier, J.L. & Vrijens, J. (1983). Cardiorespiratory response to bicycle and rowing ergometer exercise in oarsmen. *European Journal of Applied Physiology and Occupational Physiology*, *51*, 51-59.

Brown, A.M. (2001). A step-by-step guide to non-linear regression analysis of experimental data using a Microsoft Excel spreadsheet. *Computer methods and programs in biomedicine*, *65*(3), 191-200.

Brown, A.M. (2006). A non-linear regression analysis program for describing electrophysiological data with multiple functions using Microsoft Excel. *Computer methods and programs in biomedicine*, *82*(1), 51-57.

Brownlie, L., Kyle, C., Carbo, J., Demarest, N., Harber, E., MacDonald, R. & Nordstrom, M. (2009). Streamlining the time trial apparel of cyclists: the Nike Swift Spin project. *Sports Technology*, *2*(1-2), 53-60.

Burke, E.R. (1995). *Serious Cycling*. Champaign, Illinois: Human Kinetics.

Cabello, B. & Mancebo, J. (2006). Work of breathing. *Intensive Care Medicine*, *32*, 1311-1314.

Candau, R.B., Grappe, F., Menard, M., Barbier, B., Millet, G.Y., Hoffman, M.D. & Rouillon, J.D. (1999). Simplified deceleration method for assessment of resistive forces in cycling. *Medicine and science in sports and exercise*, *31*(10), 1441-1447.

Capelli, C., Rosa, G., Butti, F., Ferretti, G., Veicsteinas, A. & di Prampero, P.E. (1993). Energy cost and efficiency of

riding aerodynamic bicycles. *European journal of applied physiology and occupational physiology*, *67*(2), 144-149.

Capelli, C., Schena, F., Zamparo, P., Monte, A.D., Faina, M. & di Prampero, P.E. (1998). Energetics of best performances in track cycling. *Medicine and science in sports and exercise*, *30*(4), 614-624.

Chowdhury, H., Alam, F. & Mainwaring, D. (2011). A full scale bicycle aerodynamics testing methodology. *Procedia Engineering*, *13*, 94-99.

Chua, J.J., Fuss, F.K. & Subic, A. (2010). Rolling friction of a rugby wheelchair. *Procedia Engineering*, *2*(2), 3071-3076.

Cooke, C.B. (2003). Metabolic Rate and Energy Balance. In R. Eston & T. Reilly (Eds.), *Kinanthropometry and Exercise Physiology Laboratory Manual: Tests, Procedure and Data. Volume 2: Exercise Physiology* (pp. 137-160). London and New York: Routledge, Taylor & Francis Group.

Crouch, T., Sheridan, J., Burton, D., Thompson, M. & Brown, N.A. (2012). A quasi-static investigation of the effect of leg position on cyclist aerodynamic drag. *Procedia Engineering*, *34*, 3-8.

Cunningham, D.A., Goode, P.B. & Critz, J.B. (1975). Cardiorespiratory response to exercise on a rowing and bicycle ergometer. *Medicine and Science in Sports and Exercise*, *7*, 37-43.

Dahmen, T. & Saupe, D. (2011). Calibration of a power-speed-model for road cycling using real power and height data. *International Journal of Computer Science in Sport, 10*(2), 18-36.

Dahmen, T., Byshko, R., Saupe, D., Röder, M. & Mantler, S. (2011). Validation of a model and a simulator for road cycling on real tracks. *Sports Engineering*, *14*(2-4), 95-110.

Davies, C.T.M. (1980). Effect of air resistance on the metabolic cost and performance of cycling. *European journal of applied physiology and occupational physiology*, *45*(2-3), 245-254.

De Groot, G., Welbergen, E., Clusen, L., Clarus, J., Cabri, J. & Antonis, J. (1994). Power, muscular work, and external forces in cycling. *Ergonomics*, *37*(1), 31-42.

De Groot, G., Sargeant, A. & Geysel, J. (1995). Air friction and rolling resistance during cycling. *Medicine and science in sports and exercise*, *27*(7), 1090-1095.

Debraux, P., Bertucci, W., Manolova, A.V., Rogier, S. & Lodini, A. (2009). New method to estimate the cycling frontal area. *International journal of sports medicine*, *30*(04), 266-272.

Debraux, P., Grappe, F., Manolova, A.V. & Bertucci, W. (2011). Aerodynamic drag in cycling: methods of assessment. *Sports Biomechanics*, *10*(3), 197-218.

Defraeye, T., Blocken, B., Koninckx, E., Hespel, P. & Carmeliet, J. (2010). Aerodynamic study of different cyclist positions: CFD analysis and full-scale wind-tunnel tests. *Journal of biomechanics*, *43*(7), 1262-1268.

# REFERENCES

Díaz, V., Benito, P.J., Peinado, A.B., Álvarez, M., Martín, C., di Salvo, V., Pigozzi, F., Maffulli, N. & Calderón, F.J. (2008). Validation of a new portable metabolic system during an incremental running test. *Journal of sports science & medicine*, *7*(4), 532-536.

Di Prampero, P.E. (2000). Cycling on Earth, in space, on the Moon. *European journal of applied physiology*, *82*(5-6), 345-360.

Dorel, S., Couturier, A. & Hug, F. (2009). Influence of different racing positions on mechanical and electromyographic patterns during pedalling. *Scandinavian Journal of Medicine and Science in Sports*, *19*, 44-54.

Draper, N.R. & Smith, H. (1998). *Applied Regression Analysis*. New York: John Wiley & Sons, Inc.

Edwards, A.G. & Byrnes, W.C. (2007). Aerodynamic characteristics as determinants of the drafting effect in cycling. *Medicine and science in sports and exercise*, *39*(1), 170-176.

Egaña, M., Smith, S. & Green, S. (2006). Effect of posture on high-intensity constant-load cycling performance in men and women. *European journal of applied physiology*, *96*, 1-9.

Eriksson, J.S., Rosdahl, H. & Schantz, P. (2012). Validity of the Oxycon Mobile metabolic system under field measuring conditions. *European journal of applied physiology*, *112*(1), 345-355.

Eston, R.G. (2003). Lung Function. In R. Eston & T. Reilly (Eds.), *Kinanthropometry and Exercise Physiology Laboratory Manual: Tests, Procedure and Data. Volume 2: Exercise Physiology* (pp. 137-160). London and New York: Routledge, Taylor & Francis Group.

Evangelisti, M.I., Verde, T.J., Andres, F.F. & Flynn, M.G. (1995). Effects of handlebar position on physiological responses to prolonged cycling. *Journal of Strength and Conditioning Research*, *9*, 243-246.

Faria, E.W., Parker, D.L. & Faria, I.E. (2005). The science of cycling: factors affecting performance - part 2. *Sports medicine*, *35*(4), 313-337.

Faria, I., Dix, C. & Frazer, C. (1978). Effect of body position during cycling on heart rate, pulmonary ventilation, oxygen uptake and work output. *Journal of Sports Medicine and physical fitness*, *18*, 49-56.

Faria, I.E. (1992). Energy expenditure, aerodynamics and medical problems in cycling. An update. *Sports medicine*, *14*(1), 43-63.

Foss, M.L. & Keteyian, S.J. (1998). *Fox's Physiological Basis for Exercise and Sport*. Boston, Massachusetts: WCB/McGraw-Hill.

Franke, W.D., Betz, C.B. & Humphrey, R.H. (1994). Effects of rider position on continuous wave Doppler responses to maximal cycle ergometry. *British Journal of Sports Medicine*, *28*, 38-42.

García-López, J., Rodríguez-Marroyo, J.A., Juneau, C.E., Peleteiro, J., Martínez, A.C. & Villa, J.G. (2008). Reference

values and improvement of aerodynamic drag in professional cyclists. *Journal of sports sciences*, *26*(3), 277-286.

Gibertini, G., Campanardi, G., Grassi, D. & Macchi, C. (2008). Aerodynamics of biker position. In *Proceedings of the BBAA VI International Colloquium on: Bluff Bodies Aerodynamics and Applications*.

Gnehm, P., Reichenbach, S., Altpeter, E., Widmer, H. & Hoppeler, H. (1997). Influence of different racing positions on metabolic cost in elite cyclists. *Medicine and Science in Sports and Exercise*, *29*, 818-823.

Grappe, F., Candau, R., Belli, A. & Rouillon, J.D. (1997). Aerodynamic drag in field cycling with special reference to the Obree's position. *Ergonomics*, *40*(12), 1299-1311.

Grappe, F., Candau, R., Busso, T. & Rouillon, J.D. (1998). Effect of cycling position on ventilatory and metabolic variables. *International Journal of Sports Medicine*, *19*, 336-341.

Grappe, F., Candau, R., McLean, B. & Rouillon, J.D. (1999a). Aerodynamic drag and physiological responses in classical positions used in cycling. *Science et motricité*, *n° 38-39*, 21-24.

Grappe, F., Candau, R., Barbier, B., Hoffman, M.D., Belli, A. & Rouillon, J.D. (1999b). Influence of tyre pressure and vertical load on coefficient of rolling resistance and simulated cycling performance. *Ergonomics*, *42*(10), 1361-1371.

Gross, A.C., Kyle, C.R. & Malewicki, D.J. (1983). The aerodynamics of human-powered land vehicles. *Scientific American*, *249*, 126-134.

Gregor, R.J. & Conconi, F. (2000). *Road cycling*. Osney Mead, Oxford: Blackwell Science Ltd.

Hall, S.J. (1999). *Basic Biomechanics*. Boston, Massachusetts: WCB/McGraw-Hill.

Harris, D.C. (1998). Nonlinear least-squares curve fitting with Microsoft Excel Solver. *Journal of Chemical Education*, *75*(1), 119-121.

Heil, D.P. (1997). The pressor response to submaximal cycle ergometry while using aerodynamic handlebars. *International Journal of Sports Medicine*, *18*, 1-7.

Heil, D.P. (2001). Body mass scaling of projected frontal area in competitive cyclists. *European journal of applied physiology*, *85*(3-4), 358-366.

Heil, D.P. (2002). Body mass scaling of frontal area in competitive cyclists not using aero-handlebars. *European journal of applied physiology*, *87*(6), 520-528.

Heil, D.P., Wilcox, A.R. & Quinn, C.M. (1995). Cardiorespiratory responses to seat-tube angle variation during steady-state cycling. *Medicine and Science in Sports and Exercise*, *27*, 730-735.

Heil, D.P., Derrick, T.R. & Whittlesey, S. (1997). The relationship between preferred and optimal positioning during

submaximal cycle ergometry. *European Journal of Applied Physiology and Occupational Physiology*, *75*, 160-165.

Henchoz, Y., Crivelli, G., Borrani, F. & Millet, G.P. (2010). A new method to measure rolling resistance in treadmill cycling. *Journal of sports sciences*, *28*(10), 1043-1046.

Hennekam, W. (1990). The speed of a cyclist. *Physics Education*, *25*(3), 141-146.

Hennekam, W. & Bontsema, J. (1991). Determination of Fr and Kd from the solution of the equation of motion of a cyclist. *European Journal of Physics*, *12*(2), 59-63.

Hennekam, W. & Govers, M. (1996). The freewheeling cyclist. *Physics Education*, *31*(5), 320-328.

Hertz, P.B. & Ukrainetz, P.R. (1967). Auto-aerodynamic drag-force analysis. *Experimental Mechanics*, *7*(3), 19A-22A.

Hoffman, M.D., Millet, G.Y., Hoch, A.Z. & Candau, R.B. (2003). Assessment of wheelchair drag resistance using a coasting deceleration technique. *American journal of physical medicine & rehabilitation*, *82*(11), 880-889.

Hubenig, L.R., Game, A.B. & Kennedy, M.D. (2011). Effect of different bicycle body positions on power output in aerobically trained females. *Research in Sports Medicine*, *19*, 245-258.

Janna, W.S. (1993). *Introduction to Fluid Mechanics*. Boston: PWS-KENT Publishers.

Jensen, R.L., Balasubramani, S., Burley, K.C., Kaukola, D.R. & LaChapelle, J.A. (2010). Reliability of a digital method to determine frontal area of a cyclist. *Measurement in Physical Education and Exercise Science*, *14*(2), 130-136.

Jeukendrup, A.E. & Martin, J. (2001). Improving cycling performance: how should we spend our time and money. *Sports Medicine*, *31*(7), 559-569.

Jobson, S.A., Nevill, A.M., George, S.R., Jeukendrup, A.E. & Passfield, L. (2008). Influence of body position when considering the ecological validity of laboratory time-trial cycling performance. *Journal of Sports Sciences*, *26*, 1269-1278.

Kreighbaum, E. & Barthels, K.M. (1996). *Biomechanics: A Qualitative Approach for Studying Human Movement*. Boston, Massachusetts: Allyn and Bacon.

Kroidl, R.F., Schwarz, S. & Lehnigk, B. (2007). *Kursbuch Spiroergometrie: Technik und Befundung verständlich gemacht*. Stuttgart: Georg Thieme.

Kyle, C.R. (1979). Reduction of wind resistance and power output of racing cyclists and runners travelling in groups. *Ergonomics, 22*(4), 387-397.

Kyle, C.R. (1996). Selecting Cycling Equipment. In E.R. Burke (Ed.), *High-Tech Cycling* (pp. 1-43). Champaign, Illinois: Human Kinetics.

Kyle, C.R. & Weaver, M.D. (2004). Aerodynamics of human-powered vehicles. *Proceedings of the Institution of Mechanical Engineers, Part A: Journal of Power and Energy*, *218*(3), 141-154.

# REFERENCES

Liengme, B.V. (2009). *A guide to Microsoft Excel 2007 for scientists and engineers*. London: Academic Press.

Lim, A.C., Homestead, E.P., Edwards, A.G., Carver, T.C., Kram, R. & Byrnes, W.C. (2011). Measuring changes in aerodynamic/rolling resistances by cycle-mounted power meters. *Medicine and science in sports and exercise*, *43*(5), 853-860.

Lucía, A., Carvajal, A., Calderón, F.J., Alfonso, A. & Chicharro, J.L. (1999). Breathing pattern in highly competitive cyclists during incremental exercise. *European Journal of Applied Physiology and Occupational Physiology*, *79*, 512-521.

Lucía, A., Hoyos, J., Rardo, J. & Chicharro, J.L. (2001). Effects of endurance training on the breathing pattern of professional cyclists. *Japanese Journal of Physiology*, *51*, 133-141.

Lukes, R.A., Chin, S.B. & Haake, S.J. (2005). The understanding and development of cycling aerodynamics. *Sports Engineering*, *8*(2), 59-74.

Martin, J.C., Milliken, D.L., Cobb, J.E., McFadden, K.L. & Coggan, A.R. (1998). Validation of a mathematical model for road cycling power. *Journal of Applied Biomechanics*, *14*, 276-291.

Martin, J.C., Gardner, A.S., Barras, M. & Martin, D.T. (2006). *Modeling sprint cycling using field-derived parameters and forward integration. Medicine and Science in Sports and Exercise*, *38*(3), 592-597.

Martin, J.C., Davidson, C.J. & Pardyjak, E.R. (2007). Understanding sprint-cycling performance: the integration of muscle power, resistance, and modeling. *International journal of sports physiology and performance*, *2*(1), 5-21.

Mognoni, P. & di Prampero, P.E. (2003). Gear, inertial work and road slopes as determinants of biomechanics in cycling. *European journal of applied physiology*, *90*(3-4), 372-376.

Origenes, M.M., Blank, S.E. & Schoene, R.B. (1993). Exercise ventilatory response to upright and aero-posture cycling. *Medicine and Science in Sports and Exercise*, *25*, 608-612.

Olds, T. & Olive, S. (1999). Methodological considerations in the determination of projected frontal area in cyclists. *Journal of sports sciences*, *17*(4), 335-345.

Peveler, W., Bishop, P., Smith, J. & Richardson, M. (2005). Effects of training in an aero position on metabolic economy. *Journal of Exercise Physiology online*, *8*, 44-50.

Price, D. & Donne, B. (1997). Effect of variation in seat tube angle at different seat heights on submaximal cycling performance in man. *Journal of Sports Sciences*, *15*, 395-402.

Reiser, R.F., Peterson, M.L. & Broker, J.P. (2002). Influence of hip orientation on Wingate power output and cycling technique. *Journal of Strength and Conditioning Research*, *16*, 556-560.

Ricard, M.D., Hills-Meyer, P., Miller, M.G. & Michael, T.J. (2006). The effects of bicycle frame geometry on muscle activation and power during a Wingate anaerobic test. *Journal of Sports Science and Medicine*, *5*, 25-32.

# REFERENCES

Richardson, R.S. & Johnson, S.C. (1994). The effect of aerodynamic handlebars on oxygen consumption while cycling at a constant speed. *Ergonomics*, *37*, 859-863.

Rohdin, M., Petersson, J., Sundblad, P., Mure, M., Glenny, R.W., Lindahl, S.G.E. & Linnarsson, D. (2003). Effects of gravity on lung diffusing capacity and cardiac output in prone and supine humans. *Journal of Applied Physiology*, *95*, 3-10.

Rosdahl, H., Gullstrand, L., Salier-Eriksson, J., Johansson, P. & Schantz, P. (2009). Evaluation of the Oxycon Mobile metabolic system against the Douglas bag method. *European journal of applied physiology*, *109*(2), 159-171.

Ryschon, T.W. & Stray-Gundersen, J. (1991). The effect of body position on the energy cost of cycling. *Medicine and Science in Sports and Exercise*, *23*, 949-953.

Savelberg, H.H.C.M., Van de Port, I.G. & Willems, P.J. (2003). Body configuration in cycling affects muscle recruitment and movement pattern. *Journal of Applied Biomechanics*, *19*, 310-324.

Schlegelmilch, R.M. & Kramme, R. (2011). Pulmonary Function Testing. In R. Kramme, K.P. Hoffmann & R.S. Pozos (Eds.), *Springer Handbook of Medical Technology* (pp. 95-117). Heidenberg: Springer.

Sheel, A.W., Lama, I., Potvin, P., Coutts, K.D. & McKenzie, D.C. (1996). Comparison of aero-bars versus traditional cycling postures on physiological parameters during submaximal cycling. *Canadian Journal of Applied Physiology*, *21*, 16-22.

Szal, S.E. & Schoene, R.B. (1989). Ventilatory response to rowing and cycling in elite oarswomen. *Journal of Applied Physiology*, *67*, 264-269.

Too, D. (1990). Biomechanics of cycling and factors affecting performance. *Sports Medicine*, *10*, 286-302.

Too, D. (1991). The effect of hip position/configuration on anaerobic power and capacity in cycling. *International Journal of Sport Biomechanics*, *7*, 359-370.

Van Dyke, M. (1982). *An Album of Fluid Motion*. Parabolic Press.

Versteeg, H.K. & Malalasekera, W. (2007). *An Introduction to Computational Fluid Dynamics: The Finite Volume Method*. Edinburgh Gate: Pearson Education.

Welbergen, E. & Clijsen, L.P.V.M. (1990). The influence of body position on maximal performance in cycling. *European Journal of Applied Physiology and Occupational Physiology*, *61*, 138-142.

Wilmore, J.H. & Costill, D.L. (2004). *Physiology of Sport and Exercise*. Champaign, Illinois: Human Kinetics.

Whitt, F.R. & Wilson, D.G. (1982). *Bicycling science*. Cambridge: The MIT Press.

Wohlhart, K. (1998). *Dynamik: Grundlagen und Beispiele*. Braunschweig/Wiesbaden: Vieweg.

Wolf, S. (2010). *Optimization of Pacing Strategies for Cycling Time Trials.* Dissertation, Universität Konstanz.

# APPENDIX A: FIGURES

| Shape and Flow | Form Drag | Skin Friction | Shape and Flow | Form Drag | Skin Friction |
|---|---|---|---|---|---|
|  | 0% | 100% | 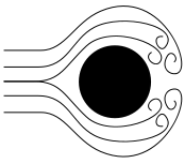 | ~90% | ~10% |
|  | ~10% | ~80% | 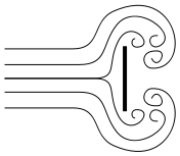 | 100% | 0% |

Figure 1 Illustration of relative proportions in percentage for various shapes such as a parallel plate, streamline, sphere, and perpendicular plate between their form drag and skin friction while flowing through a fluid. (Resource: http://en.wikipedia.org/wiki/Drag_(physics))

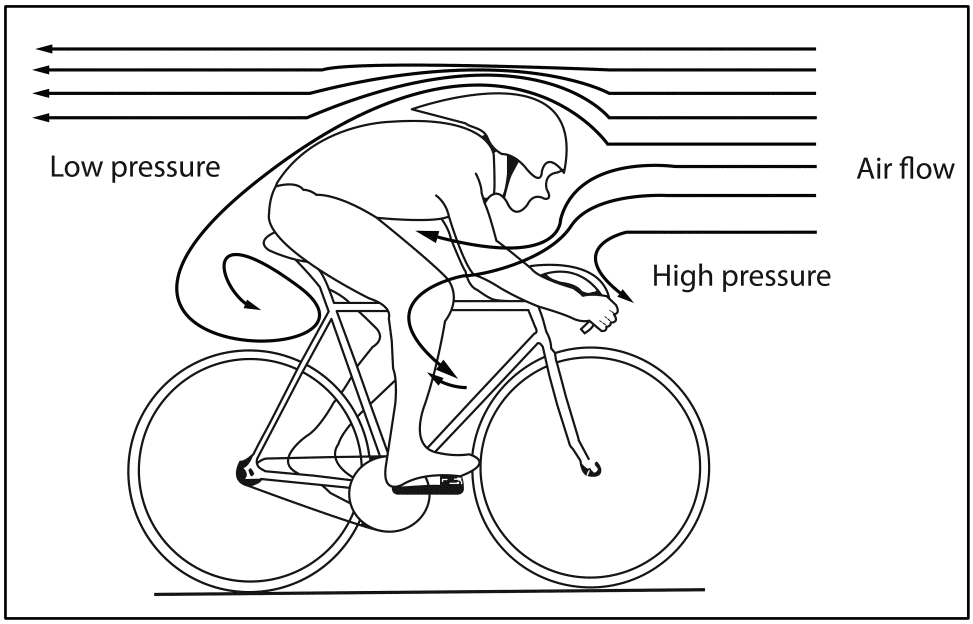


Figure 2 Illustration of air pressure drag during cycling acting between leading region (high-pressure) and trailing region (low-pressure) of a cyclist and bicycle.

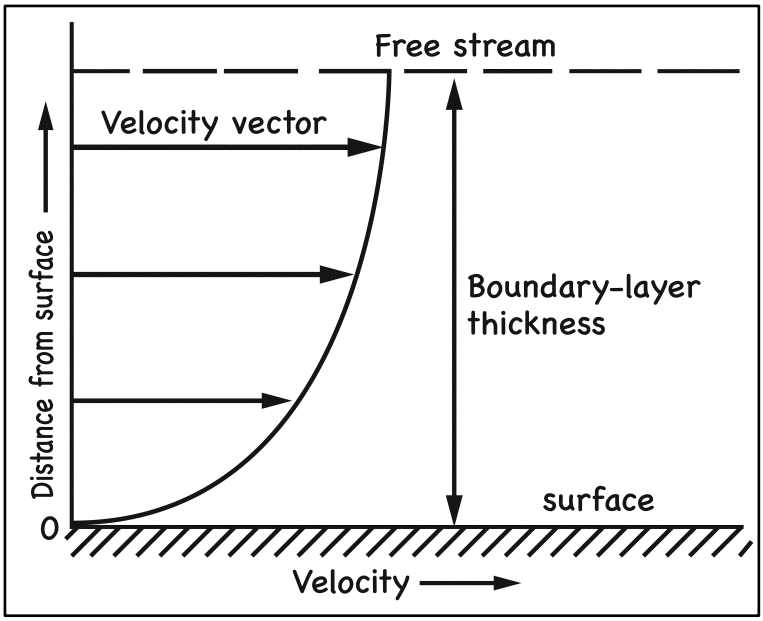


Figure 3 Illustration which represents the various velocity vectors of the boundary-layer thickness from the body surface to the free stream. (Resource: Versteeg & Malalasekera, 2007)

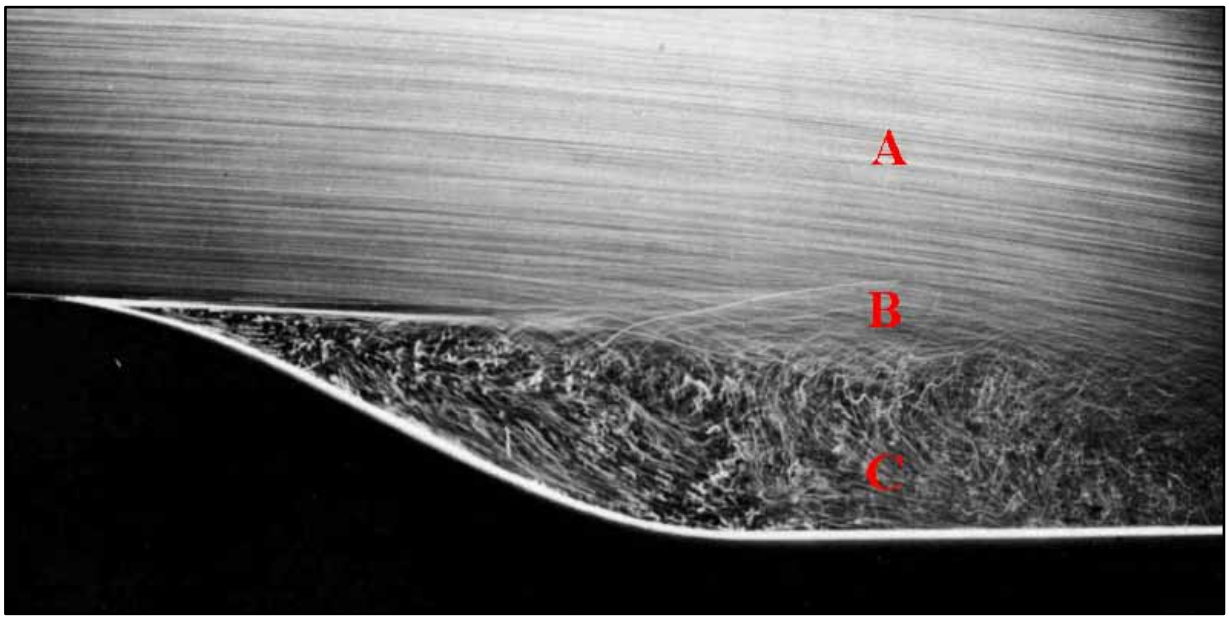


Figure 4 Illustration of three forms of boundary layers: (A) laminar flow, (B) separated flow, and (C) turbulent flow. (Resource: Van Dyke, 1982)

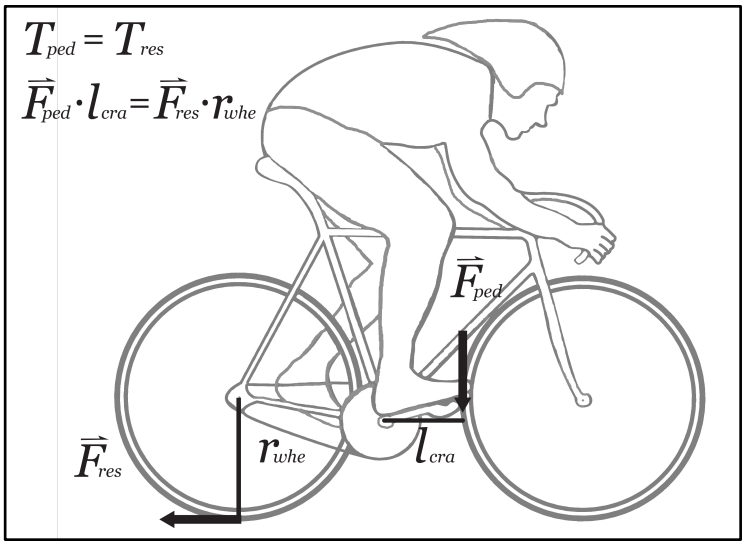


Figure 5 Schematic representation of equilibrium of resistive torque ( $T_{res}$ ) and pedal torque ( $T_{ped}$ ) during cycling on the road. The $T_{res}$ is equal to the resistive force ( $F_{res}$ ) that consists of aerodynamic drag force ( $F_{aer}$ ), rolling friction ( $F_{rol}$ ), gravitational force ( $F_{gra}$ ), bearing friction ( $F_{bea}$ ), and inertial force ( $F_{ine}$ ) multiple by the wheel radius ( $r_{whe}$ ), and the $T_{ped}$ is equal to the pedal force ( $F_{res}$ ) that generated by cyclist multiple by the length of crank ( $l_{cra}$ ).

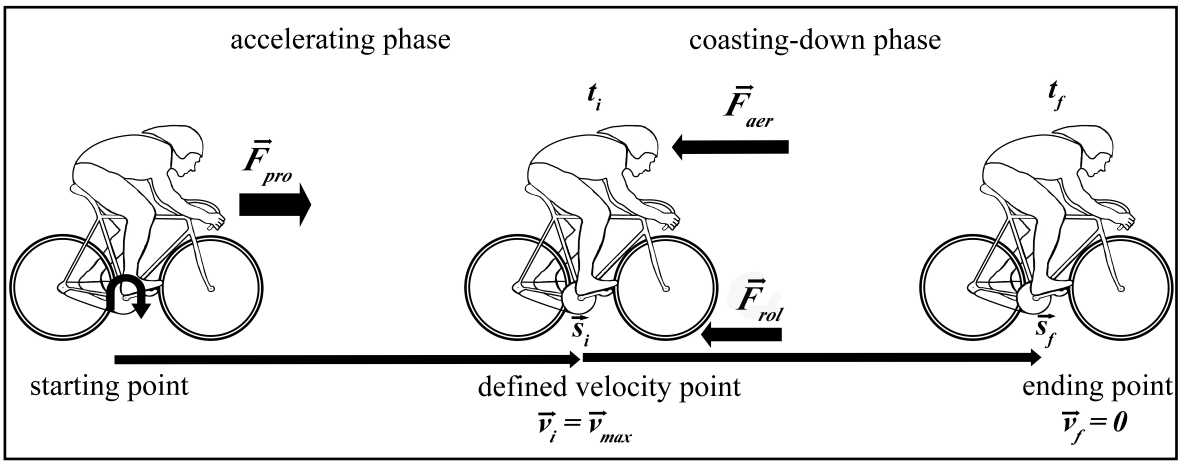


Figure 6 Schematic representation of the technique of coasting down motion from the starting point through the defined point (accelerated by propulsive force $F_{pro}$ ) to the ending point (decelerated by air drag $F_{aer}$ and rolling friction $F_{rol}$ ). The measured velocities respect to time are recorded from the defined velocity point until the ending point in order to estimate the values of best-fit aerodynamic parameters. Note: $v_i$ , $v_f$ and $v_{max}$ are initial, final and maximal velocity. $s_i$ and $s_f$ are initial and final displacement. $t_i$ and $t_f$ are initial and final time.

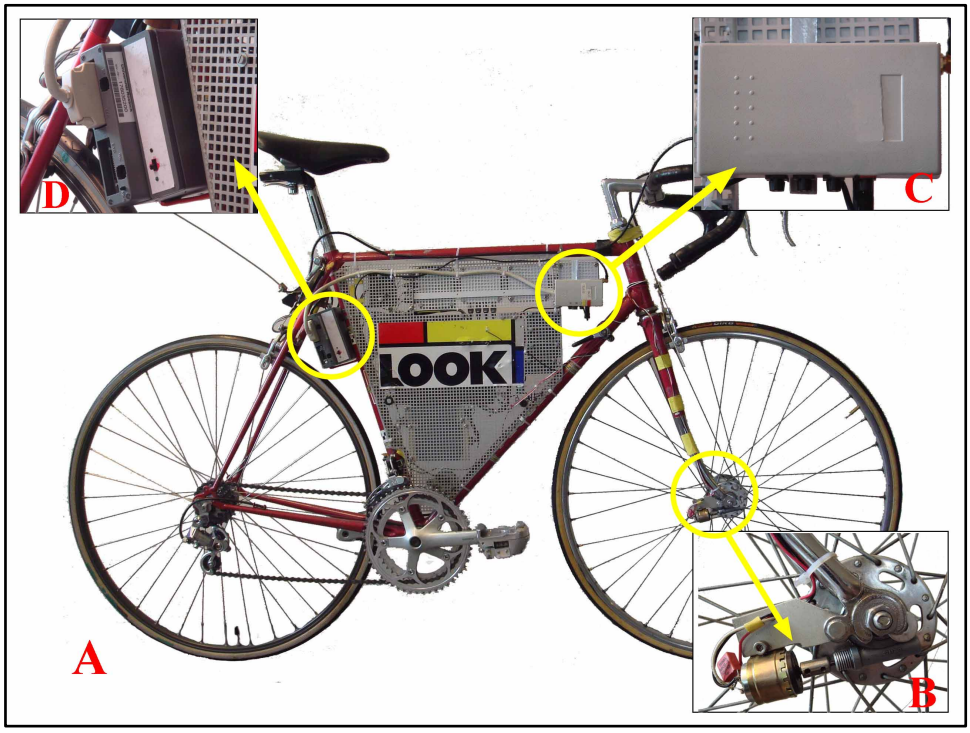


Figure 7 Illustration of (A) telemetry-bicycle system consists of (B) a tachogenerator (speed sensor), (C) a connector box, and (D) a transmitter unit with an antenna.


Figure 8 Illustration of wireless telemetry systems for coasting down testing consisting of (A) a telemetry bicycle, (B) a receiver antenna, (C) a receiver device, (D) a connector block, (E) a DAQCard™, and (F) a laptop with DIAdem® software.

# APPENDIX A: FIGURES

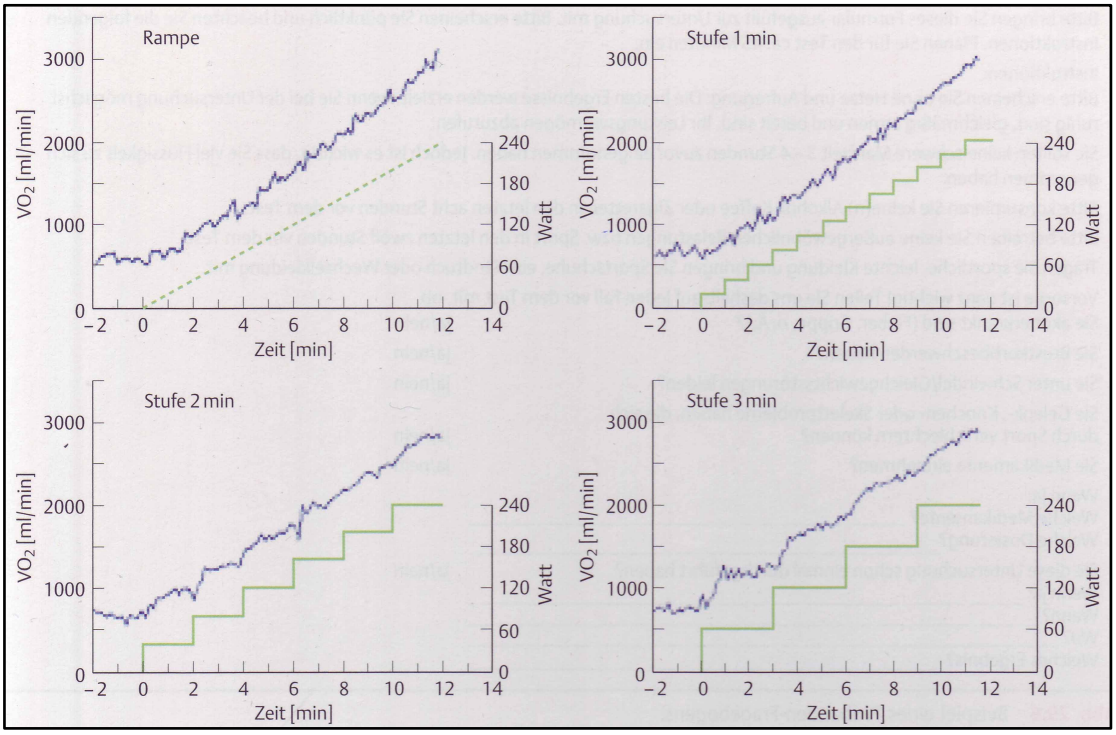


Figure 9 Illustration of the oxygen consumption (ml/min) over time for a ramp protocol and steady-state protocols at 1, 2 and 3 minute, and increased intensities 20, 40 and 60 Watt, respectively. (Resource: Kroidl et al., 2007)

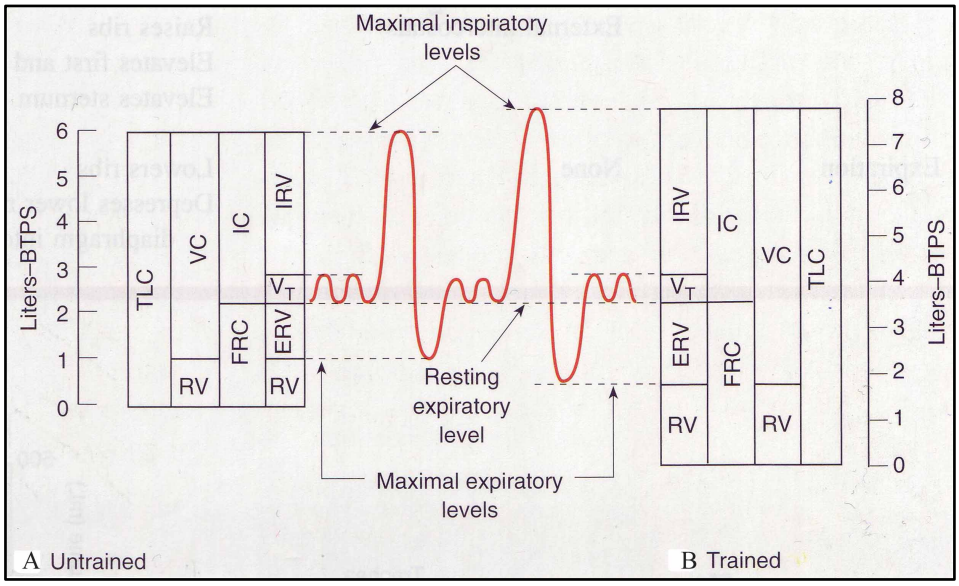


Figure 10 As shown in these spirograms, various lung volumes at rest (except $V_T$) can be smaller in untrained (A) than in trained (B) individuals. Note: $V_T$ = tidal volume, IC = inspiratory capacity, VC = vital capacity, RV = residual volume, IRV = inspiratory reserve volume, ERV = expiratory reserve volume, FRC = functional residual capacity, and TLC = total lung capacity. (Resource: Foss & Keteyian, 1998)

# APPENDIX A: FIGURES

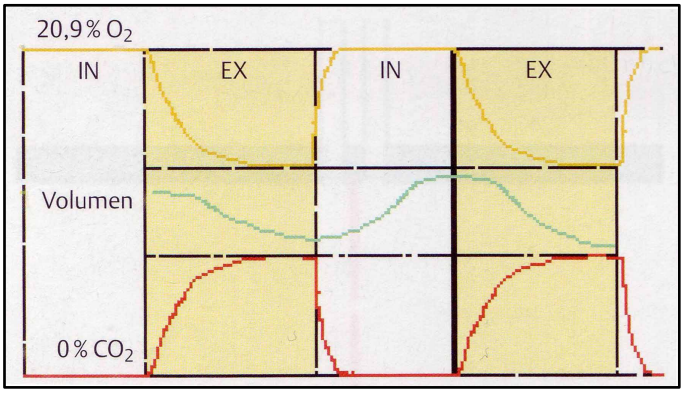


Figure 11 Illustration shows the synchronization of respiratory gas volumes in percentage by the breath-by-breath technique. In fresh air, the proportion of gases that are inspired by the body typically consist of fractional concentration of oxygen 0.2093 (20.93%) and fractional concentration of carbon dioxide 0.0004 (0.04%). Note: IN = Inspiration, EX = Expiration, $O_2$ = Oxygen, and $CO_2$ = Carbon Dioxide. (Resource: Kroidl et al., 2007)

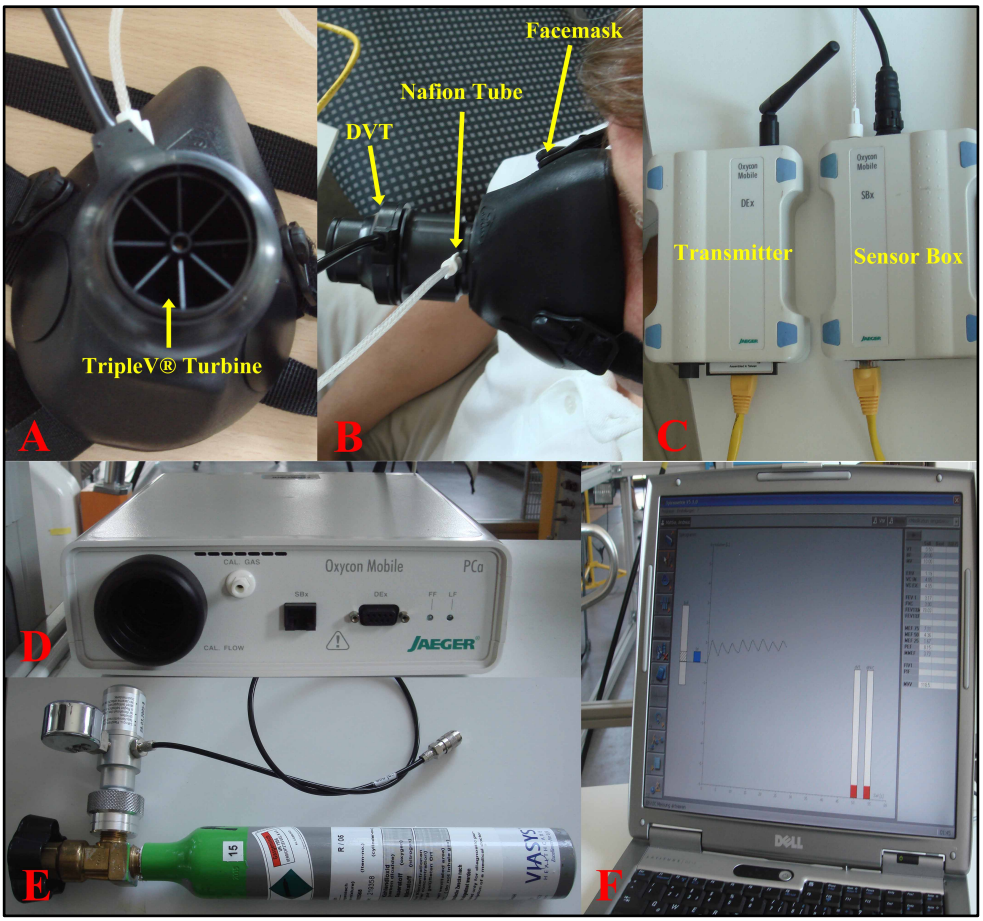


Figure 12 Illustrations of Oxycon Mobile® system, which consists of (A) a TripleV® turbine, (B) a DVT and a Nafion tube connected to a facemask, (C) a sensor box and a transmitter, (D) a telemetry unit with a calibration module, (E) a pressure reducer with an optional gas cylinder, and (F) a laptop with Oxycon Mobile®'s software.

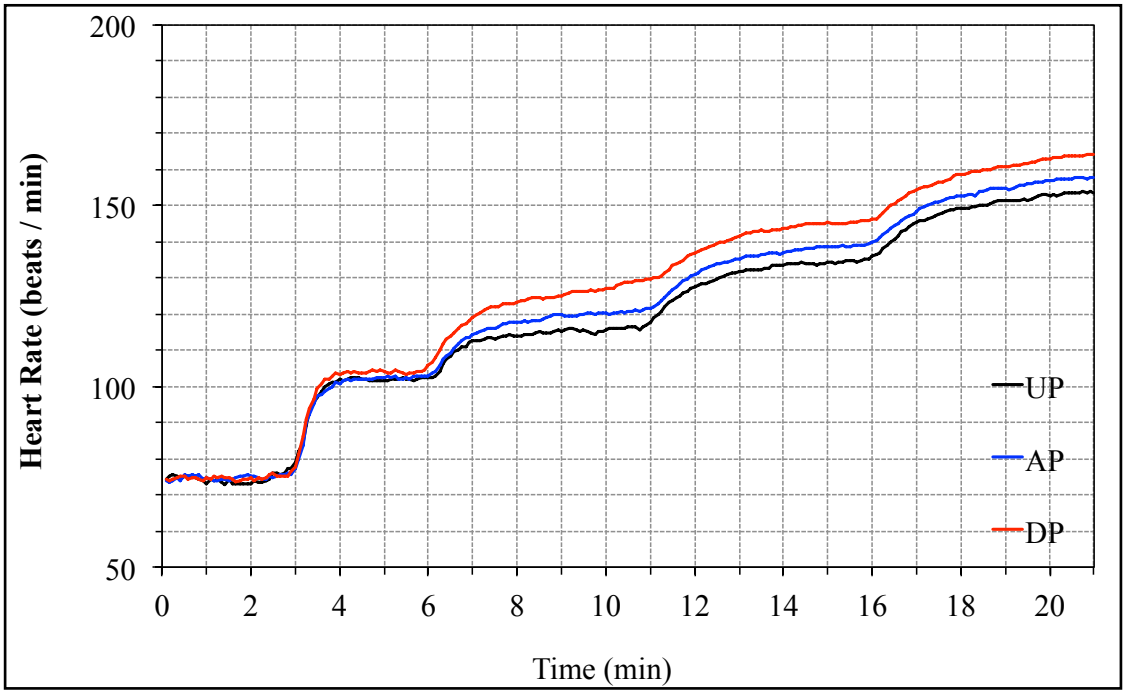


Figure 13 Average of heart rate from online record for the three cycling positions ($n$ = 24).

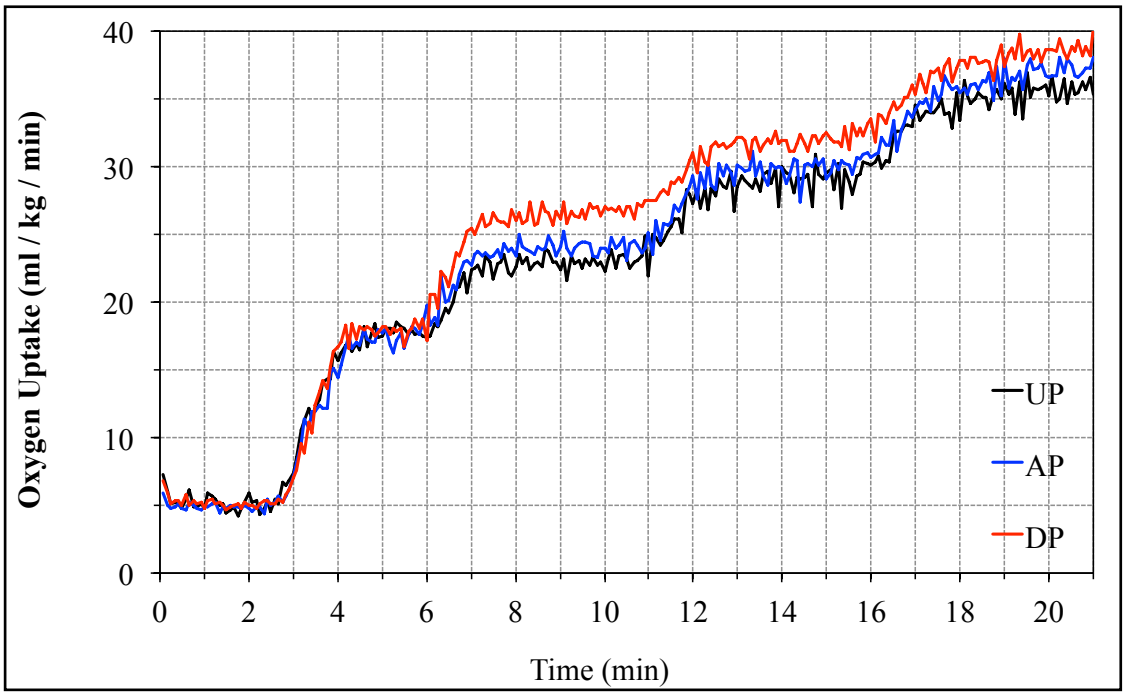


Figure 14 Average of oxygen uptake per body weight from online record for the three cycling positions ($n$ = 24).

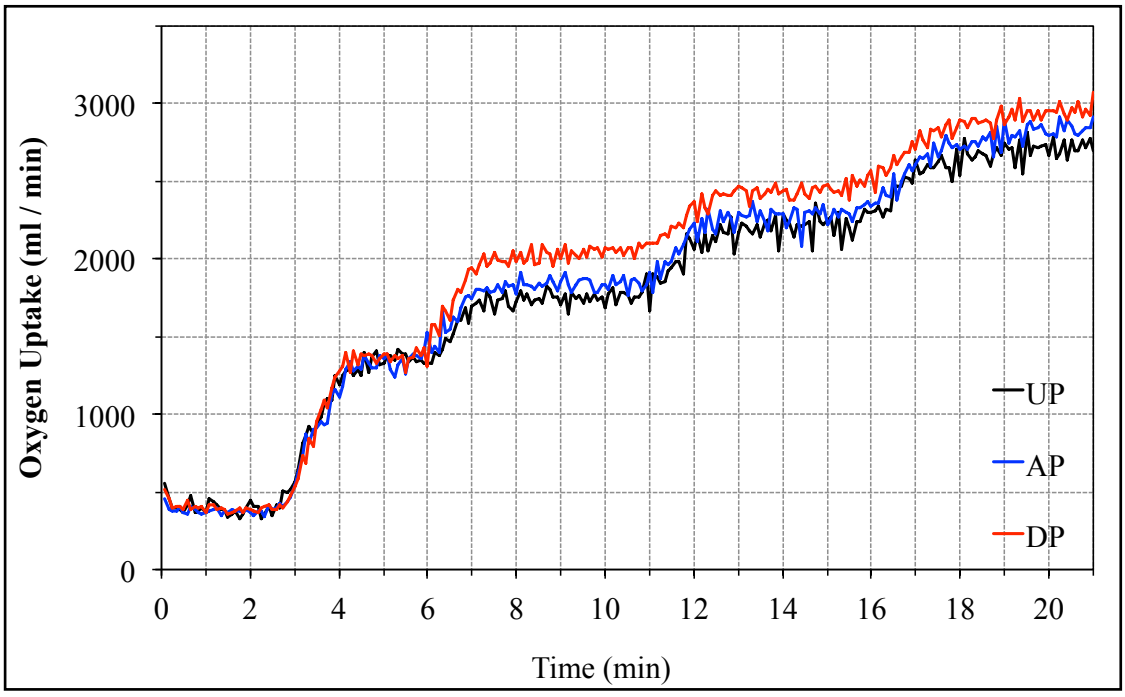


Figure 15 Average of oxygen uptake from online record for the three cycling positions ($n$ = 24).

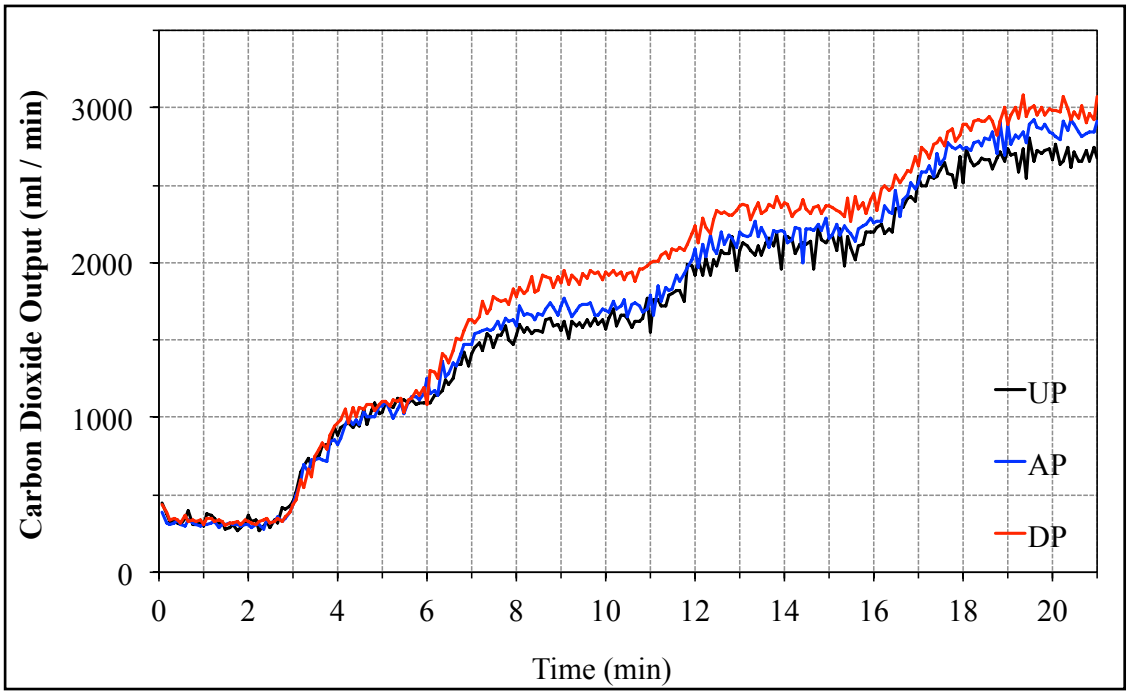


Figure 16 Average of carbon dioxide output from online record for the three cycling positions ($n$ = 24).

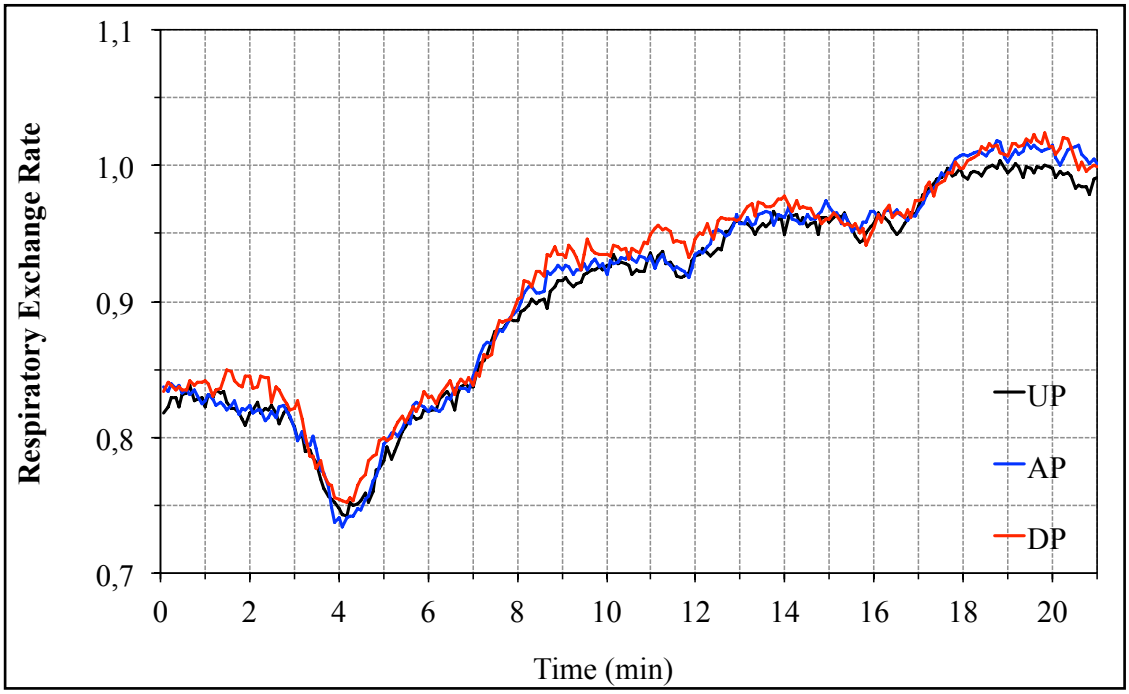


Figure 17 Average of respiratory exchange rate from online record for the three cycling positions ($n$ = 24).

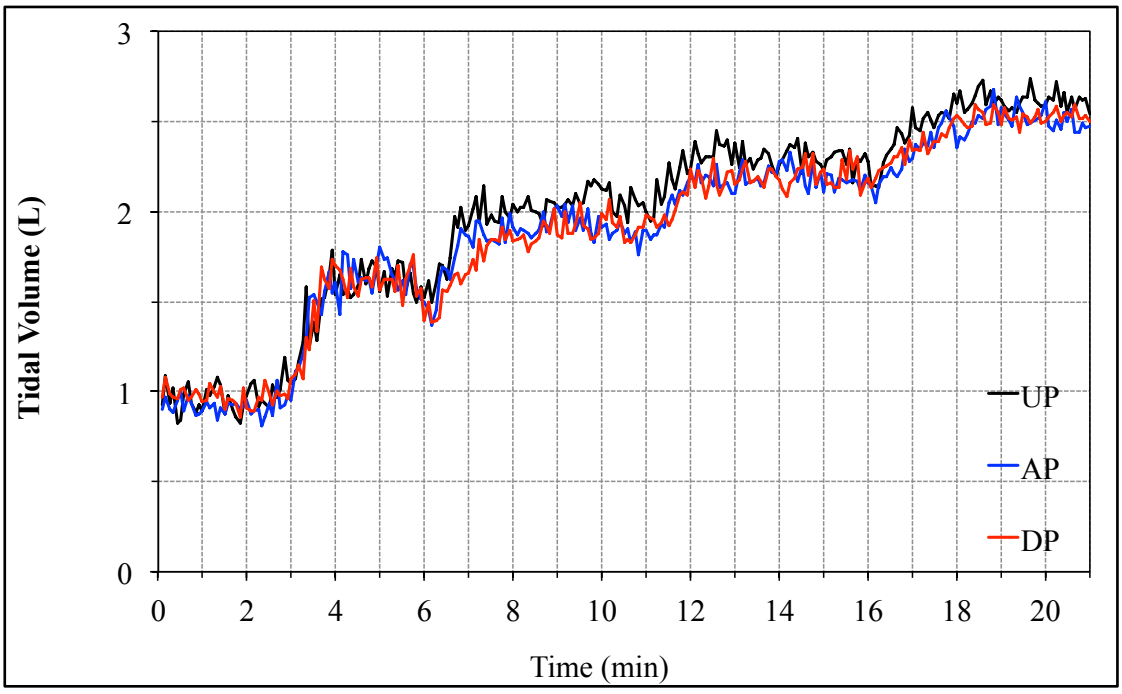


Figure 18 Average of tidal volume from online record for the three cycling positions ($n$ = 24).

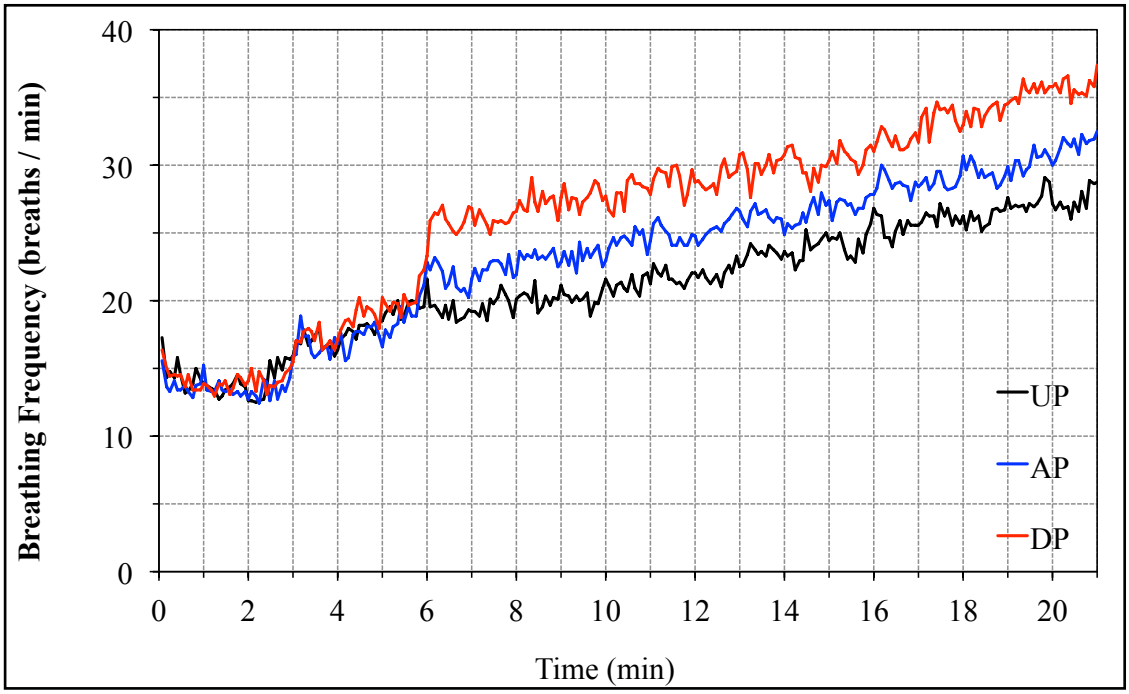


Figure 19 Average of breathing frequency from online record for the three cycling positions ($n$ = 24).

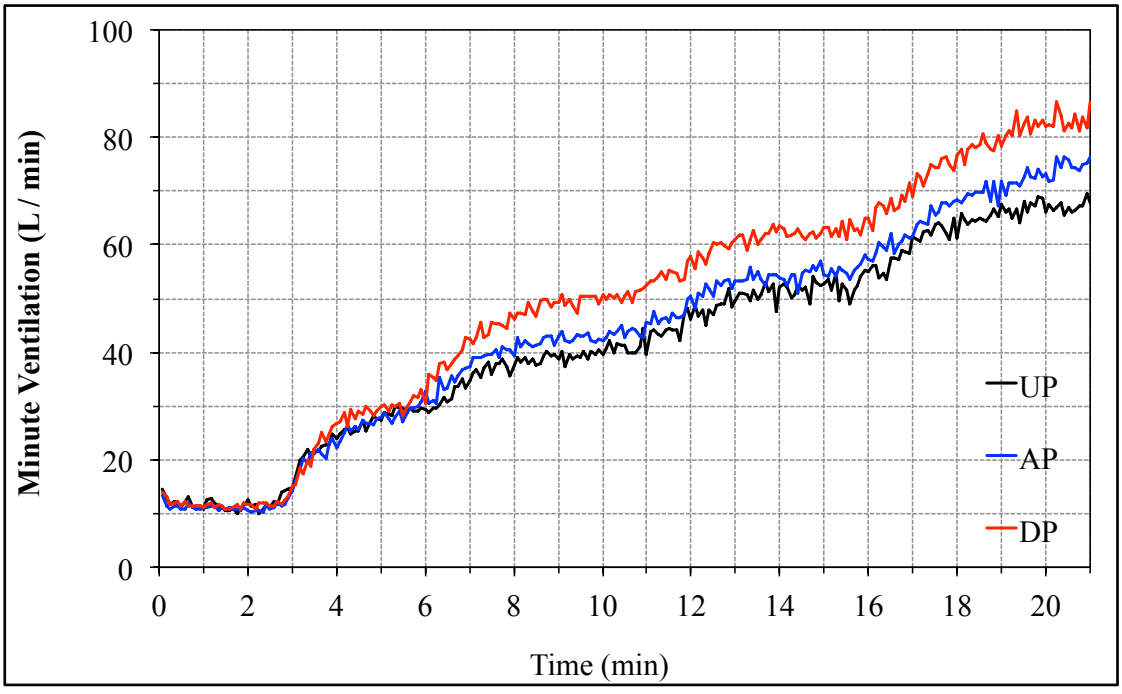


Figure 20 Average of minute ventilation from online record for the three cycling positions ($n$ = 24).

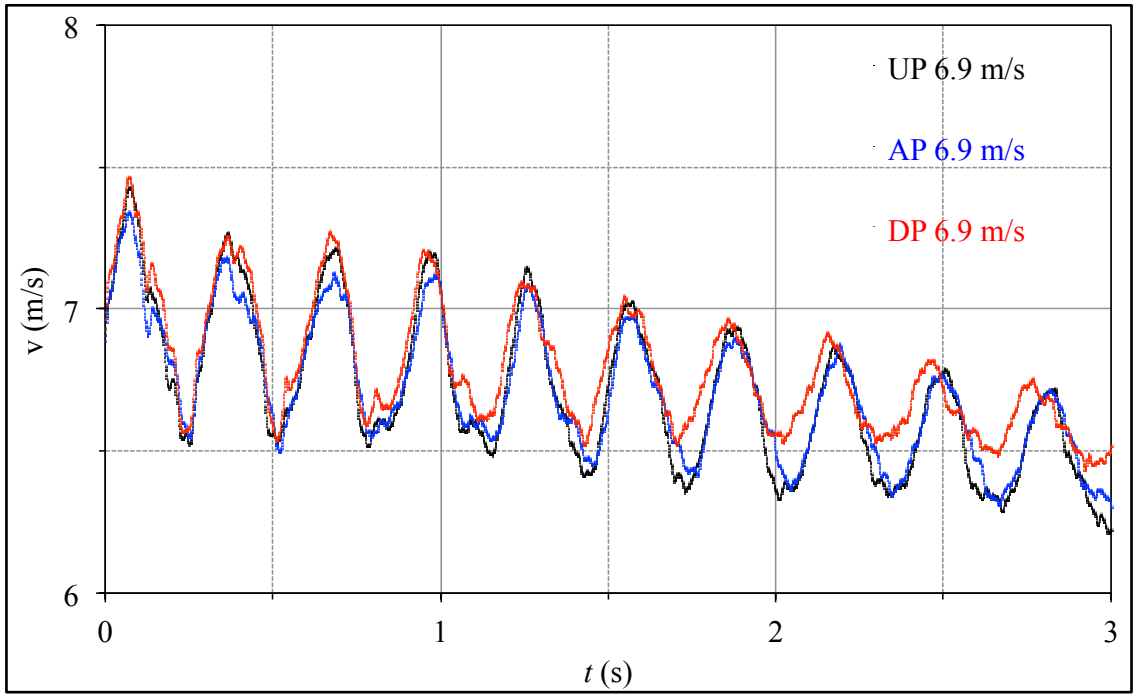


Figure 21 Average of measured velocity of 6.9 $m \cdot s^{-1}$ (25 $km \cdot h^{-1}$) for the three cycling positions ($n$ = 4).

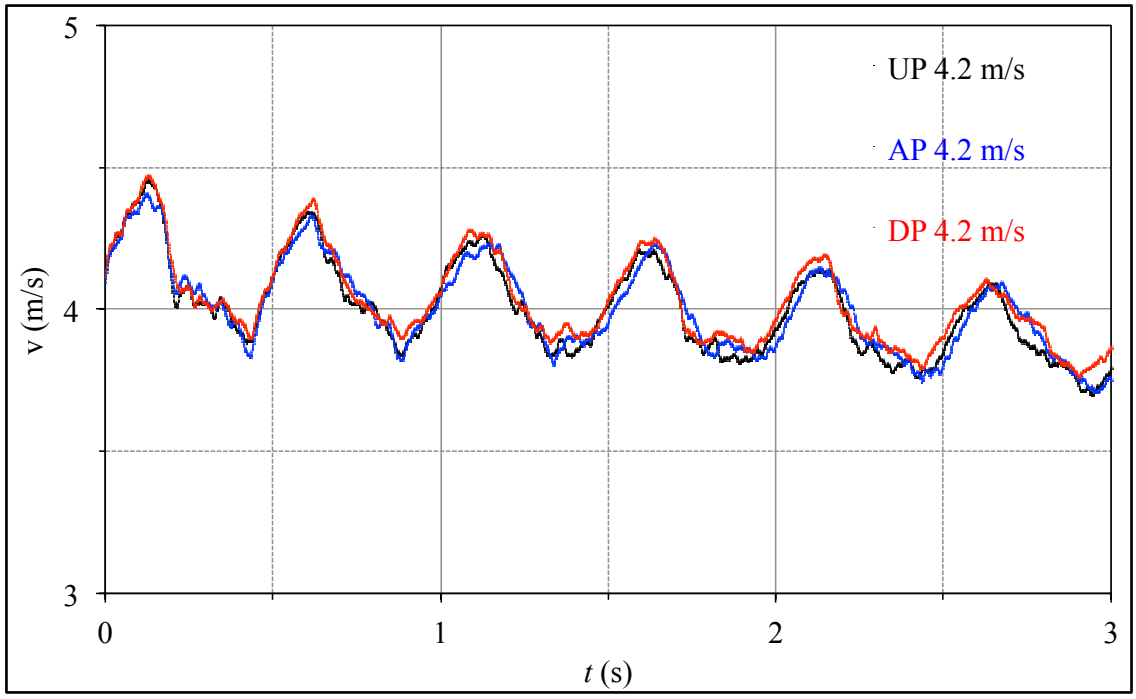


Figure 22 Average of measured velocity of 4.2 $m \cdot s^{-1}$ (15 $km \cdot h^{-1}$) for the three cycling positions ($n$ = 4).

# APPENDIX B: TABLES

Table 1 Definitions of lung volumes and capacities, typical values at rest, and their changes during exercise as compared with rest. (Resource: Foss & Keteyian, 1998)

| Lung volume or capacity | Definition | Typical values at rest (Litre) | Change during exercise |
|---|---|---|---|
| Tidal volume ($V_T$) | Volume inspired or expired per breath | 0.4-0.6 | Increase |
| Inspiratory reserve volume (IRV) | Maximal volume inspired from end-inspiration | 3.1 | Decrease |
| Expiratory reserve volume (ERV) | Maximal volume expired from end-expiration | 1.2 | Decrease |
| Residual volume (RV) | Volume remaining at end of maximal expiration | 1.2 | Slight decrease |
| Total lung capacity (TLC) | Volume in lung at end of maximal inspiration | 6.0 | Slight decrease |
| Vital capacity (VC) | Maximal volume forcefully expired after maximal inspiration | 4.8 | Slight decrease |
| Inspiratory capacity (IC) | Maximal volume inspired from resting expiratory level | 3.6 | Increase |
| Functional residual capacity (FRC) | Volume in lung at end of passive expiration | 2.4 | Decrease |

# APPENDIX B: TABLES

Table 2 Individual physical data of the twenty-four participants and the sequential cycling positions of the six groups for spiroergometry testing.

| No. | Code-Subject | Age (years) | Height (cm) | Weight (kg) | Sequential Cycling Positions | | |
|---|---|---|---|---|---|---|---|
| | | | | | 1st Day | 2nd Day | 3rd Day |
| 1 | 16-AH | 24 | 181 | 69 | UP | AP | DP |
| 2 | 17-NY | 26 | 179 | 79 | UP | AP | DP |
| 3 | 20-SB | 34 | 178 | 71 | UP | AP | DP |
| 4 | 24-FZ | 22 | 178 | 70 | UP | AP | DP |
| 5 | 12-LB | 24 | 181 | 79 | UP | DP | AP |
| 6 | 15-ES | 30 | 175 | 71 | UP | DP | AP |
| 7 | 18-MH | 25 | 180 | 74 | UP | DP | AP |
| 8 | 08-SO | 26 | 178 | 83 | UP | DP | AP |
| 9 | 11-AL | 29 | 180 | 69 | AP | DP | UP |
| 10 | 19-RB | 27 | 177 | 90 | AP | DP | UP |
| 11 | 22-YL | 36 | 165 | 62 | AP | DP | UP |
| 12 | 04-CJ | 24 | 181 | 79 | AP | DP | UP |
| 13 | 03-HK | 25 | 186 | 90 | AP | UP | DP |
| 14 | 13-RH | 25 | 183 | 76 | AP | UP | DP |
| 15 | 21-SL | 30 | 170 | 75 | AP | UP | DP |
| 16 | 10-RK | 22 | 192 | 97 | AP | UP | DP |
| 17 | 01-WN | 35 | 175 | 76 | DP | UP | AP |
| 18 | 02-TN | 23 | 180 | 71 | DP | UP | AP |
| 19 | 05-MJ | 28 | 190 | 78 | DP | UP | AP |
| 20 | 14-SB | 24 | 180 | 82 | DP | UP | AP |
| 21 | 06-UC | 29 | 171 | 70 | DP | AP | UP |
| 22 | 07-KS | 21 | 194 | 85 | DP | AP | UP |
| 23 | 23-KV | 29 | 183 | 72 | DP | AP | UP |
| 24 | 09-HL | 32 | 177 | 74 | DP | AP | UP |
| (*n*=24) | Mean | 27.1 | 179.8 | 76.8 | | | |
| | SD | 4.2 | 6.5 | 8.0 | | | |

# APPENDIX C: LEAST-SQUARES METHOD

| Time t (s) | Measuring points v mea. (m/s) | Model function v fit. (m/s) | Residuals Differences between v mea. and v fit. (v mea. - v fit.) | Residuals Squared Squares of Differences between v mea. and v fit. (v mea. - v fit.)^2 |
|---|---|---|---|---|
| 0 | 10,00 | 9,900931 | 0,099069 | 0,009815 |
| 10 | 7,00 | 8,153095 | -1,153095 | 1,329629 |
| 20 | 8,00 | 6,771236 | 1,228764 | 1,509862 |
| 30 | 6,50 | 5,634021 | 0,865979 | 0,749920 |
| 40 | 4,00 | 4,666854 | -0,666854 | 0,444694 |
| 50 | 5,00 | 3,821038 | 1,178962 | 1,389950 |
| 60 | 2,00 | 3,063114 | -1,063114 | 1,130211 |
| 70 | 2,50 | 2,368982 | 0,131018 | 0,017166 |
| 80 | 1,00 | 1,720470 | -0,720470 | 0,519077 |
| 90 | 1,50 | 1,103192 | 0,396808 | 0,157456 |
| 100 | 0,00 | 0,505145 | -0,505145 | 0,255171 |
| | | | Sum of Squares (SS) = | 7,512950 |

A

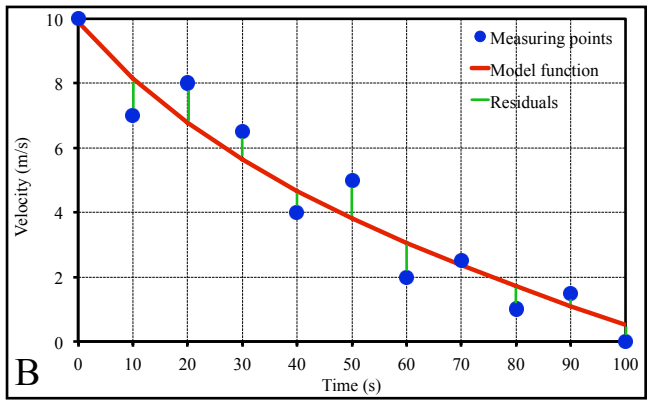


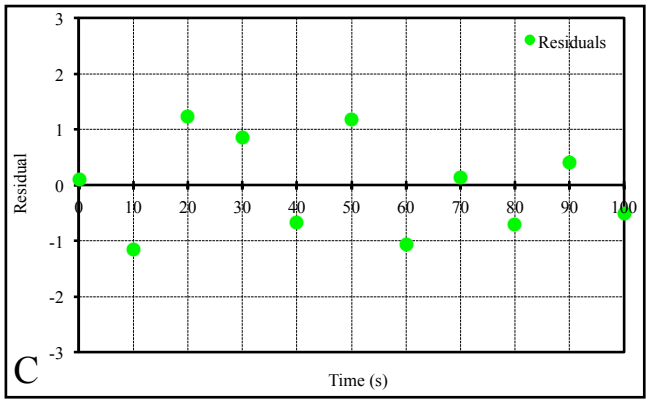


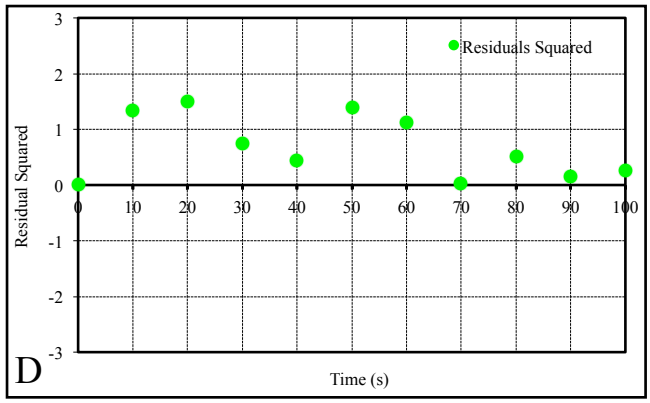


Figure 1 Illustration of curve fitting by using the least-squares principle: (A) measured data, (B) nonlinear mathematical model as $y = f(x)$, (C) residual, and (D) residual squares.

Figures 1A and 1B demonstrate a nonlinear model of Equation (2.26), namely the coasting down model (red line), the measuring points as function $y = f(x)$ (blue dot), and the residuals (green line). The red curve indicates that a nonlinear regression is used to fit the data to the model that defines y (dependent variable, such as velocity) as a function of x (independent variable, such as time). This model is created by determining of best-fit values of parameters of Equation (2.26) by the least-squared method through a nonlinear regression algorithm. The main technique of the least squares method is to minimize the sum of the squared errors or vertical distances (Y-axis) between the data points and the curve. These errors are also called residuals (Draper & Smith, 1998). The value of a residual is positive when the point is above the curve, and negative when the point is below the curve (Figure 1C). By iterative processing, the algorithm will try to find the best set of parameter values that make the curve fit the data points as closely as possible, i.e. which provide the smallest value for the sum of the squared residuals (Figure 1D).

# APPENDIX C: CALCULATION OF RESPIRATORY GASES

***Oxygen consumption***

By concept, oxygen uptake is the amount of oxygen that is consumed per minute ($\dot{V}O_2$), which is equal to the difference between the amount of inhaled oxygen ($\dot{V}_{in}O_2$) and the amount of exhaled oxygen ($\dot{V}_{ex}O_2$) (Foss & Keteyian, 1998). This must be corrected in units of the standard temperature and pressure dry (STPD), which can be conceptualized by:

$$\dot{V}O_2 = \dot{V}_{in}O_2 - \dot{V}_{ex}O_2 \qquad \text{(Apd. 1)}$$

In Equation (Apd. 1) the amount should actually be defined as a volume times a fractional concentration of gases; thus, the true amount of oxygen consumption is:

$$\dot{V}O_2 = \left(\dot{V}_{in} \cdot F_{in}O_2\right) - \left(\dot{V}_{ex} \cdot F_{ex}O_2\right) \qquad \text{(Apd. 2)}$$

where, $\dot{V}O_2$ is the oxygen consumption per minute ($L \cdot min^{-1}$); $\dot{V}_{in}$ and $\dot{V}_{ex}$ are the volumes of air inspired and expired per minute ($L \cdot min^{-1}$); and $F_{in}O_2$ and $F_{ex}O_2$ are the fractional concentrations of oxygen in the inspired and expired air. From Equation (Apd. 2), only $\dot{V}O_2$ and $\dot{V}_{in}$ are unknown, whereas $F_{in}O_2$ (= 0.2093), $\dot{V}_{ex}$, and $F_{ex}O_2$ are either known or can be directly measured by the detector (Wilmore & Costill, 2004). Consequently, $\dot{V}_{in}$ needs to be measured or calculated in order to solve for $\dot{V}O_2$ in Equation (Apd. 2).

In accordance with the inspired air volume and the gas relationship of inhalation and exhalation:

$$\dot{V}_{in} = \dot{V}_{ex} \cdot \left(\frac{F_{ex}N_2}{F_{in}N_2}\right) \qquad (2.36)$$

$$F_{in}O_2 + F_{in}CO_2 + F_{in}N_2 = 1 \qquad (2.38)$$

$$F_{ex}N_2 = 1 - F_{ex}O_2 - F_{ex}CO_2 \qquad (2.41)$$

From unknown value of $\dot{V}_{in}$ in Equation (2.36) (see Chapter 2: Theories 2.5.3), the value of $F_{in}N_2$ (= 0.7903) is known, whereas the values of $\dot{V}_{ex}$ and $F_{ex}N_2$ as well as the values of $F_{ex}O_2$ and $F_{ex}CO_2$ in Equation (2.41) (see Chapter 2: Theories 2.5.3) must be obtained from measurements. Thus, the values of these variables are needed to calculate $\dot{V}O_2$.

Considering Equation (Apd. 2) aganin, this seems to be a simple procedure, except for the simultaneous measurement of $\dot{V}_{in}$ and $\dot{V}_{ex}$. Wilmore and Costill, 2004 noted that, if we measure one of the two and assume them both to be equal, we will make mistakes because under some circumstances, the inspired and expired ventilation

volumes can be quite different, the main difference being that the inspired gas is dry, whereas the expired gas is saturated with water vapour. Theoretically, the value of the respiratory gases will fluctuate with the barometric pressure, the inspired and expired gas temperatures, and the relative humidity. It is relatively simple to know both $\dot{V}_{in}$ and $\dot{V}_{ex}$ while only measuring the one. This is due to the nitrogen concentrations as nitrogen is neither used nor given off by the body (Cooke, 2003). Therefore, instead of measuring $\dot{V}_{in}$ directly, as mentioned above, the principle of the Haldane transformation uses a simpler technique for accurately calculating $\dot{V}_{in}$. Substituting Equation (2.36) into Equation (Apd. 2) gives:

$$\dot{V}O_2 = \left(\dot{V}_{ex} \cdot \left(\frac{F_{ex}N_2}{F_{in}N_2}\right) \cdot F_{in}O_2\right) - \left(\dot{V}_{ex} \cdot F_{ex}O_2\right) \qquad \text{(Apd. 3)}$$

$F_{ex}N_2 / F_{in}N_2$ is the ratio of the fractional concentration of $N_2$ expired to inspired and is referred to as the Nitrogen factor. Then, substituting Equation (2.41) in Equation (Apd. 3) leads to:

$$\dot{V}O_2 = \left(\dot{V}_{ex} \cdot \left(\frac{1 - F_{ex}O_2 - F_{ex}CO_2}{F_{in}N_2}\right) \cdot F_{in}O_2\right) - \left(\dot{V}_{ex} \cdot F_{ex}O_2\right) \qquad \text{(Apd. 4)}$$

which can be rearranged to the following:

$$\dot{V}O_2 = \dot{V}_{ex} \cdot \left(\left(1 - F_{ex}O_2 - F_{ex}CO_2\right) \cdot \frac{F_{in}O_2}{F_{in}N_2} - F_{ex}O_2\right) \qquad \text{(Apd. 5)}$$

As mentioned above in Equation (2.38) (see Chapter 2: Theories 2.5.3), the sum of the fractional concentrations for the inspired oxygen $F_{in}O_2$ = 0.2093 (20.93%), carbon dioxide $F_{in}CO_2$ = 0.0004 (0.04%), and gaseous nitrogen $F_{in}N_2$ = 0.7903 (79.03%) is known and equal to 1 (Cooke, 2003). Then, finally, by substituting these known values into Equation (Apd. 5), the modified equation for calculating $\dot{V}O_2$ becomes:

$$\dot{V}O_2 = \dot{V}_{ex} \cdot \left(\left(1 - F_{ex}O_2 - F_{ex}CO_2\right) \cdot 0.2648 - F_{ex}O_2\right) \qquad \text{(Apd. 6)}$$

assuming $F_{in}O_2 / F_{in}N_2$ = 0.2093 / 0.7903 = 0.2468, and that $\dot{V}_{ex}$, $F_{ex}O_2$ and $F_{ex}CO_2$ are obtained from measurements. The factor $\left(F_{ex}N_2\right) \cdot 0.2648 - F_{ex}O_2$ or is called the true oxygen (Foss & Keteyian, 1998).

***Carbon dioxide production***

Under the same principle, carbon dioxide production per minute ($\dot{V}CO_2$) is equal to the difference between the amount of exhaled carbon dioxide ($\dot{V}_{ex}CO_2$) and the amount of inhaled carbon dioxide ($\dot{V}_{in}CO_2$) (Foss & Keteyian, 1998), which can be conceptualized by:

$$\dot{V}CO_2 = \dot{V}_{ex}CO_2 - \dot{V}_{in}CO_2 \quad \text{(Apd. 7)}$$

Or, if expressed as a volume times a fractional concentration of gases:

$$\dot{V}CO_2 = \left(\dot{V}_{ex} \cdot F_{ex}CO_2\right) - \left(\dot{V}_{in} \cdot F_{in}CO_2\right) \quad \text{(Apd. 8)}$$

where, $\dot{V}CO_2$ is the carbon dioxide production per minute ($L \cdot min^{-1}$); $\dot{V}_{ex}$ and $\dot{V}_{in}$ are the volumes of air expired and inspired per minute ($L \cdot min^{-1}$); and $F_{ex}CO_2$ and $F_{in}CO_2$ are the fractional concentrations of carbon dioxide in the expired and inspired air. The calculation of $\dot{V}CO_2$ is based on the same process as the calculation of the oxygen uptake, by using the principle of the Haldane transformation because $\dot{V}_{ex}$ and $F_{ex}CO_2$ are measured, $\dot{V}_{in}$ is calculated using the nitrogen factor, and $F_{in}CO_2$ is assumed to be 0.0004. Thus, substituting Equation (2.36) into Equation (Apd. 8) gives:

$$\dot{V}CO_2 = \left(\dot{V}_{ex} \cdot F_{ex}CO_2\right) - \left(\dot{V}_{ex} \cdot \left(\frac{F_{ex}N_2}{F_{in}N_2}\right) \cdot F_{in}CO_2\right) \quad \text{(Apd. 9)}$$

Then, substituting Equation (2.41) into Equation (Apd. 9) becomes:

$$\dot{V}CO_2 = \left(\dot{V}_{ex} \cdot F_{ex}CO_2\right) - \left(\dot{V}_{ex} \cdot \left(\frac{1 - F_{ex}O_2 - F_{ex}CO_2}{F_{in}N_2}\right) \cdot F_{in}CO_2\right) \quad \text{(Apd. 10)}$$

Which can be rearranged as follows:

$$\dot{V}CO_2 = \dot{V}_{ex} \cdot \left(F_{ex}CO_2 - \left(1 - F_{ex}O_2 - F_{ex}CO_2\right) \cdot \frac{F_{in}CO_2}{F_{in}N_2}\right) \quad \text{(Apd. 11)}$$

Finally, by inserting the known values $F_{in}CO_2$ = 0.0004 (0.04%) and $F_{in}N_2$ = 0.7903 (79.03%) into Equation (Apd. 11), the modified equation for calculating $\dot{V}CO_2$ becomes:

$$\dot{V}CO_2 = \dot{V}_{ex} \cdot \left(F_{ex}CO_2 - \left(1 - F_{ex}O_2 - F_{ex}CO_2\right) \cdot 0.0005\right) \quad \text{(Apd. 12)}$$

where, $F_{in}CO_2 / F_{in}N_2$ = 0.0004 / 0.7903 = 0.0005, and $\dot{V}_{ex}$, $F_{ex}CO_2$ and $F_{ex}O_2$ are measured by the detector. The factor $F_{ex}CO_2 - \left(1 - F_{ex}O_2 - F_{ex}CO_2\right) \cdot 0.0005$ or $F_{ex}CO_2 - \left(F_{ex}N_2\right) \cdot 0.0005$ is called the true carbon dioxide (Foss & Keteyian, 1998).

# Selbständigkeitserklärung

Ich versichere hiermit an Eides statt, dass ich die vorliegende Arbeit selbstständig angefertigt und ohne fremde Hilfe verfasst habe, keine außer den von mir angegebenen Hilfsmitteln und Quellen dazu verwendet habe und die den benutzten Werken inhaltlich und wörtlich entnommenen Stellen als solche kenntlich gemacht habe.

Rostock, 18. März 2016 Wuttigrai Noipant

# Curriculum Vitae

**PROFILE**


| | |
|---|---|
| Name: | Mr. Wuttigrai Noipant |
| Date of birth: | Oktober 6, 1975 |
| Place of birth: | Lop Buri, Thailand |
| Nationality: | Thai |
| Marital status: | Married |
| Occupation: | University lecturer |
| Teaching Area: | Sports Biomechanics |
| Research Area: | Cycling Science |
| Address: | Department of Athletic Training and Movement Science, Faculty of Sports Science, Kasetsart University, Kampheang Saen Campus. Malaiman Road, Nakornprathom Province, 73140, Thailand. |
| E-mail: | fsswgn@ku.ac.th |
| Phone: | (+66) 3435 5258 |


**EDUCATIONAL BACKGROUND**

| | |
|---|---|
| 2007-Present: | PhD candidate in the field of sports biomechanics and movement science, Department of Sports Science, Philosophy Faculty, University of Rostock, Germany |
| Dissertation: | The effect of cycling positions on cardiorespiratory and aerodynamic parameters for road cyclists |
| Funding: | Kasetsart University |
| 1998-2001: | Master of Science (Sports Sciences), Department of Sports Science, Faculty of Education, Kasetsart University, Bangkok |
| Thesis: | The Study of Cycling Position upon Aerodynamics Drag Force |
| Funding: | Sports Authority of Thailand |
| 1994-1998: | Bachelor of Science (Physical Education), Department of Physical Education, Faculty of Education, Kasetsart University, Bangkok |
| 1988-1994: | Secondary School Grade 7 to 12 (Sciences and Mathematics), Banmiwittaya School, Lob Buri |

**WORKS AND TRAINING EXPERIENCES**

2002-2006: University lecturer in Sports Science Program, Faculty of Science, Rajabhat Chandrakasem University, Bangkok

25-28/07/2005: Sports Science Workshop on Modern Speed Strength Training: From Beginner to Elite Athletes, Sports Authority of Thailand, Bangkok

17-28/12/2004: Technical Course in Cycling (Level 1), Cycling Association of Thailand, Bangkok

19-22/07/2004: Sports Science Workshop on How to Prevent Sports Injuries, Sports Authority of Thailand, Bangkok

01-04/09/2003: Sports Science Workshop on Modern Speed Training, Sports Authority of Thailand, Bangkok

04-08/03/2008: Workshop on Muscular Stimulation with Prof. Dr. Volker Zschorlich, Department of Sports Science, University of Rostock, Germany

**PUBLICATIONS**

1. Wuttigrai Noipant, The Study of Cycling Position upon Aerodynamics Drag Force, Journal of The Sports Medicine Association of Thailand. Volume.7, No.2, August 2003.
2. Wuttigrai Noipant, The Study of Cycling Position upon Aerodynamics Drag Force, Sports Science Bulletin (Sports Authority of Thailand). Volume.5, No.48, April 2004.

**SEMINARS AND CONFERENCES**

26-027/08/2011: 1st International Symposium on Numerical Simulation in Orthopaedic Biomechanics, University of Rostock, Germany

**GERMAN LANGUAGE SKILLS**

1. Deutsch als Fremdsprache – Niveaustufe: B2.1, B1.2, B1, und A2.2 des Europäischen Referenzrahmens für Sprachen, Volkshocschule Hansestadt Rostock.

2. Deutsch als Fremdsprache – Niveaustufe: Aufbaustufe, Modul 2 und 3 des Europäischen Referenzrahmens für Sprachen, Sprachenzentrum Universität Rostock.